Identification and characterization of novel filament-forming proteins in cyanobacteria

Benjamin L. Springstein[1‡*], Christian Woehle[1‡‡], Julia Weissenbach[1‡‡‡], Andreas O. Helbig[2], Tal Dagan[1], Karina Stucken[3*]

[1] Institute of General Microbiology, Christian-Albrechts-Universität zu Kiel, Kiel, Germany

[2] Institute for Experimental Medicine, Christian-Albrechts-Universität zu Kiel, Kiel, Germany

[3] Department of Food Engineering, University of La Serena, La Serena, Chile.

‡ Present address: Department of Microbiology, Blavatnick Institute, Harvard Medical School, Boston, MA, 02115 USA

‡‡ Present address: Max Planck Institute for Plant Breeding Research, Max Planck-Genome-Center Cologne, Cologne, Germany

‡‡‡ Present address: Faculty of Biology, Technion-Israel Institute of Technology, Haifa, 32000, Israel

* Corresponding authors: BLS: benjamin_springstein@hms.harvard.edu
KS: kstucken@userena.cl

Abstract

Filament-forming proteins in bacteria function in stabilization and localization of proteinaceous complexes and replicons; hence they are instrumental for myriad cellular processes such as cell division and growth. Here we present two novel filament-forming proteins in cyanobacteria. Surveying cyanobacterial genomes for coiled-coil-rich proteins (CCRPs) that are predicted as putative filament-forming proteins, we observed a higher proportion of CCRPs in filamentous cyanobacteria in comparison to unicellular cyanobacteria. Using our predictions, we identified nine protein families with putative intermediate filament (IF) properties. Polymerization assays revealed four proteins that formed polymers *in vitro* and three proteins that formed polymers *in vivo*. Fm7001 from *Fischerella muscicola* PCC 7414 polymerized *in vitro* and formed filaments *in vivo* in several organisms. Additionally, we identified a tetratricopeptide repeat protein - All4981 - in *Anabaena* sp. PCC 7120 that polymerized into filaments *in vitro* and *in vivo*. All4981 interacts with known cytoskeletal proteins and is indispensable for *Anabaena* viability. Although it did not form filaments *in vitro*, Syc2039 from *Synechococcus elongatus* PCC 7942 assembled into filaments *in vivo* and a Δ*syc2039* mutant was characterized by an impaired cytokinesis. Our results expand the repertoire of known prokaryotic filament-forming CCRPs and demonstrate that cyanobacterial CCRPs are involved in cell morphology, motility, cytokinesis and colony integrity.

Introduction

Species in the phylum Cyanobacteria present a wide morphological diversity, ranging from unicellular to multicellular organisms. Unicellular cyanobacteria of the *Synechocystis* and *Synechococcus* genera are characterized by a round or rod-shaped morphology, respectively, and many strains are motile. Species of the Nostocales order are multicellular and differentiate specialized cells, known as heterocysts, which fix atmospheric nitrogen under aerobic conditions. Within the Nostocales, species of the Nostocaceae (e.g., *Anabaena*, *Nostoc*) form linear trichomes, while cells in the Hapalosiphonaceae and Chlorogloepsidaceae divide in more than one plane to form true-branching trichomes as in *Fischerella* or multiseriate

trichomes (more than one filament in a row) as in *Chlorogloeopsis* (Rippka *et al.*, 1979). Notably, cells within a single trichome of a multicellular cyanobacterium can differ in size, form or cell wall composition (Rippka *et al.*, 1979). Cells in the *Anabaena* sp. PCC 7120 (hereafter *Anabaena*) trichome are linked by a shared peptidoglycan sheet and an outer membrane (Wilk *et al.*, 2011). *Anabaena* cells communicate and exchange nutrients through intercellular cell-cell connections, called septal junctions, which are thought to comprise the septal junction proteins SepJ, FraC and FraD (Herrero, Stavans and Flores, 2016; Weiss *et al.*, 2019). SepJ is essential for the multicellular phenotype in *Anabaena* (Flores *et al.*, 2007; Nayar *et al.*, 2007).

Studies of the molecular basis of cyanobacterial morphogenesis have so far focused on the function of FtsZ and MreB, the prokaryotic homologs of tubulin and actin, respectively (Wagstaff and Löwe, 2018). FtsZ functions in a multi-protein complex called the divisome, and is known as a key regulator of cell division and septal peptidoglycan (PG) biogenesis (Bi and Lutkenhaus, 1991; Wagstaff and Löwe, 2018). FtsZ has been shown to be an essential cellular protein in *Anabaena* and in the coccoid cyanobacterium *Synechocystis* sp. PCC 6803 (hereafter *Synechocystis*) (Zhang *et al.*, 1995). The FtsZ cellular concentration in *Anabaena* is tightly controlled by a so far undescribed protease (Lopes Pinto *et al.*, 2011). Apart from its function in cell division, the FtsZ-driven divisome also mediates the localization of SepJ (Ramos-León *et al.*, 2015). MreB functions in a multi-protein complex called the elongasome, where it is a key mediator of longitudinal PG biogenesis that controls the cell shape (Jones, Carballido-López and Errington, 2001; Wagstaff and Löwe, 2018). In cyanobacteria, MreB plays a role in cell shape determination in *Anabaena*, nonetheless, it is not essential for cell viability (Hu *et al.*, 2007). In contrast, in *Synechococcus* sp. PCC 7942 (hereafter *Synechococcus*) MreB is essential, where partially segregated mutants display a coccoid morphology resembling the morphology of *E. coli mreB* deletion strains (Kruse, Bork-Jensen and Gerdes, 2005; Jain, Vijayan and O'Shea, 2012).

Proteins resembling the eukaryotic intermediate filaments (IFs) have been discovered in several bacterial species and were shown to form filaments *in vitro* and *in vivo* and to impact

essential cellular processes (Lin and Thanbichler, 2013). IF proteins exhibit an intrinsic nucleotide-independent *in vitro* polymerization capability that is mediated by the high frequency of coiled-coil-rich regions in their amino acid sequence (Shoeman and Traub, 1993; Fuchs and Weber, 1994; Löwe and Amos, 2009; Wagstaff and Löwe, 2018). Eukaryotic IF proteins are generally characterized by a conserved domain buildup consisting of discontinuous coiled-coil segments that form a central rod domain. This rod domain is N- and C-terminally flanked by globular head and tail domains of variable length (Fuchs and Weber, 1994; Herrmann *et al.*, 1996; Herrmann and Aebi, 2004). Crescentin is a bacterial IF-like CCRP from *Caulobacter crescentus*, which exhibits a striking domain similarity to eukaryotic IF proteins. Crescentin filaments that align at the inner cell curvature are essential for the typical crescent-like cell shape of *C. crescentus*; possibly, by locally exuding a constriction force which coordinates the MreB-driven peptidoglycan (PG) synthesis machinery (Ausmees, Kuhn and Jacobs-Wagner, 2003; Cabeen *et al.*, 2009; Charbon, Cabeen and Jacobs-Wagner, 2009). Reminiscent of eukaryotic IF proteins, Crescentin was found to assemble into filamentous structures *in vitro* in a nucleotide-independent manner (Ausmees, Kuhn and Jacobs-Wagner, 2003). However, so far no Crescentin homologs have been found in other bacteria, indicating that non-spherical or rod-shaped prokaryotic morphologies are putatively controlled by other polymerizing proteins (Bagchi *et al.*, 2008; Wickstead and Gull, 2011). Apart from Crescentin, many other coiled-coil-rich proteins (CCRPs) with IF-like functions have been identified to polymerize into filamentous structures and to perform cytoskeletal-like roles; however, none of them resembled the eukaryotic IF domain architecture (reviewed by Lin & Thanbichler, 2013). Examples are two proteins from *Streptomyces coelicolor* whose function has been studied in more detail: FilP and Scy (Bagchi *et al.*, 2008; Walshaw, Gillespie and Kelemen, 2010; Holmes *et al.*, 2013). Gradients of FilP localize at the tip of a growing hyphae and contribute to cellular stiffness (Bagchi *et al.*, 2008). Scy forms patchy clusters at the sites of novel tip-formation and, together with the scaffolding CCRP DivIVA, orchestrates the polar hyphal growth (Holmes *et al.*, 2013). Together with FilP and a cellulose-synthase, these proteins form the polarisome, which guides peptidoglycan biogenesis and hyphal tip growth in *S. coelicolor* (Flärdh *et al.*,

2012; Hempel *et al.*, 2012; Holmes *et al.*, 2013). Another example are four CCRPs in the human pathogen *Helicobacter pylori*, which were found to assemble into filaments *in vitro* and *in vivo*, with a function in determination of the helical cell shape as well as cell motility (Waidner *et al.*, 2009; Specht *et al.*, 2011). Consequently, filament-forming CCRPs with essential cellular functions have been found in numerous prokaryotes having various cellular morphologies. The presence of filament-forming CCRPs in cyanobacteria is so far understudied. Here we search for CCRPs with presumed IF-like functions in cyanobacteria using a computational prediction of CCRPs. Putative filament-forming proteins were further investigated experimentally by structural analyses and *in vitro* and *in vivo* localization assays in morphologically diverse cyanobacteria.

Results

Coiled-coil-rich proteins are widespread in cyanobacteria

For the computational prediction of putative filament-forming proteins, we surveyed 364 cyanobacterial genomes including 1,225,314 protein-coding sequences (CDSs) for CCRPs. All CDSs in the cyanobacterial genomes where clustered by sequence similarity into families of homologous proteins (see Methods). The frequency of CCRPs in each CDS was calculated using the COILS algorithm (Lupas, Van Dyke and Stock, 1991). The algorithm yielded a list of 28,737 CDSs with high coiled-coil content (≥80 amino acids in coiled-coil conformation; Supplementary File 1). CCRPs were predicted in 158,466 protein families covering all cyanobacterial species. To examine the overall distribution of CCRPs in cyanobacterial genomes, we investigated 1,504 families of homologous proteins that include at least three CCRP members (Fig. 1). Notably, most protein families (1,142; 76%) include CCRP and non-CCRP members, indicating that protein properties might differ among homologous proteins. The presence/absence pattern of families including CCRPs further shows that those are less abundant in picocyanobacterial genomes (SynProCya group) in comparison to the remaining specie in the phylum. Furthermore, the proportion of CCRPs in the genome is significantly higher in multicellular cyanobacteria in comparison to unicellular cyanobacteria ($P=2.65x10^{-46}$

using Kruskal-Wallis test and Tukey test with α=0.05). This indicates that a high frequency of CCRPs is one characteristic of multicellular cyanobacteria.

For the experimental validation, the complete list of CCRPs was filtered to include candidates from freshwater unicellular and filamentous cyanobacteria that are genetically accessible, including *Thermosynechococcus elongatus* BP-1 (*Thermosynechococccus*), *Synechocystis*, *Synechococcus*, *Anabaena* and *Fischerella muscicola* PCC 7414 (*Fischerella*). In addition to cytoskeleton functions, coiled-coils are common motifs of proteins involved in other cellular processes such as transcription, the extracellular matrix, chemotaxis and host–pathogen interactions (Rackham *et al.*, 2010). Consequently, the remaining CCPRs were further sorted to include proteins having similar properties to known prokaryotic IF-like CCRPs (e.g., crescentin, FilP) and are annotated as hypothetical proteins with an unknown function. Additionally, proteins lacking an unstructured N-terminal head and C-terminal tail domain, which are characteristics of prokaryotic IF-like proteins (Bagchi *et al.*, 2008), were excluded. Furthermore, proteins with an assigned function or predicted to be involved in other cellular processes were excluded (using publicly available online bioinformatic tools: NCBI Blast, NCBI CD search, PSORTb, TMHMM, InterPro, PSIPRED and I-TASSER). In the screening for protein characteristics and annotation, Crescentin, FilP and other eukaryotic IF proteins (e.g., Vimentin and Desmin) were chosen as reference for our predictions, where proteins displaying similar results were favored. An additional *Fischerella* CDS, Fm7001, was added to the list as earlier analyses suggested that it has a cell shape-determining function. The preliminary filtration resulted in a list of nine candidates, which we investigated experimentally here (Fig. 1C,D and Supplementary Table 1).

Candidate coding sequences varied in size and ranged from ca. 280 amino acids (Synpcc7942_2039, abbreviated Syc2039) to ca. 650 amino acids (All4981). The coiled-coil domain distribution was variable among the candidates in both coiled-coil domain count and length (Fig. 1D). Only Slr7083 exhibited a somewhat characteristic domain architecture of eukaryotic IF proteins, whereas the coiled-coil domain distribution in the other candidates had

major differences in coiled-coil domain number and lengths. None of the predicted CCRPs exhibited a stutter-like structure in the last coiled-coil segment. Besides coiled-coil domains, the COILS algorithm also predicted tetratricopeptide repeats (TPRs) as coiled-coils, thus we also included All4981 into our analysis, even though conserved domain searches reliably predicted these domains as TPRs and not coiled-coils. Many protein candidates contained conserved domains from eukaryotic IF proteins, found in Crescentin and FilP or from the bacterial cell division protein EzrA (Supplementary Table 1). The presence of these domains may be regarded as support for our classification. Additionally, structural maintenance of chromosomes (SMC) domains were predicted in almost all chosen candidates, all eukaryotic IF proteins as well as in Crescentin and FilP (Supplementary Table 1). The MscS_TM domain from Desmin was found in Slr7083 and Tlr0420 contains a Neuromodulin_N as well as a CCDC158 domain, both present in FilP or Crescentin, respectively.

The presence of homologs across all cyanobacterial morphotypes serves as a hint for universal protein function while a restricted distribution in specific subsections or morphotypes indicates a functional specialization within the respective taxon. An example for such species-specific candidate in our list is *slr7083* that is encoded on the pSYSA toxin-antitoxin plasmid in *Synechocystis*, similarly to *parM* and *tubZ*, which mediate plasmid segregation (Larsen *et al.*, 2007; Bharat *et al.*, 2015). In contrast, the homologous proteins Synpcc7942_1139 (abbreviated Syc1139) and Slr1301 are highly conserved and have homologs among all cyanobacterial groups (Fig. 1), including CypS from *Anabaena*, which we previously identified as a filament-forming CCRP (Springstein *et al.*, 2019). As our candidate CCRPs annotated as hypothetical proteins, we initially verified the transcription of the respective genes by RT-PCR from cDNA (Supplementary Fig. 1A-D). Our results showed that *slr7083* was only weakly transcribed during mid-exponential culture growth phase and *all4981* was found to be transcribed in an operon with its upstream genes *all4982* and *all4983* (Supplementary Fig. 1B,C).

Cyanobacterial CCRPs assemble into diverse filamentous structures *in vitro*

A major characteristic of filament-forming proteins is their ability to self-polymerize into filaments intra and extracellularly (Fuchs and Weber, 1994; Köster *et al.*, 2015). Unlike actin and tubulin, IFs are able to form filamentous structures *in vitro* in a nucleotide-independent manner without additional co-factors upon renaturation from a denaturing buffer (Köster *et al.*, 2015). To examine the self-polymerization property of the nine tested CCRPs, we purified His_6-tagged CCRPs under denaturing conditions and subjected them to subsequent renaturation by dialysis. Here we used protein concentrations in a similar range (0.5-1 mg ml^{-1}) to previously investigated proteins shown to form filaments *in vitro* (e.g., Crescentin (Ausmees, Kuhn and Jacobs-Wagner, 2003) and Scc (England *et al.*, 2005), the metabolic enzyme CtpS (Ingerson-Mahar *et al.*, 2010) and the bactofilins BacA, BacB (Kühn *et al.*, 2010) and BacM (Koch, McHugh and Hoiczyk, 2011)). When applicable, the purified proteins were labeled with NHS-Fluorescein and the formation of *in vitro* filaments was assessed by epifluorescence or bright field microscopy. Several candidates did not form discernible structures *in vitro* and were consequently excluded from further investigation (including Slr6096, Tlr0420 and Fm6009; Supplementary Fig. 2A). The remaining CCRPs assembled into highly diverse structures *in vitro* (Fig. 2). Direct dialysis of Fm7001 from a high urea-containing buffer to a physiological buffer led to protein precipitation. However, upon slow stepwise renaturation (removing 0.5 M every 2 h), Fm7001 polymerized into a flat two-dimensional sheet floating on top of the dialysate in 4,5 M urea (Supplementary Fig. 2D). We addressed the eventuality that these structures could be the product of crystalized urea, but control experiments did not reveal filaments. Polymerized Fm7001 revealed two-dimensional filamentous sheets as well as single filamentous fibers (Fig. 2). Similar structures were observed for purified Fm7001-GFP and MBP-Fm7001-His_6 (Supplementary Fig 2E,F). A two-dimensional filamentation pattern was observed also for Slr7083, which formed single, long and straight filamentous strings that were interconnected by two-dimensional sheets, thereby producing an irregular net (Fig. 2). Similarly, All4981 assembled into an interconnected filamentous net with thin single filaments (Fig. 2). The heterologous expression of Syc2039-His_6 in *E. coli* failed, but we successfully

purified Syc2039-GFP-His_6 from *Synechococcus* instead. The polymerization pattern of Syc2039-GFP-His_6 revealed sphere or cell shape-like three-dimensional sheets (Fig. 2). However, we note that most of the protein precipitated upon renaturation, hence it is unlikely that Syc2039 has *in vitro* polymerizing properties. Syc1139 polymerized into similar cell shape-like three-dimensional sheets but without any detectable aggregates (Fig. 2). The resemblance between Syc2039 and Syc1139 sheets raised the possibility that the sheet-like structures observed in the Syc2039-GFP-His_6 sample represented co-precipitated and polymerized Syc1139. In accordance with this suggestion, we identified direct interactions of Syc1139 and Syc2039 using the bacterial adenylate cyclase two-hybrid (BACTH) assays (Supplementary Fig. 3A). For Slr1301, no clear *in vitro* structures were observed (Fig. 2). Nonetheless, we included this protein in further analyses since its homolog in *Anabaena* (CypS) has been recently reported as a filament-forming protein (Springstein *et al.*, 2019). Notably, Crescentin, which we used as a positive control, polymerized into smooth and filigree filaments only in the presence of monovalent ions (i.e. NaCl; Supplementary Fig. 2B). This observation highlights the importance of suitable buffer conditions for the detection of filament-forming proteins. To further confirm our *in vitro* observations, we included the monomeric and highly soluble maltose binding protein (MBP) as well as the oligomeric proteins GroEL1.2 (from *Chlorogloeopsis fritschii* PCC 6912; (Weissenbach *et al.*, 2017)) and the UMP kinase (from *Anabaena*) as negative controls. While both, the MBP and the UMP kinase readily clumped into comparably small aggregates, GroEL1.2 formed large proteinaceous aggregates *in vitro*, likely as a result of uncoordinated multimerization (Supplementary Fig. 2C). Consequently, we conclude that the *in vitro* filaments of the cyanobacterial CCRPs we observed here are unlikely to be oligomerization artifacts. We further validated the self-binding properties of the remaining six CCRPs using the BACTH assay and found that all proteins are able to self-interact (Supplementary Fig. 3A).

Putative filament-forming proteins form filaments *in vivo*

To investigate whether the genetic background influences the filamentation properties of the candidate proteins, we expressed GFP or YFP translational fusion constructs of the putative filament-forming CCRPs in multiple hosts: 1) *E. coli*, 2) their native cyanobacterium and 3) in cyanobacteria of a different morphotype or subsection. Gene expression was driven by inducible or constitutive promoters commonly used in cyanobacteria. These included P_{cpc560} (for *Synechocystis*) (Zhou *et al.*, 2014), P_{trc} (for *E. coli*, *Synechocystis* and *Synechococcus*) (Huang *et al.*, 2010) or P_{petE} (for *Anabaena* and *Fischerella*) (Buikema and Haselkorn, 2001). As a positive control for *in vivo* filamentation, we expressed Crescentin-GFP in *Anabaena*, which formed round and helical filaments in the cells, thereby showing that P_{petE} is suitable for studying filament-forming IF-like CCRPs in *Anabaena*. (Supplementary Fig. 4A).

Fm7001 forms protein filaments *in vivo* independent of the host

The *in vivo* localization of Fm7001 in *Fischerella* showed different results depending on the tag orientation. Only the expression of N-terminal YFP fusions of Fm7001 resulted in filamentous structures (Fig. 3 and Supplementary Fig. 4B). In *Synechocystis*, YFP-Fm7001 formed filaments throughout the cell (Fig. 3A) while in *Anabaena* we observed septum-arising filamentous strings (Fig. 3B). In its host, *Fischerella*, YFP-Fm7001 only rarely assembled into short filamentous strings (Fig. 3C inlays). Despite of the low abundance of filaments in *Fischerella*, induction of heterologous expression of YFP-Fm7001 induced an altered cell phenotype and trichomes seemingly divided in more than one plane resulting in a multiseriate (more than one trichome in a row) phenotype characteristic of *C. fritschii*. While under non-inducing conditions (i.e. in the absence of copper), *Fischerella* cells carrying a plasmid that expresses YFP-Fm7001 from P_{petE} had a WT phenotype, an altered morphotype and multiseriate growth was observed after around 4 rounds of replication (i.e. after 7 d) under inducing conditions (Fig. 3C). We also observed that, although expressed from a non-native promoter, YFP-Fm7001 was initially localized at branching points (Fig. 3C, 19 h after induction). Those effects suggest that Fm7001 may be involved in cell shape control and in

the true-branching phenotype of *Fischerella*. Our attempts to generate a *Fischerella* Δ*fm7001* mutant strain remained unsuccessful, hence the function of Fm7001 remains unknown.

Slr7083 and Slr1301 are involved in twitching motility in *Synechocystis*

The *in vivo* localization of Slr7083-GFP in *Synechocystis* showed that it was localized to the cell periphery as well as rare focal spots and S-shaped filaments (Fig. 4A). We also attempted to localize Slr7083-GFP in the motile *Synechocystis* PCC-M substrain (hereafter PCC-M) but never obtained any successfully transformed clone, suggesting that overrepresentation of Slr7083 is deleterious for this strain. The localization of Slr1301-YFP in *Synechocystis* and PCC-M was at indistinct peripheral sites as assemblies of crescent-like shapes and rarely as S-shaped filaments (Fig. 4A and Supplementary Fig. 4C). Similar structures have been previously reported for the pilus ATPase PilB (Schuergers *et al.*, 2015). The localization of Slr7083-GFP and YFP-Slr7083 in *Anabaena* was at the cell periphery (Supplementary Fig. 4D). Furthermore, extended expression of YFP-Slr7083 in *Anabaena* altered the cellular morphology and disturbed the linear *Anabaena* trichome growth pattern (Supplementary Fig. 4E). In *E. coli*, Slr7083-GFP localized next to the cell poles (Supplementary Fig. 1E). When expressed in *E. coli*, Slr1301-GFP revealed a similar polar localization (Supplementary Fig. 1E). Additionally, reminiscent of Slr7083, the heterologous expression of Slr1301-YFP in *Anabaena* had an effect on the *Anabaena* cell-shape where it localized at the periphery and also formed single filaments or thick filamentous bundles that seemingly traversed through several cells (Supplementary Fig. 4C). To further assess the role of Slr1301 and Slr7083 in *Synechocystis* motility, we generated *Synechocystis* and PCC-M Δ*slr7083* and Δ*slr1301* mutant strains. The *Synechocystis* Δ*slr7083* and Δ*slr1301* mutants revealed no phenotypic defects compared to the WT (Fig. 4B,C). In contrast, the PCC-M Δ*slr7083* mutant is characterized by a decrease in twitching motility and a defect in cytokinesis (Fig. 4B). PCC-M Δ*slr7083* mutant cells often lacked internal chlorophyll signal entirely and failed to properly divide internal thylakoid membrane (assessed by the lack of chlorophyll autofluorescence) during cell division (Fig. 4B). Similarly, the PCC-M Δ*slr1301* mutant lost its twitching motility

(Fig. 4B; confirming previous results from Bhaya, Takahashi, Shahi, & Arthur (2001)). Attempts to complement the motility defect in the PCC-M Δ*slr1301* mutant by expressing Slr1301-YFP from the conjugation plasmid pRL153 failed, possibly as a result of the comparably high expression of Slr1301-YFP from P_{trc} (we note that P_{trc} cannot be regulated by IPTG in *Synechocystis*). Additional attempts to complement the PCC-M Δ*slr7083* mutant never resulted in exconjugants. In order to further explore how Slr1301 affects motility, we analyzed co-precipitated proteins of Slr1301-YFP expressed in *Synechocystis* by mass spectrometry. This revealed multiple putative interaction partners involved in motility, including a twitching motility protein (Slr0161), two methyl-accepting chemotaxis proteins (McpA and PilJ) and the type IV pilus assembly ATPase PilB (Fig. 4D). The interaction of Slr1301 with PilB, together with their similar *in vivo* localization, prompted us to characterize the interaction of both proteins. For this purpose, we attempted to express PilB-GFP in *Synechocystis* WT, and in the Δ*slr1301* and Δ*slr7083* mutants. In *Synechocystis* WT, PilB-GFP localized to the cell periphery and often formed crescent-like formations (reminiscent of Slr1301-YFP and Slr7083-GFP; Fig. 4A), confirming previous results by Schuergers *et al.* (2015). However, we never observed any PilB-GFP expression in the *Synechocystis* or PCC-M Δ*slr7083* and Δ*slr1301* mutants. The similarity between our observations so far for Slr1301 and Slr7083 led us to test for an interaction between these two proteins. Indeed, a bacterial two-hybrid assay confirmed a direct interaction between Slr7083 and Slr1301 (Fig. 4E). Taken together, our investigation identified two *Synechocystis* CCRPs that are involved in cell motility. Slr7083 is a cell envelope-localized protein involved in cytokinesis and motility. It polymerized into filaments *in vitro* but only few filaments were identified *in vivo*. Slr1301, although failing to assemble into filaments *in vitro*, occasionally polymerized into filaments *in vivo* and was found to be an interaction partner of proteins that function in *Synechocystis* twitching motility.

All4981 is an *Anabaena* TPR protein that forms septal-arising filaments

The expression of All4981-GFP in *Anabaena* revealed numerous filaments that traversed the cell while in other cells All4981-GFP was associated with the cell septa (Fig. 5A). All4981-GFP

316 filaments also occasionally spread in a star-like pattern into the cytosol. Additionally, in freshly
317 ruptured All4981-GFP-expressing cells, filamentous *ex vivo* structures assembled in the
318 medium into an interconnected network (Supplementary Fig. 4F), resembling the *in vitro*
319 polymerization pattern of All4981 (Fig 2). We confirmed a host-independent *in vivo*
320 polymerization capacity of All4981 by expressing All4981-GFP in *Synechocystis*, which lacks
321 homologs to that protein (Fig. 5B). Intrigued by the septal localization, we tested for an
322 interaction with SepJ, a septal junction protein in *Anabaena* (Flores *et al.*, 2007) and found
323 weak, albeit significant physical interactions (Supplementary Fig. 3A). In addition, bacterial
324 two-hybrid assays revealed that All4981 interacted with two other *Anabaena* filament-forming
325 CCRPs, namely LfiA and LfiB (Springstein *et al.*, 2019), and strongly interacted with the cell
326 shape-determining protein MreB (Supplementary Fig. 3A). Notably, MreB has previously been
327 shown to form similar filamentous structures in *Anabaena*. However, in contrast to genes in
328 the *mreBCD* operon, whose overexpression induces abnormal cell morphologies (Hu *et al.*,
329 2007), no direct morphogenic influence was detected for All4981 in *Anabaena*. Notably, it is
330 likely that All4981 is an essential protein in *Anabaena* as we were not able to generate an
331 *all4981* deletion strain. Initially, we accidently also created a YFP-All4981 fusion construct with
332 a deletion of 240 bp between nt 735 and nt 975 of the *all4981* CDS, resulting in a deletion of
333 the third and fourth TPR (YFP-All4981$^{\Delta TPR3-4}$) leaving the remaining ORF intact. Remarkably,
334 this fusion protein, like All4981-GFP, formed cell-traversing filaments in *Anabaena* and
335 sometimes assembled into a filamentous structure within the cells (Supplementary Fig. 4G). In
336 contrast, full length YFP-All4981 localized to the septa between two neighboring cells but also
337 revealed indistinct cytosolic localization (Supplementary Fig. 4G). Co-immunoprecipitation
338 experiments following LC-MS/MS analytics from *Anabaena* WT expressing YFP-All4981$^{\Delta TPR3-}$
339 ^{4} revealed an association of YFP-All4981$^{\Delta TPR3-4}$ with ParB, MinD and MreB (Fig. 5C). Thus,
340 All4981 might be involved in ParA/B/S-driven plasmid or chromosome segregation. The
341 interaction with MreB agrees with the *in vivo* localization of YFP-All4981$^{\Delta TPR3-4}$ in *Anabaena*
342 (Supplementary Fig. 4G) and the results from the bacterial two-hybrid assay (Supplementary
343 Fig. 3A). Further interactions were found with a variety of putative S-layer and prohibitin-like

proteins and with DevH, an essential protein for heterocyst glycolipid layer synthesis. Notably, we never observed All4981 expression in heterocysts, regardless of the fluorescence tag. All4981 also interacted with All4982, a protein encoded directly upstream of *all4981*, but not with All4983, which is encoded upstream of *all4982* (Supplementary Fig. 1C). This observation, together with the common transcript of *all4981* and *all4982* (Supplementary Fig. 1C) argues for a common function of both proteins. Thus, we attempted to localize All4982 with an eCFP tag in *Anabaena* but could not observe a coherent localization pattern. Overall, our results demonstrate that All4981 is connected to other *Anabaena* filament-forming CCRPs, the MreB cytoskeleton, the septal junctions and the protective S-layer. Additionally, All4981 polymerizes *in vitro*, *in vivo* and *ex vivo*, is likely essential for *Anabaena* and is thus accordingly classified as a novel cyanobacterial filament-forming TPR-repeat protein.

***Synechococcus* CCRPs are involved in cytokinesis and colony integrity**

The results of the *in vivo* localization of a functional Syc2039-GFP fusion protein (Supplementary Fig. 5E,F) contrasted the ambiguous *in vitro* polymerization pattern (Fig. 2). Filaments were readily observed in different cyanobacterial hosts, indicating that in Syc2039 self-polymerization is independent of the host (Fig. 6A). Notably, however, Syc2039 formed different structures in each host. In *Anabaena*, filaments were long, curved and intertwined; in *Synechocystis* filaments appeared as spindle-like structures and in *Synechococcus* filaments were long, sometimes helical and often aligned with or in close proximity to the cell envelope (Fig. 6A). A similar helical or cell periphery-aligned localization pattern was also observed in *E. coli* (Supplementary Fig. 1E). In *Synechocystis* and *Synechococcus* Syc1139-GFP localized as spots at the cell periphery, while in *E. coli* it seemingly coated the entire cell envelope (Fig. 6A, Supplementary Fig. 1E). Syc1139-GFP failed to be expressed in *Anabaena*, suggesting that (over-)expression of this protein has a negative impact on that organism. Using double homologous gene replacement, we generated a *Synechococcus* Δ*syc2039* mutant strain and a non-segregated *Synechococcus* Δ*syc1139* mutant strain (Supplementary Fig. 5A-C). The non-segregated nature of the Δ*syc1139* mutant suggests that this gene performs an essential

371 cellular function and cannot be fully deleted. Colony integrity of the Δ*syc2039* mutant was
372 unaltered while the Δ*syc1139* mutant was characterized by apparent changes in colony
373 morphology (Fig. 6B), which were lost upon growth on non-selective plates (Supplementary
374 Fig. 5D). Additionally, both mutants presented an impairment in liquid culture growth: the
375 Δ*syc2039* mutant grew in standard BG11 medium but failed to grow upon addition of several
376 osmotic stressors, whereas the Δ*syc1139* mutant failed to grow in liquid culture entirely (Fig.
377 6C). Spot assays confirmed a decreased viability of the Δ*syc1139* mutant and showed that it
378 is highly sensitive to Proteinase K but unaffected by lysozyme (Supplementary Fig. 6A). These
379 cell wall defects, together with the *in vitro* cell shape-like filamentation pattern suggest that
380 Syc1139 might form a protective and protease-resistant proteinaceous layer below the
381 cytoplasmic membrane. This possibility would also be in concert with the distorted colony
382 morphology of the non-segregated Δ*syc1139* mutant strain. The Δ*syc2039* mutant was
383 unaffected by cell wall and membrane destabilizers (Supplementary Fig. 6B). To investigate
384 the role of these proteins in cell division, we stained intracellular DNA with DAPI and
385 localization of FtsZ was detected by immunofluorescence in *Synechococcus* WT and both
386 mutant strains. A proportion of Δ*syc2039* mutant cells exhibited a segregated DNA distribution
387 either to both cell poles or to just one pole (Fig. 6D). Furthermore, some cells of both mutants
388 lacked any discernible intracellular DNA or perceptible chlorophyll signal and were elongated
389 compared to the WT (Fig. 6D,E). The WT phenotype of the Δ*syc2039* mutant could be rescued
390 by insertion of P_{trc}::*syc2039-gfp* or $P_{syc2039}$::*syc2039* into the neutral NS1 (Bustos and Golden,
391 1992) locus (Supplementary Fig. 5E,F). Although both mutant cells were elongated compared
392 to WT cells (Fig. 6E), the intracellular localization of FtsZ was unaffected (Supplementary Fig.
393 6C). And despite the defect in cytokinesis, the Δ*syc2039* mutant strain revealed similar liquid
394 culture growth properties as the WT (Supplementary Fig. 6D). Taken together, Syc2039 forms
395 abundant filamentous networks *in vivo* and is involved in cytokinesis or cell cycle control. We
396 could further show that *syc1139* is an essential gene important for cytokinesis, cellular integrity
397 and colony formation, implicating structural functions.

Discussion

Earlier studies suggested that there is likely a broad spectrum of coiled-coil-rich and rod-domain containing proteins with IF-like function in prokaryotes (Bagchi *et al.*, 2008). And indeed, reports on such proteins followed with the discovery of Scy (in *Streptomyces coelicolor*) and several CCRPs from *Helicobacter pylori* (Waidner *et al.*, 2009; Walshaw, Gillespie and Kelemen, 2010; Specht *et al.*, 2011; Holmes *et al.*, 2013). Here we further investigated the presence and function of CCRPs with filament-forming IF-like properties in prokaryotes, by predicting and evaluating CCPRs in cyanobacteria. Our *in vitro* polymerization assay allowed for a rapid detection of protein filaments *in vitro* using fluorescence microscopy thus bypassing the need to investigate filament-formation by laborious electron microscopy procedures. The observed protein filament lengths were in the range of previously described *in vitro* filaments of FtsZ (Camberg, Hoskins and Wickner, 2009) and of the human prion protein in its amyloid form (Bocharova *et al.*, 2005) that were obtained by a similar experimental procedure.

Our results show that Fm7001 assembles into polymers *in vitro* upon renaturation from urea as well as *in vivo,* and that this protein has an impact on cellular and trichome morphology, thereby fulfilling major IF criteria (Köster *et al.*, 2015; Kelemen, 2017). Consequently, we propose that Fm7001 constitutes a novel filament-forming CCRP specific to multicellular, cell-differentiating and branching cyanobacteria. The floating Fm7001 polymer sheet in high molar urea (i.e. 4.5 M urea) indicates an exceptionally high self-association capacity of Fm7001. In comparison, the eukaryotic IF protein Vimentin exists only as tetramers in 5 M urea (Herrmann *et al.*, 1996). *In vivo* localization experiments revealed an essential role of the Fm7001 C-terminus for filamentation, which is a common observation for known prokaryotic filament-forming proteins, including MreB (Swulius and Jensen, 2012), Crescentin (Ausmees, Kuhn and Jacobs-Wagner, 2003) as well as eukaryotic IF proteins (Geisler and Weber, 1982; Weber and Geisler, 1982; Traub and Vorgias, 1983; Nakamura *et al.*, 1993; Herrmann *et al.*, 1996). Additionally, the assigned structural similarities of Fm7001 with the acetyl-CoA-carboxylase may provide further support for the theory that filament-forming proteins originated from

metabolic enzymes that obtained polymerization features (Ingerson-Mahar and Gitai, 2012). Notwithstanding, the metabolic activity of Fm7001 was not evaluated in our study hence its presumed enzymatic activity remains to be tested. Additionally, so far, no sufficient genome modification systems exist for *Fischerella* (Stucken *et al.*, 2012; Stucken, Koch and Dagan, 2013), as such a precise analysis of the function of Fm7001 is currently not possible.

Several prokaryotic tubulin-like and actin-like cytoskeletal proteins, such as ParM and TubZ, are known to be encoded on plasmids or on bacteriophages (Hurme *et al.*, 1994; Wagstaff and Löwe, 2018). In *Synechocystis*, *slr7083* is encoded on the large toxin-antitoxin defense plasmid (pSYSA) (Kopfmann and Hess, 2013), thus it adds another protein to the list of those filament-forming CCRPs carried by an autonomously replicating genetic element. Preliminarily we suspected that Slr7083 has a role in plasmid-segregation similar to ParM. However, Slr7083 showed no indications of dynamic properties, which would be indispensable for a plasmid segregation mechanism. Furthermore, unlike ParM (Carballido-Lopez, 2006), Slr7083 did not localize in a spindle-like pattern *in vivo* and was only expressed at later growth phases, which is contradictory to a possible involvement in the cell cycle. In contrast, the polymers formed by Slr7083 *in vitro* and *in vivo* rather suggest that it could form a proteinaceous layer below the cytoplasmic membrane. Notably, Slr7083 *in vitro* structures resemble the nuclear lamina formed by nuclear lamins and FilP lace-like *in vitro* filaments (Stuurman, Heins and Aebi, 1998; Bagchi *et al.*, 2008; Fuchino *et al.*, 2013). It is thus conceivable that Slr7083 has a role in cellular stiffness as well as rigidity and mediates mechanical cell stabilization. However, restriction of transcription to only a comparably short period of the culture growth phase challenges the idea of a cell-stabilizing function for Slr7083. In contrast, cell motility in *Synechocystis* seems to be partially regulated by Slr7083, reminiscent of the role of the actin cytoskeleton in eukaryotes.

The role of Slr7083 in cell motility is possibly mediated by means of its interaction with Slr1301, which has already previously been shown to be essential for twitching motility in *Synechocystis* (Bhaya *et al.*, 2001). So far it is unknown how photoreceptors transduce the

perceived light stimuli to the motility apparatus in *Synechocystis* ultimately resulting in phototactic movements (Schuergers, Mullineaux and Wilde, 2017). It is tenable to hypothesize that Slr1301 might constitute the missing link between the two systems, possibly in combination with Slr7083. This hypothesis is supported by the physical interaction of Slr1301 with PilB and the *in vivo* localization of Slr1301 that is similar to that observed for PilB (Schuergers *et al.*, 2015). A comparable complex was observed in *Pseudomonas aeruginosa*, where FimL (a proposed scaffolding protein with a weakly predicted coiled-coil) was shown to connect the chemosensory receptor system to the type IV pili apparatus, regulating the chemotactic and virulence pathways (Inclan *et al.*, 2016). In eukaryotes, cellular motility is strongly dependent on cytoskeletal proteins (Cappuccinelli, 1980), thus it is possible that filament-forming proteins are also key factors for cell locomotion in prokaryotes. Although IFs do not directly participate in cell motility in eukaryotes (Lodish *et al.*, 2000), an adaptation of filament-forming CCRPs in prokaryotes for this task is conceivable. Bactofilins constitute a separate class of prokaryotic-specific polymerizing proteins and were proposed to be involved in coordinated motility in *C. crescentus* (Kühn *et al.*, 2010). Additionally, the filament-forming CCRP AglZ from *Myxococcus xanthus* was previously shown to govern gliding motility together with a multi-protein complex that also involves the MreB cytoskeleton (Yang *et al.*, 2004; Nan *et al.*, 2010). The interaction of Slr1301 with twitching motility proteins was prevailed in the non-motile *Synechocystis* strain, hinting for additional beneficial functions of this interaction besides motility. Notably, we previously reported filament-forming properties for Alr0931 (CypS), which is a homolog of Slr1301 in *Anabaena* (Springstein *et al.*, 2019). While CypS polymerizes into filaments *in vitro*, Slr1301 does not, which could indicate a specific adaptation of CypS to filament-formation in multicellular cyanobacteria. Despite their different cellular functions and *in vitro* polymerization properties, the homologous proteins Slr1301, Syc1139 and CypS retained the ability to cross-interact (Supplementary Fig. 3A). Further studies may focus on identifying the protein domains that mediate this interaction, likely residing within the highly conserved amino acid sequence region in this homologous protein family

(Supplementary Fig. 3B). These regions are likely important for an interaction with species-specific proteins that lead to their species-specific cellular function.

TPR proteins are known to mediate protein-protein interactions and can assemble into multimers, but their ability to polymerize into filaments has not been described so far (Blatch and Lässle, 1999). Nonetheless, All4981 polymerizes *in vitro* and *in vivo* in all tested hosts. Additionally, it forms extracellular filaments and is presumably an essential protein in *Anabaena*. These observations suggest that All4981 is a *bona fide* prokaryotic filament-forming TPR protein. The association of All4981 with MreB, FtsZ-regulators, the S-layer and SepJ indicates that it might function as a bridge that connects the shape-determinants outside of the cell wall and inside of the cytoplasmic membrane to the sites of cell-cell connections (i.e. septal junctions). A function of All4981 in *Anabaena* cell and filament shape is also supported by its interaction with the *Anabaena* filament and cell shape stabilizing proteins LfiA and LfiB (Springstein *et al.*, 2019).

Considering the presence of an N-terminal transmembrane domain and the lack of clear *in vitro* filaments, it is unlikely that Syc2039 constitutes a genuine filament-forming protein. Nonetheless, the highly abundant filamentous network formed in all tested bacterial hosts suggests that Syc2039 is associated with cytoskeletal structures. Specifically, the elongated phenotype and the disturbed cytokinesis in the *Synechococcus* Δ*syc2039* mutant and the non-segregated Δ*syc1139* mutant suggest an association with the FtsZ-driven elongasome. Direct interaction with FtsZ or MreB could not be shown, as such, future studies will likely attempt to unravel the presumed connection of the *Synechococcus* CCRPs to those two major cytoskeletal systems. Notably, besides its cytokinetic defect, the Δ*syc2039* mutant showed growth characteristics like the WT, suggesting that feedback mechanisms between cytokinesis and cell division are disturbed in the Δ*syc2039* mutant.

Our results reveal two novel filament-forming CCRPs - Fm7001 and All4981 - from different cyanobacterial subsections and morphotypes (Fig. 7). Our study thus extends the spectrum of known filament-forming CCRPs in prokaryotes and expands the set of functional

properties associated with IF-like proteins in prokaryotes. Notably, as indicated by Bagchi *et al*. (2008), we demonstrate that the sole observation of coiled-coil-rich regions within a protein sequence cannot be regarded as a sole predictor of protein polymerization, hence identification of novel filament-forming proteins requires additional *in vitro* and *in vivo* assays. The cyanobacterial CCRPs we report here, like other bacterial CCRPs (Ausmees, Kuhn and Jacobs-Wagner, 2003; Bagchi *et al.*, 2008; Waidner *et al.*, 2009; Fiuza *et al.*, 2010; Specht *et al.*, 2011; Holmes *et al.*, 2013) and eukaryotic IFs (Alberts *et al.*, 2014) are essential cellular components (All4981), are important for cell shape determination (Fm7001, Syc1139 and Syc2039), mediate cellular motility (Slr7083 and Slr1301), DNA segregation (Syc1139 and Syc2039) and colony integrity (Syc1139). Our study thus strengthens the perception that like eukaryotes, prokaryotes require organized internal complexes and even microcompartments to maintain cell shape, size and proper cell function and highlights the usefulness of polymerized proteinaceous structures for cellular processes. Remarkably, some of the identified CCRPs were highly conserved among all cyanobacterial morphotypes, suggesting that their function is conserved. Future studies are required in order to evaluate the functional conservation of homologous proteins in different cyanobacterial species and morphotypes. On the other hand, Syc2039 and Slr7083 are highly strain specific, possibly performing a function that is adapted to the very needs of their hosts. Similarly to the eukaryotic cytolinker proteins (Leung, Green and Liem, 2002; Wiche, Osmanagic-Myers and Castañón, 2015), cyanobacterial CCRPs were often associated with other cytoskeletal systems (MreB, FtsZ and other filament-forming CCRPs) and sites of cell-cell connections (i.e. SepJ), which demonstrates the necessity for those structures to be in a constant interplay even in comparably small cells. The discovery of filament-forming CCRPs with different levels of conservation in various cyanobacterial morphotypes thus opens up new avenues of research on their contribution to cyanobacterial morphological diversity.

Material and Methods

Data and CCRP prediction

The cyanobacteria protein families were constructed from completely sequenced genomes available in RefSeq database (O'Leary *et al.*, 2015) (ver. May 2016; Supplementary File 2). For the construction of protein families, at the first stage, all protein sequences annotated in the genomes were blasted all-against-all using stand-alone BLAST (Altschul *et al.*, 1990) (V. 2.2.26). Protein sequence pairs that were found as reciprocal best BLAST hits (rBBHs; Tatusov, Koonin and Lipman, 1997) with a threshold of E-value ≤ $1x10^{-5}$ were further compared by global alignment using needle (EMBOSS package, V. 6.6.0.0; (Rice, Longden and Bleasby, 2000). Sequence pairs having ≥30% identical amino acids were clustered into protein families using the Markov clustering algorithm (MCL) (Enright, Van Dongen and Ouzounis, 2002) (ver. 12-135) with the default parameters. For the CCRPs prediction, 1,535 protein sequences containing non-standard amino acids were discarded. Coiled-coil regions in protein sequences were predicted using PEPCOIL (EMBOSS package, V. 6.6.0.0; (Rice, Longden and Bleasby, 2000). The algorithm was executed with a window size of 21 and the threshold for amino acids in coiled-coil conformation was set to ≥ 80 amino acid residues similarly as described by Bagchi *et al.* (2008). Statistical tests were performed with MatLab©. For the comparison of CCRPs proportion, the compared groups included: 1) SynProCya group, 2) unicellular cyanobacteria, 3) unicellular cyanobacteria that divide in more than one plane, and 4) multicellular cyanobacteria. Identification of conserved amino acid domains within cyanobacterial CCRP homologs (CypS (Alr0931), Slr1301 and Syc1139) was done using MULTALIGN (Corpet, 1988).

Protein candidates were further manually examined with online available bioinformatic tools (NCBI Conserved Domain (CD) Search (Marchler-Bauer *et al.*, 2016), TMHMM Server (Krogh *et al.*, 2001) (V. 2.0), PSIPRED (McGuffin, Bryson and Jones, 2000), PSORTb (Yu *et al.*, 2010) (ver. 3.0), I-TASSER (Zhang, 2009). CCRPs exhibiting similar predictions to known

IF and IF-like proteins like CreS, FilP, vimentin, desmin or keratin were selected, and proteins predicted to be involved in other cellular processes were excluded.

Bacterial strains and growth conditions

Fischerella, *Anabaena* and *Synechocystis* were obtained from the Pasteur Culture Collection (PCC) of cyanobacteria (France). *Synechococcus* was a gift from Martin Hagemann (University Rostock). Glucose-tolerant motile *Synechocystis* PCC-M substrain was a gift from Annegret Wilde (University Freiburg). Cells were grown photoautotropically in BG11 or without combined nitrogen ($BG11_0$) at a 16h/8h light/dark regime (*Fischerella*) or at constant light (*Anabaena*, *Synechococcus* and *Synechocystis*) with a light intensity of 20 µmol m^{-2} s^{-1}. When appropriate, 50 µg ml^{-1} kanamycin (Km), 2.5 µg ml^{-1} spectinomycin (Sp), 2.5 µg ml^{-1} streptomycin (Sm) or 30 µg ml^{-1} neomycin (Nm) was added. Non-segregated Δ*syc1139* cells were always grown in the presence of Km. *E. coli* strains DH5α, DH5αMCR, XL1-blue and HB101 were used for cloning and conjugation by triparental mating. BTH101 was used for BACTH assays and BL21 (DE3) was used for expression of His- and GFP-tagged proteins in *E. coli*. All *E. coli* strains (Supplementary Table 2) were grown in LB medium containing the appropriate antibiotics at standard concentrations.

Plasmid and strain construction

All plasmids employed in this study were either generated by using standard restriction enzyme-base cloning procedures or using Gibson assembly (Gibson *et al.*, 2009). A detailed description of the cloning strategies for the respective plasmids is available upon request from the authors. All primers, plasmids and strains employed or generated in this study are listed in Supplementary Tables 2-5. GFP, YFP and eCFP protein tags were used as reporter proteins and His_6 tag was used for protein affinity purification. For gene replacement mutants, homologous flanks for double homologous recombination comprised 1000 bp upstream and downstream of the gene of interest. Mutant strains harboring gene replacements with antibiotic resistance cassettes (*nptII* or *CS.3*; Beck *et al.*, 1982; Sandvang, 1999) were verified by colony

PCR testing for absence of gene of interest using primers #129/#130 for Δ*slr7083*, primers #168/#169 for Δ*slr1301*, primers #146/#147 for Δ*syc2039* or primers #161/#162 for Δ*syc1139*. We also attempted to generate gene replacement mutants for *all4981* and *fm7001* but remained unsuccessful.

Transformation of cyanobacteria

Transformation of *Synechococcus* was achieved by natural transformation as described by Ivleva *et al.* (2005) and transformation of *Synechocystis* was accomplished by natural transformation as described by Vermaas *et al.* (2002) or by conjugation as described by Ungerer and Pakrasi (2016). *Anabaena* and *Fischerella* were transformed by conjugation as described by Ungerer and Pakrasi (2016) or Stucken *et al.* (2012), respectively. Ex-conjugant colonies from *Synechococcus* and *Synechocystis* carrying gene replacements were re-streaked three to four times and absence of genes of interest was verified by colony PCR. Transformation of sonicated (fragmented) and NaCl-treated *Fischerella* cells followed by the conjugational method described by Ungerer and Pakrasi (2016) was also feasible for *Fischerella*, albeit with a lower transformation frequency.

Phenotypic characterization of the mutant strains

Defects in cell viability were evaluated by spot assays adapted from Dörrich *et al.* (2014). Wild type and mutant strains from liquid cultures or BG11 plates were adjusted to an OD_{750} of about 0.4 in liquid BG11 liquid. Next, 5 µl of cells were spotted in triplicates onto BG11 plates or BG11 plates supplemented with Proteinase K or lysozyme at indicated concentrations in 10-fold serial dilutions and incubated under standard growth conditions until no further colonies arose in the highest dilution.

Growth defects were assessed with growth curves. For this, cells were grown in liquid BG11 medium, washed three times by centrifugation (6500 x *g*, RT, 3 min) in BG11, adjusted to an OD_{750} of 0.1 and then grown in triplicates or quadruples at standard growth conditions in 15 ml culture volumes. OD_{750} values were recorded every 24 h.

Cell length of *Synechococcus* WT, mutant strains and mutant complementation strains was measured using the line tool from the imaging software Fiji.

Cell wall integrity defects were evaluated by testing the influence of osmotic factors on cell growth. *Synechococcus* WT and mutant strains were grown on BG11 agar plates, transferred to BG11 liquid medium and grown under standard growth conditions with or without 5 mM glucose, 200 mM glucose, 2 mM NH_4Cl, 200 mM maltose or 500 mM NaCl.

To evaluate the motility of *Synechocystis* and PCC-M WT and mutant strains, three single colonies of the respective strain were streaked on a line on a BG11 growth plate. Growth plates were then placed into the standard culture incubator for 10 d with with illumination limited from one direction.

Protein purification and *in vitro* filamentation assays

C-terminally His_6-tagged proteins were expressed and subsequently purified under denaturing conditions using Ni-NTA affinity columns as previously described by Springstein *et al.* (2019). For expression of MBP-Fm7001-His_6, DH5α cells carrying pMAL-c2x-Fm7001-His_6 were grown and induced accordingly but in the presence of 0.2% glucose. Purified proteins were dialyzed overnight against polymerization buffer (PLB: 50 mM PIPES, 100 mM KCl, pH 7.0; HLB: 25 mM HEPES, 150 mM NaCl, pH 7.4) at 18 °C and 180 rpm with three bath changes using a Slide-A-Lyzer™ MINI Dialysis Device (10K MWCO, 0.5 ml or 2 ml; Thermo Fischer Scientific). Purified proteins were stained with 0.005 mg NHS-Fluorescein (Thermo Fischer Scientific) per 1 ml protein dialysate and *in vitro* filamentation was analyzed by epifluorescence microscopy.

For Fm7001-His_6, proteins were slowly dialyzed against 2 mM Tris-HCl, 4.5 M urea, pH 7.5 (18°C, 200 rpm) decreasing 0.5 M urea every 2 h (from 6 M to 4.5 M urea). The resulting floating filamentous web was then analyzed by bright field microscopy.

Syc2039-His_6 failed to be expressed in *E. coli* BL21 (DE3). To bypass this, Syc2039-GFP-His, under the control of an IPTG-inducible P_{trc}, was inserted into a neutral locus of

Synechococcus. Cells were grown to an OD_{750} of 0.8 and protein expression was induced with 0.05 mM IPTG for 3 d. Induced cells were harvested and washed with PBS by centrifugation (4800 x *g*, 4 °C, 10 min) and stored at -80 °C. Protein purification, dialysis and labeling was then performed as described above with the exception that BG11 growth medium was used as dialysate.

Co-immunoprecipitation

For co-immunoprecipitations of fluorescently tagged CCRP candidates, cyanobacterial strains expressing YFP-All4981 or Slr1301-YFP were grown in BG11 or $BG11_0$ liquid medium. Co-immunoprecipitation was performed using the µMACS GFP isolation kit (Miltenyl Biotec) as previously described by Springstein *et al.* (2019) using PBS-N (PBS supplemented with 1% NP-40) or HSLB (50 mM NaH_2PO_4, 500 mM NaCl, 1% NP-40, pH 7.4) lysis buffers supplemented with a protease inhibitor cocktail (cOmplete™, EDTA-free Protease Inhibitor Cocktail, Sigma-Aldrich). Proteins were identified by mass spectrometry as previously described by Springstein *et al.* (2019) for YFP-All4981 or by Kahnt *et al.* (2007) for Slr1301-YFP.

Immunofluorescence

The localization of FtsZ in *Synechococcus* WT and mutant strains was evaluated by immunofluorescence using a modified protocol from Heinz *et al.* (2016). In contrast, cells were lysed in 50 mM Tris-HCl pH 7.4, 10 mM EDTA and 0.2 mg ml^{-1} lysozyme for 30 min at 37 °C and samples were blocked in 1x Roti®-ImmunoBlock (Carl Roth) in PBS supplemented with 0.05% Tween 20. Samples were incubated with rabbit anti-FtsZ primary antibody (Agrisera; raised against *Anabaena* FtsZ; 1:250 diluted) in blocking buffer followed by incubation with 7.5 µg ml^{-1} Alexa Fluor 488-conjugated goat anti-rabbit IgG (H+L) secondary antibody (Thermo Fischer Scientific) in blocking buffer. Before microscopy, cells were stained with 10 µg ml^{-1} DAPI (final concentration) in PBS.

660 Brightfield and fluorescence microscopy analysis

661 Bacterial strains grown in liquid culture were either directly applied to a microscope slide or
662 previously immobilized on a 2% low-melting agarose in PBS agarose pad and air dried before
663 microscopic analysis. Epifluorescence microscopy was performed using an Axio Imager.M2
664 light microscope (Carl Zeiss) equipped with Plan-Apochromat 63x/1.40 Oil M27 objective and
665 the AxioCam MR R3 imaging device (Carl Zeiss). GFP, Alexa Fluor 488, eCFP and YFP
666 fluorescence was visualized using filter set 38 (Carl Zeiss; excitation: 470/40 nm band pass
667 (BP) filter; emission: 525/50 nm BP). Chlorophyll auto-fluorescence was recorded using filter
668 set 15 (Carl Zeiss; excitation: 546/12 nm BP; emission: 590 nm long pass). When applicable,
669 cells were previously incubated in the dark at RT for about 5 min with 10 µg ml^{-1} DAPI in PBS
670 to stain intracellular DNA. For visualization of DAPI fluorescence filter set 49 (Carl Zeiss;
671 excitation: G 365 nm; emission: 455/50 nm) was employed. *E. coli* BL21 (DE3) cells expressing
672 C-terminally GFP-tagged protein candidates were grown over night in LB and then diluted 1:40
673 in the same medium the following day. Cells were grown for 2 h at 37 °C, briefly acclimated to
674 20 °C for 10 min and induced with 0.05 mM IPTG at 20 °C. Protein localization of GFP/YFP-
675 tagged proteins was then observed after indicated time points of cells immobilized on an
676 agarose pad.

677 Statistical analysis

678 Beta-galactosidase values were measured in triplicates from three independent colonies and
679 significant differences compared to WT were determined by a one-way ANOVA using
680 Dunnett's multiple comparison test. For statistical evaluation of *Synechococcus* WT and
681 mutant cell length, a one-way ANOVA using Turkey's multiple comparison test was used.
682 Significance levels are the same as for the beta-galactosidase assay. Statistical tests were
683 performed with the GraphPad Prims 8.0.0 software. Significance levels are indicated by stars
684 (*) and correspond to: *: $P < 0.05$, **: $P < 0.01$, ***: $P < 0.001$, ****: $P < 0.0001$.

685 RNA isolation and RT-PCR

686 Total RNA was isolated from 10 ml culture using either the Direct-zol™ RNA MiniPrep Kit
687 (Zymo Research; *Synechocystis*, *Synechococcus* and *Anabaena*) according to the
688 manufacturer's instructions or the Plant RNA Reagent (Thermo Fischer Scientific; *Anabaena*,
689 *Fischerella* and *Synechocystis*). For RNA isolation using the Plant RNA Reagent, a modified
690 protocol was employed. To this end, cells were pelleted by centrifugation (4800 x *g*, 10 min, 4
691 °C) and the supernatant was discarded. The pellet was resuspended in 0.5 ml of Plant RNA
692 Reagent und lysed in a Precellys® 24 homogenizer (Bertin) with 3 strokes at 6500 rpm for 30
693 s in 2 ml soil grinding (SK38) or tough microorganism (VK05) lysis tubes (Bertin). RNA was
694 then isolated according to the manufacturer's instructions. Isolated RNA was treated with DNA-
695 free™ Kit (2 units rDNAs/reaction; Thermo Fischer Scientific) and 1 µg (*Fischerella*,
696 *Synechocystis* and *Synechococcus*) or 200 ng (*Anabaena*) RNA was reverse transcribed using
697 the Maxima™ H Minus cDNA Synthesis Master Mix (with dsDNase; Thermo Fischer Scientific,
698 for *Fischerella*, *Synechocystis* and *Synechococcus*) or the qScript™ cDNA Synthesis Kit
699 (Quanta Biosciences, for *Anabaena*). RT-PCR of cDNA samples for *fm7001*, *ftsZ*, *slr7083*,
700 *rnpB*, *slr1301*, *syc2039*, *syc1139*, *all4981*, *all4981+all4982* and *all4981+all4983* was done
701 using primer pairs #1/#2, #3/#4, #5/#6, #7/#8, #9/#10, #11/#12, #13/#14, #15/#16, #17/#15
702 and #18/#15, respectively.

703 Bacterial two hybrid assays

704 In this study, the BACTH system (Euromedex) was employed. Gene candidates were cloned
705 into the expression vectors pKNT25, pKT25, pUT18 and pUT18C by GIBSON assembly,
706 thereby generating C and N-terminal translational fusions to the T25 or T18 subunit.
707 Chemically competent *E. coli* BTH101 (Δ*cya*) cells were co-transformed with 5 ng of the
708 indicated plasmids, plated onto LB plates supplemented with 200 µg ml^{-1} X-gal, 0.5 mM IPTG,
709 Amp, Km and grown at 30 °C for 24-36 h. Interactions were quantified by beta-galactosidase
710 assays from three colonies for each combination according to the protocol described by
711 Euromedex or in a 96 well format according to Karimova, Davi and Ladant (2012). For this aim,

712 cultures were either grown over night at 30 °C or for 2 d at 20 °C in LB Amp, Km, 0.5 mM IPTG
713 and interaction strength of the investigated proteins was by quantified by beta-galactosidase-
714 mediated hydrolyzation of ONPG (ortho-Nitrophenyl-β-galactoside), which is then recorded in
715 Miller units (Miller, 1992).

716

717 **Acknowledgements**

718 We thank Katrin Schumann, Myriam Barz, Lisa Stuckenschneider, Lisa-Marie Philipp and
719 Marius Lasse Theune for their assistance in the experimental work. Furthermore, we thank
720 Martin Thanbichler and Daniela Kiekebusch (both from Philipps University, Marburg, Germany)
721 for their support with mass spectrometry analysis. The study was supported by the German
722 science foundation (DFG) (Grant No. STU513/2-1 awarded to KS).

723 **Author contribution**

724 BLS and KS designed the study. BLS established and performed the experimental work with
725 contributions from JW. CW and TD performed the comparative genomics analysis. AOH
726 analyzed protein samples by mass spectrometry. BLS, TD and KS drafted the manuscript with
727 contributions from all coauthors.

References

Alberts, B. *et al.* (2014) *Molecular Biology of the Cell*. 6th editio. Garland Science.

Altschul, S. F. *et al.* (1990) 'Basic local alignment search tool', *Journal of Molecular Biology*. Academic Press, 215(3), pp. 403–410. doi: 10.1016/S0022-2836(05)80360-2.

Ausmees, N., Kuhn, J. R. and Jacobs-Wagner, C. (2003) 'The bacterial cytoskeleton: An intermediate filament-like function in cell shape', *Cell*, pp. 705–713. doi: 10.1016/S0092-8674(03)00935-8.

Bagchi, S. *et al.* (2008) 'Intermediate filament-like proteins in bacteria and a cytoskeletal function in Streptomyces', *Molecular Microbiology*, 70(4), pp. 1037–1050. doi: 10.1111/j.1365-2958.2008.06473.x.

Beck, E. *et al.* (1982) 'Nucleotide sequence and exact localization of the neomycin phosphotransferase gene from transposon Tn5', *Gene*, 19(3), pp. 327–336. doi: 10.1016/0378-1119(82)90023-3.

Bharat, T. A. M. *et al.* (2015) 'Structures of actin-like ParM filaments show architecture of plasmid-segregating spindles', *Nature*. Nature Publishing Group, a division of Macmillan Publishers Limited. All Rights Reserved., 523, p. 106. Available at: https://doi.org/10.1038/nature14356.

Bhaya, D. *et al.* (2001) 'Novel Motility Mutants of Synechocystis Strain PCC 6803 Generated by In Vitro Transposon Mutagenesis Novel Motility Mutants of Synechocystis Strain PCC 6803 Generated by In Vitro Transposon Mutagenesis †', *Journal of Bacteriology*, 183(20), pp. 1–5. doi: 10.1128/JB.183.20.6140.

Bi, E. and Lutkenhaus, J. (1991) 'FtsZ ring structure associated with division in Escherichia coli', *Nature*, 354(6349), pp. 161–164. doi: 10.1038/354161a0.

Blatch, G. L. and Lässle, M. (1999) 'The tetratricopeptide repeat: A structural motif mediating protein-protein interactions', *BioEssays*, 21(11), pp. 932–939. doi: 10.1002/(SICI)1521-

753 1878(199911)21:11<932::AID-BIES5>3.0.CO;2-N.

754 Bocharova, O. V. *et al.* (2005) 'In vitro conversion of full-length mammalian prion protein
755 produces amyloid form with physical properties of PrPSc', *Journal of Molecular Biology*,
756 346(2), pp. 645–659. doi: 10.1016/j.jmb.2004.11.068.

757 Boyer, H. and Roulland-Dessoix, D. (1969) 'A complementation analysis of the restrcition and
758 modification of DNA in Escherichia coli.', *J. Mol. Biol.*, 41, pp. 459–472.

759 Buikema, W. J. and Haselkorn, R. (2001) 'Expression of the Anabaena hetR gene from a
760 copper-regulated promoter leads to heterocyst differentiation under repressing conditions',
761 *Proceedings of the National Academy of Sciences*, 98(5), pp. 2729–2734. doi:
762 10.1073/pnas.051624898.

763 Bustos, S. A. and Golden, S. S. (1992) 'Light-regulated expression of the psbD gene family in
764 Synecbococcus sp. strain PCC 7942: evidence for the role of duplicated psbD genes in
765 cyanobacteria', *Molecular and General Genetics MGG*, 232(2), pp. 221–230. doi:
766 10.1007/BF00280000.

767 Cabeen, M. T. *et al.* (2009) 'Bacterial cell curvature through mechanical control of cell growth',
768 *The EMBO Journal*, pp. 1208–1219. doi: 10.1038/emboj.2009.61.

769 Cai, Y. and Wolk, C. P. (1990) 'Use of a conditionally lethal gene in Anabaena sp. strain PCC
770 7120 to select for double recombinats and to entrap insertion sequnces', *Journal of*
771 *Bacteriology*, 172(6), pp. 3138–3145.

772 Camberg, J. L., Hoskins, J. R. and Wickner, S. (2009) 'ClpXP protease degrades the
773 cytoskeletal protein, FtsZ, and modulates FtsZ polymer dynamics', *Proc Natl Acad Sci U S A*,
774 106(26), pp. 10614–10619. doi: 10.1073/pnas.0904886106.

775 Cappuccinelli, P. (1980) 'The movement of eukaryotic cells', in *Motility of Living Cells*.
776 Dordrecht: Springer Netherlands, pp. 59–74. doi: 10.1007/978-94-009-5812-8_4.

777 Carballido-Lopez, R. (2006) 'The Bacterial Actin-Like Cytoskeleton', *Microbiology and*

778 *Molecular Biology Reviews*, 70(4), pp. 888–909. doi: 10.1128/MMBR.00014-06.

779 Charbon, G., Cabeen, M. T. and Jacobs-Wagner, C. (2009) 'Bacterial intermediate filaments:
780 In vivo assembly, organization, and dynamics of crescentin', *Genes and Development*, pp.
781 1131–1144. doi: 10.1101/gad.1795509.

782 Corpet, F. (1988) 'Multiple sequence alignment with hierarchical clustering.', *Nucleic acids*
783 *research*, 16(22), pp. 10881–90. doi: 10.1093/nar/16.22.10881.

784 Dörrich, A. K. *et al.* (2014) 'Deletion of the Synechocystis sp. PCC 6803 kaiAB1C1 gene cluster
785 causes impaired cell growth under light???dark conditions', *Microbiology (United Kingdom)*,
786 160(2014), pp. 2538–2550. doi: 10.1099/mic.0.081695-0.

787 England, P. *et al.* (2005) 'The Scc Spirochetal Coiled-Coil Protein Forms Helix-Like Filaments
788 and Binds to Nucleic Acids Generating Nucleoprotein Structures', *Journal of Bacteriology*,
789 188(2), pp. 469–476. doi: 10.1128/jb.188.2.469-476.2006.

790 Enright, A. J., Van Dongen, S. and Ouzounis, C. A. (2002) 'An efficient algorithm for large-
791 scale detection of protein families', *Nucleic acids research*. Oxford University Press, 30(7), pp.
792 1575–1584.

793 Fiuza, M. *et al.* (2010) 'Phosphorylation of a novel cytoskeletal protein (RsmP) regulates rod-
794 shaped morphology in Corynebacterium glutamicum', *Journal of Biological Chemistry*, pp.
795 29387–29397. doi: 10.1074/jbc.M110.154427.

796 Flärdh, K. *et al.* (2012) 'Regulation of apical growth and hyphal branching in Streptomyces',
797 *Current Opinion in Microbiology*, 15(6), pp. 737–743. doi:
798 https://doi.org/10.1016/j.mib.2012.10.012.

799 Flores, E. *et al.* (2007) 'Septum-localized protein required for filament integrity and diazotrophy
800 in the heterocyst-forming cyanobacterium Anabaena sp. strain PCC 7120', *Journal of*
801 *Bacteriology*, 189(10), pp. 3884–3890. doi: 10.1128/JB.00085-07.

802 Fuchino, K. *et al.* (2013) 'Dynamic gradients of an intermediate filament-like cytoskeleton are

803 recruited by a polarity landmark during apical growth', *Proceedings of the National Academy*
804 *of Sciences*, pp. E1889–E1897. doi: 10.1073/pnas.1305358110.

805 Fuchs, E. and Weber, K. (1994) 'INTERMEDIATE FILAMENTS: Structure, Dynamics, Function
806 and Disease', *Annual Review of Biochemistry*, 63, pp. 345–382.

807 Geisler, N. and Weber, K. (1982) 'The amino acid sequence of chicken muscle desmin
808 provides a common structural model for intermediate filament proteins', *The EMBO journal*,
809 1(12), pp. 1649–1656. Available at: https://www.ncbi.nlm.nih.gov/pubmed/6202512.

810 Gibson, D. G. *et al.* (2009) 'Enzymatic assembly of DNA molecules up to several hundred
811 kilobases', *Nature Methods*, 6(5), pp. 343–345. doi: 10.1038/nmeth.1318.

812 Grant, S. G. *et al.* (1990) 'Differential plasmid rescue from transgenic mouse DNAs into
813 Escherichia coli methylation-restriction mutants.', *Proceedings of the National Academy of*
814 *Sciences*, 87(12), pp. 4645–4649. doi: 10.1073/pnas.87.12.4645.

815 Heinz, S. *et al.* (2016) 'Thylakoid Membrane Architecture in *Synechocystis* Depends on CurT,
816 a Homolog of the Granal CURVATURE THYLAKOID1 Proteins', *The Plant Cell*, 28(9), pp.
817 2238–2260. doi: 10.1105/tpc.16.00491.

818 Hempel, A. M. *et al.* (2012) 'The Ser/Thr protein kinase AfsK regulates polar growth and hyphal
819 branching in the filamentous bacteria Streptomyces', *Proceedings of the National Academy of*
820 *Sciences of the United States of America*. 2012/08/06. National Academy of Sciences,
821 109(35), pp. E2371–E2379. doi: 10.1073/pnas.1207409109.

822 Herrero, A., Stavans, J. and Flores, E. (2016) 'The multicellular nature of filamentous
823 heterocyst-forming cyanobacteria', *FEMS Microbiology Reviews*, 40(6), pp. 831–854. doi:
824 10.1093/femsre/fuw029.

825 Herrmann, H. *et al.* (1996) 'Structure and assembly properties of the intermediate filament
826 protein vimentin: The role of its head, rod and tail domains', *Journal of Molecular Biology*,
827 264(5), pp. 933–953. doi: 10.1006/jmbi.1996.0688.

828 Herrmann, H. and Aebi, U. (2004) 'Intermediate Filaments: Molecular Structure, Assembly
829 Mechanism, and Integration Into Functionally Distinct Intracellular Scaffolds', *Annual Review*
830 *of Biochemistry*, 73(1), pp. 749–789. doi: 10.1146/annurev.biochem.73.011303.073823.

831 Holmes, N. A. *et al.* (2013) 'Coiled-coil protein Scy is a key component of a multiprotein
832 assembly controlling polarized growth in Streptomyces', *Proceedings of the National Academy*
833 *of Sciences*, pp. E397–E406. doi: 10.1073/pnas.1210657110.

834 Hu, B. *et al.* (2007) 'MreB is important for cell shape but not for chromosome segregation of
835 the filamentous cyanobacterium Anabaena sp. PCC 7120', *Molecular Microbiology*, 63(6), pp.
836 1640–1652. doi: 10.1111/j.1365-2958.2007.05618.x.

837 Huang, H.-H. *et al.* (2010) 'Design and characterization of molecular tools for a Synthetic
838 Biology approach towards developing cyanobacterial biotechnology', *Nucleic acids research*.
839 2010/03/17. Oxford University Press, 38(8), pp. 2577–2593. doi: 10.1093/nar/gkq164.

840 Hurme, R. *et al.* (1994) 'Intermediate filament-like network formed in vitro by a bacterial coiled
841 coil protein', *Journal of Biological Chemistry*, pp. 10675–10682.

842 Inclan, Y. F. *et al.* (2016) 'A scaffold protein connects type IV pili with the Chp chemosensory
843 system to mediate activation of virulence signaling in Pseudomonas aeruginosa', *Molecular*
844 *Microbiology*, 101(4), pp. 590–605. doi: 10.1111/mmi.13410.

845 Ingerson-Mahar, M. *et al.* (2010) 'The metabolic enzyme CTP synthase forms cytoskeletal
846 filaments', *Nature Cell Biology*, pp. 739–746. doi: 10.1038/ncb2087.

847 Ingerson-Mahar, M. and Gitai, Z. (2012) 'A growing family: the expanding universe of the
848 bacterial cytoskeleton', *FEMS Microbiol Rev*, 36(1), pp. 256–266. doi: 10.1111/j.1574-
849 6976.2011.00316.x.

850 Ivleva, N. B. *et al.* (2005) 'LdpA: A component of the circadian clock senses redox state of the
851 cell', *EMBO Journal*, 24(6), pp. 1202–1210. doi: 10.1038/sj.emboj.7600606.

852 Jain, I. H., Vijayan, V. and O'Shea, E. K. (2012) 'Spatial ordering of chromosomes enhances

the fidelity of chromosome partitioning in cyanobacteria.', *Proceedings of the National Academy of Sciences of the United States of America*, 109(34), pp. 13638–43. doi: 10.1073/pnas.1211144109.

Jones, L. J. F., Carballido-López, R. and Errington, J. (2001) 'Control of cell shape in bacteria: Helical, actin-like filaments in Bacillus subtilis', *Cell*, 104(6), pp. 913–922. doi: 10.1016/S0092-8674(01)00287-2.

Kahnt, J. *et al.* (2007) 'Post-translational modifications in the active site region of methyl-coenzyme M reductase from methanogenic and methanotrophic archaea', *The FEBS journal*. Wiley Online Library, 274(18), pp. 4913–4921.

Karimova, G., Davi, M. and Ladant, D. (2012) 'The β-lactam resistance protein Blr, a small membrane polypeptide, is a component of the Escherichia coli cell division machinery', *Journal of Bacteriology*, 194(20), pp. 5576–5588. doi: 10.1128/JB.00774-12.

Kelemen, G. H. (2017) 'Intermediate Filaments Supporting Cell Shape and Growth in Bacteria BT - Prokaryotic Cytoskeletons: Filamentous Protein Polymers Active in the Cytoplasm of Bacterial and Archaeal Cells', in Löwe, J. and Amos, L. A. (eds). Cham: Springer International Publishing, pp. 161–211. doi: 10.1007/978-3-319-53047-5_6.

Koch, M. K., McHugh, C. A. and Hoiczyk, E. (2011) 'BacM, an N-terminally processed bactofilin of Myxococcus xanthus, is crucial for proper cell shape', *Mol Microbiol .*, 80(4), pp. 1031–1051. doi: 10.1111/j.1365-2958.2011.07629.x.

Kopfmann, S. and Hess, W. R. (2013) 'Toxin-antitoxin systems on the large defense plasmid pSYSA of synechocystis sp. pCC 6803', *Journal of Biological Chemistry*, 288(10), pp. 7399–7409. doi: 10.1074/jbc.M112.434100.

Köster, S. *et al.* (2015) 'Intermediate filament mechanics in vitro and in the cell: From coiled coils to filaments, fibers and networks', *Current Opinion in Cell Biology*, 32, pp. 82–91. doi: 10.1016/j.ceb.2015.01.001.

878 Krogh, A. *et al.* (2001) 'Predicting transmembrane protein topology with a hidden Markov
879 model: application to complete genomes', *Journal of molecular biology*. Elsevier, 305(3), pp.
880 567–580.

881 Kruse, T., Bork-Jensen, J. and Gerdes, K. (2005) 'The morphogenetic MreBCD proteins of
882 Escherichia coli form an essential membrane-bound complex', *Molecular Microbiology*, 55(1),
883 pp. 78–89. doi: 10.1111/j.1365-2958.2004.04367.x.

884 Kühn, J. *et al.* (2010) 'Bactofilins, a ubiquitous class of cytoskeletal proteins mediating polar
885 localization of a cell wall synthase in Caulobacter crescentus', *EMBO Journal*, pp. 327–339.
886 doi: 10.1038/emboj.2009.358.

887 Kunert, A., Hagemann, M. and Erdmann, N. (2000) 'Construction of promoter probe vectors
888 for Synechocystis sp. PCC 6803 using the light-emitting reporter systems Gfp and LuxAB',
889 *Journal of Microbiological Methods*, 41(3), pp. 185–194. doi: 10.1016/S0167-7012(00)00162-
890 7.

891 Larsen, R. A. *et al.* (2007) 'Treadmilling of a prokaryotic tubulin-like protein, TubZ, required for
892 plasmid stability in Bacillus thuringiensis', *Genes and Development*, 21(11), pp. 1340–1352.
893 doi: 10.1101/gad.1546107.

894 Leung, C. L., Green, K. J. and Liem, R. K. H. (2002) 'Plakins: A family of versatile cytolinker
895 proteins', *Trends in Cell Biology*, 12(1), pp. 37–45. doi: 10.1016/S0962-8924(01)02180-8.

896 Lin, L. and Thanbichler, M. (2013) 'Nucleotide-independent cytoskeletal scaffolds in bacteria',
897 *Cytoskeleton*, 70(8), pp. 409–423. doi: 10.1002/cm.21126.

898 Lodish, H. *et al.* (2000) *Molecular Cell Biology*. 4th edn. New York: W. H. Freeman. Available
899 at: https://www.ncbi.nlm.nih.gov/books/NBK21560/ (Accessed: 27 February 2018).

900 Lopes Pinto, F. *et al.* (2011) 'FtsZ degradation in the cyanobacterium Anabaena sp. strain PCC
901 7120', *Journal of Plant Physiology*. Elsevier GmbH., 168(16), pp. 1934–1942. doi:
902 10.1016/j.jplph.2011.05.023.

Löwe, J. and Amos, L. A. (2009) 'Evolution of cytomotive filaments: The cytoskeleton from prokaryotes to eukaryotes', *International Journal of Biochemistry and Cell Biology*, 41(2), pp. 323–329. doi: 10.1016/j.biocel.2008.08.010.

Lupas, A., Van Dyke, M. and Stock, J. (1991) 'Predicting coiled coils from protein sequences', *Science*, pp. 1162–1164. doi: 10.1126/science.252.5009.1162.

Marchler-Bauer, A. *et al.* (2016) 'CDD/SPARCLE: functional classification of proteins via subfamily domain architectures', *Nucleic acids research*. Oxford University Press, 45(D1), pp. D200–D203.

McGuffin, L. J., Bryson, K. and Jones, D. T. (2000) 'The PSIPRED protein structure prediction server', *Bioinformatics*. Oxford University Press, 16(4), pp. 404–405.

Meselson, M. and Yuan, R. (1968) 'DNA restriction enzyme from E. coli.', *Nature*, 217(5134), pp. 1110–4. Available at: http://www.ncbi.nlm.nih.gov/pubmed/4868368 (Accessed: 22 February 2018).

Miller, J. H. (1992) *A Short Course in Bacterial Genetics – A Laboratory Manual and Handbook for Escherichia coli and Related Bacteria*, *Cold Spring Harbor Laboratory Press*. Cold Spring Harbor. doi: 10.1002/jobm.3620330412.

Nakamura, Y. *et al.* (1993) 'Acceleration of bovine neurofilament L assembly by deprivation of acidic tail domain', *European Journal of Biochemistry*, 212(2), pp. 565–571. doi: 10.1111/j.1432-1033.1993.tb17694.x.

Nan, B. *et al.* (2010) 'A multi-protein complex from Myxococcus xanthus required for bacterial gliding motility', *Molecular Microbiology*, 76(6), pp. 1539–1554. doi: 10.1111/j.1365-2958.2010.07184.x.

Nayar, A. S. *et al.* (2007) 'FraG is necessary for filament integrity and heterocyst maturation in the cyanobacterium Anabaena sp. strain PCC 7120', *Microbiology*, 153(2), pp. 601–607. doi: 10.1099/mic.0.2006/002535-0.

928 O'Leary, N. A. *et al.* (2015) 'Reference sequence (RefSeq) database at NCBI: current status,
929 taxonomic expansion, and functional annotation', *Nucleic acids research*. Oxford University
930 Press, 44(D1), pp. D733–D745.

931 Rackham, O. J. L. *et al.* (2010) 'The Evolution and Structure Prediction of Coiled Coils across
932 All Genomes', *Journal of Molecular Biology*. Academic Press, 403(3), pp. 480–493. doi:
933 10.1016/J.JMB.2010.08.032.

934 Ramos-León, F. *et al.* (2015) 'Divisome-dependent subcellular localization of cell-cell joining
935 protein SepJ in the filamentous cyanobacterium Anabaena', *Molecular Microbiology*, 96(3), pp.
936 566–580. doi: 10.1111/mmi.12956.

937 Rice, P., Longden, I. and Bleasby, A. (2000) 'EMBOSS: the European Molecular Biology Open
938 Software Suite.', *Trends in genetics : TIG*. Elsevier, 16(6), pp. 276–7. doi: 10.1016/S0168-
939 9525(00)02024-2.

940 Rippka, R. *et al.* (1979) 'Generic Assignments, Strain Histories and Properties of Pure Cultures
941 of Cyanobacteria', *Microbiology*, 111(1), pp. 1–61. doi: 10.1099/00221287-111-1-1.

942 Sandvang, D. (1999) 'Novel streptomycin and spectinomycin resistance gene as a gene
943 cassette within a class 1 integron isolated from Escherichia coli', *Antimicrobial Agents and*
944 *Chemotherapy*, 43(12), pp. 3036–3038. doi: 10.1128/AAC.44.2.475-475.2000.

945 Schuergers, N. *et al.* (2015) 'PilB localization correlates with the direction of twitching motility
946 in the cyanobacterium Synechocystis sp. PCC 6803', *Microbiology (Reading, England)*,
947 161(2015), pp. 960–966. doi: 10.1099/mic.0.000064.

948 Schuergers, N., Mullineaux, C. W. and Wilde, A. (2017) 'Cyanobacteria in motion', *Current*
949 *Opinion in Plant Biology*. Elsevier Ltd, 37, pp. 109–115. doi: 10.1016/j.pbi.2017.03.018.

950 Shoeman, R. L. and Traub, P. (1993) 'Assembly of Intermediate Filaments', *Bioessays*, 15(9),
951 pp. 605–611. doi: 10.1002/bies.950150906.

952 Specht, M. *et al.* (2011) 'Helicobacter pylori Possesses Four Coiled-Coil-Rich Proteins That

953 Form Extended Filamentous Structures and Control Cell Shape and Motility', *Journal of*
954 *Bacteriology*, 193(17), pp. 4523–4530. doi: 10.1128/JB.00231-11.

955 Springstein, B. L. *et al.* (2019) 'A cytoskeletal network maintains filament shape in the
956 multicellular cyanobacterium Anabaena sp. PCC 7120', *bioRxiv*, p. 553073. doi:
957 10.1101/553073.

958 Stucken, K. *et al.* (2012) 'Transformation and conjugal transfer of foreign genes into the
959 filamentous multicellular cyanobacteria (subsection V) Fischerella and Chlorogloeopsis',
960 *Current Microbiology*, 65(5), pp. 552–560. doi: 10.1007/s00284-012-0193-5.

961 Stucken, K., Koch, R. and Dagan, T. (2013) 'Cyanobacterial defense mechanisms against
962 foreign DNA transfer and their impact on genetic engineering', *Biological Research*, 46(4), pp.
963 373–382. doi: 10.4067/S0716-97602013000400009.

964 Studier, F. W. and Moffatt, B. A. (1986) 'Use of bacteriophage T7 RNA polymerase to direct
965 selective high-level expression of cloned genes', *Journal of Molecular Biology*, 189(1), pp.
966 113–130. doi: 10.1016/0022-2836(86)90385-2.

967 Stuurman, N., Heins, S. and Aebi, U. (1998) 'Nuclear lamins: Their structure, assembly, and
968 interactions', *Journal of Structural Biology*, 122(1–2), pp. 42–66. doi: 10.1006/jsbi.1998.3987.

969 Swulius, M. T. and Jensen, G. J. (2012) 'The helical mreb cytoskeleton in Escherichia coli
970 MC1000/pLE7 is an artifact of the N-terminal yellow fluorescent protein tag', *Journal of*
971 *Bacteriology*, 194(23), pp. 6382–6386. doi: 10.1128/JB.00505-12.

972 Tatusov, R. L., Koonin, E. V and Lipman, D. J. (1997) 'A genomic perspective on protein
973 families', *Science*. American Association for the Advancement of Science, 278(5338), pp. 631–
974 637.

975 Tolonen, A. C., Liszt, G. B. and Hess, W. R. (2006) 'Genetic manipulation of Prochlorococcus
976 strain MIT9313: green fluorescent protein expression from an RSF1010 plasmid and Tn5
977 transposition', *Applied and environmental microbiology*. 2006/10/13. American Society for

978 Microbiology, 72(12), pp. 7607–7613. doi: 10.1128/AEM.02034-06.

979 Traub, P. and Vorgias, C. E. (1983) 'Involvement of the N-terminal polypeptide of vimentin in
980 the formation of intermediate filaments', *Journal of Cell Science*, 63(1), pp. 43 LP – 67.
981 Available at: http://jcs.biologists.org/content/63/1/43.abstract.

982 Ungerer, J. and Pakrasi, H. B. (2016) 'Cpf1 Is A Versatile Tool for CRISPR Genome Editing
983 Across Diverse Species of Cyanobacteria', *Scientific Reports*. Nature Publishing Group, 6, pp.
984 1–9. doi: 10.1038/srep39681.

985 Vermaas, W. F. J. *et al.* (2002) 'Transformation of the cyanobacterium Synechocystis sp. PCC
986 6803 as a tool for genetic mapping: optimization of efficiency', *FEMS Microbiology Letters*,
987 206(2), pp. 215–219. doi: 10.1111/j.1574-6968.2002.tb11012.x.

988 Wagstaff, J. and Löwe, J. (2018) 'Prokaryotic cytoskeletons: protein filaments organizing small
989 cells', *Nature Reviews Microbiology*. Nature Publishing Group. doi: 10.1038/nrmicro.2017.153.

990 Waidner, B. *et al.* (2009) 'A novel system of cytoskeletal elements in the human pathogen
991 Helicobacter pylori', *PLoS Pathogens*. doi: 10.1371/journal.ppat.1000669.

992 Walshaw, J., Gillespie, M. D. and Kelemen, G. H. (2010) 'A novel coiled-coil repeat variant in
993 a class of bacterial cytoskeletal proteins', *Journal of Structural Biology*, pp. 202–215. doi:
994 10.1016/j.jsb.2010.02.008.

995 Weber, K. and Geisler, N. (1982) 'The structural relation between intermediate filament
996 proteins in living cells and the alpha-keratins of sheep wool', *The EMBO journal*, 1(10), pp.
997 1155–1160. Available at: https://www.ncbi.nlm.nih.gov/pubmed/6202505.

998 Weiss, G. L. *et al.* (2019) 'Structure and Function of a Bacterial Gap Junction Analog', *Cell*.
999 Cell Press, 178(2), pp. 374-384.e15. doi: 10.1016/J.CELL.2019.05.055.

1000 Weissenbach, J. *et al.* (2017) 'Evolution of Chaperonin Gene Duplication in Stigonematalean
1001 Cyanobacteria (Subsection V)', *Genome Biology and Evolution*, 9(1), pp. 241–252. doi:
1002 10.1093/gbe/evw287.

1003 Wiche, G., Osmanagic-Myers, S. and Castañón, M. J. (2015) 'Networking and anchoring
1004 through plectin: A key to IF functionality and mechanotransduction', *Current Opinion in Cell*
1005 *Biology*, 32, pp. 21–29. doi: 10.1016/j.ceb.2014.10.002.

1006 Wickstead, B. and Gull, K. (2011) 'The evolution of the cytoskeleton', *Journal of Cell Biology*,
1007 194(4), pp. 513–525. doi: 10.1083/jcb.201102065.

1008 Wilk, L. *et al.* (2011) 'Outer membrane continuity and septosome formation between vegetative
1009 cells in the filaments of Anabaena sp. PCC 7120', *Cellular Microbiology*, 13(11), pp. 1744–
1010 1754. doi: 10.1111/j.1462-5822.2011.01655.x.

1011 Wolk, C. P. *et al.* (1988) 'Isolation and complementation of mutants of Anabaena sp. strain
1012 PCC 7120 unable to grow aerobically on dinitrogen.', *Journal of bacteriology*, 170(3), pp. 1239–
1013 1244. doi: 10.1128/jb.170.3.1239-1244.1988.

1014 Yang, J. and Zhang, Y. (2015) 'I-TASSER server: New development for protein structure and
1015 function predictions', *Nucleic Acids Research*, 43(W1), pp. W174–W181. doi:
1016 10.1093/nar/gkv342.

1017 Yang, R. *et al.* (2004) 'AglZ Is a Filament-Forming Coiled-Coil Protein Required for
1018 Adventurous Gliding Motility of Myxococcus xanthus', *Journal of bacteriology*, 186(18), pp.
1019 6168–6178. doi: 10.1128/JB.186.18.6168.

1020 Yu, N. Y. *et al.* (2010) 'PSORTb 3.0: Improved protein subcellular localization prediction with
1021 refined localization subcategories and predictive capabilities for all prokaryotes',
1022 *Bioinformatics*, 26(13), pp. 1608–1615. doi: 10.1093/bioinformatics/btq249.

1023 Zhang, C.-C. C. *et al.* (1995) 'Analysis of genes encoding the cell division protein FtsZ and a
1024 glutathione synthetase homologue in the cyanobacterium Anabaena sp. PCC 7120', *Research*
1025 *in Microbiology*, 146(6), pp. 445–455. doi: 10.1016/0923-2508(96)80290-7.

1026 Zhang, Y. (2009) 'I-TASSER: Fully automated protein structure prediction in CASP8', *Proteins:*
1027 *Structure, Function and Bioinformatics*, 77(SUPPL. 9), pp. 100–113. doi: 10.1002/prot.22588.

1028 Zhou, J. *et al.* (2014) 'Discovery of a super-strong promoter enables efficient production of
1029 heterologous proteins in cyanobacteria', *Scientific Reports*, 4, pp. 1–6. doi:
1030 10.1038/srep04500.

1031

Figures

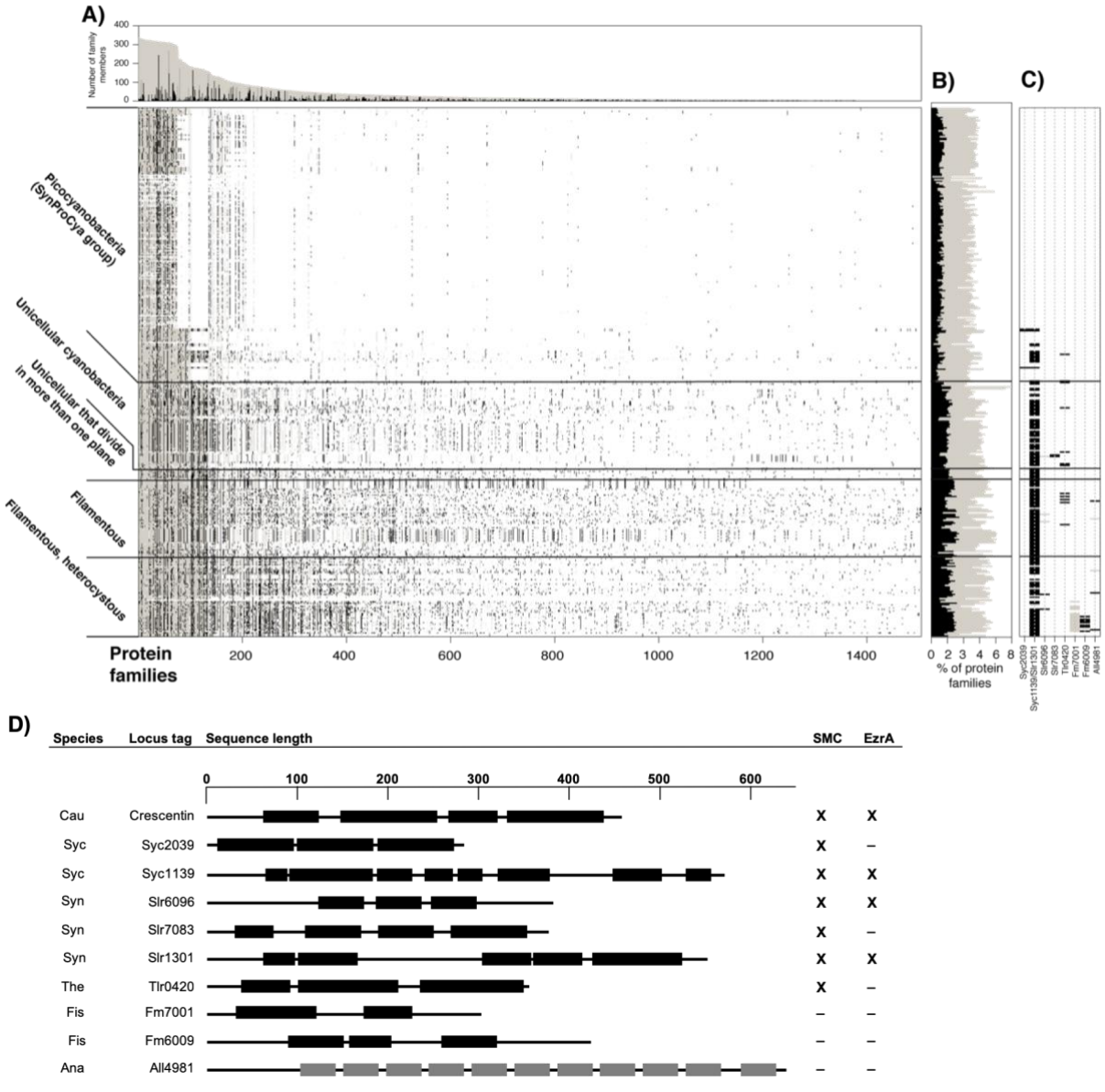

Fig. 1: Distribution of CCRP protein families within cyanobacteria

(**A**) Lines in the presence/absence matrix designate cyanobacterial genomes; each column shows a protein family. Gray dots designate any homologous protein in the same protein family and black dots represent CCRP members. Protein families are sorted according to the number of members. Protein family size and the number of CCRP members are presented in a bar graph above. (**B**) The proportion of protein families containing CCRPs (gray) and CCRP proteins (black) in each genome. (**C**) Presence/absence pattern of CCRP candidate protein families. Only protein families with at least three members predicted to be CCRPs are shown. (**D**) Domain prediction of CCRP candidates. Scale on top is given in amino acid residues. Amino acid sequences in coiled-coil conformation are depicted by black bars with non-coiled-coil sequences represented by black lines. Tetratricopeptide repeats (TPR), also predicted by the COILS algorithm, are shown as grey bars. Proteins are given as cyanobase locus tags. Fm7001 and Fm6009 correspond to NCBI accession numbers WP_016868005.1 and WP_020476706, respectively. Abbreviations: Cau: *C. crescentus*; Syc: *Synechococcus*, Syn: *Synechocystis*; Ana: *Anabaena*; The: *Thermosynechococcus elongatus* BP-1; Fis: *Fischerella*. Cyanobacterial CCRPs had conserved domains present in prokaryotic IF-like CCRPs and eukaryotic IF proteins (Supplementary Table 1). Presence of a structural maintenance of chromosomes (SMC) domain or structural similarities to the cell division protein EzrA are marked with "**X**", absence is indicated with "**-**". Full list is given in Supplementary Table 1. Note: *Anabaena* CCRPs have been described elsewhere before: *Springstein et al*. (2019), bioRxiv, doi: 10.1101/553073.

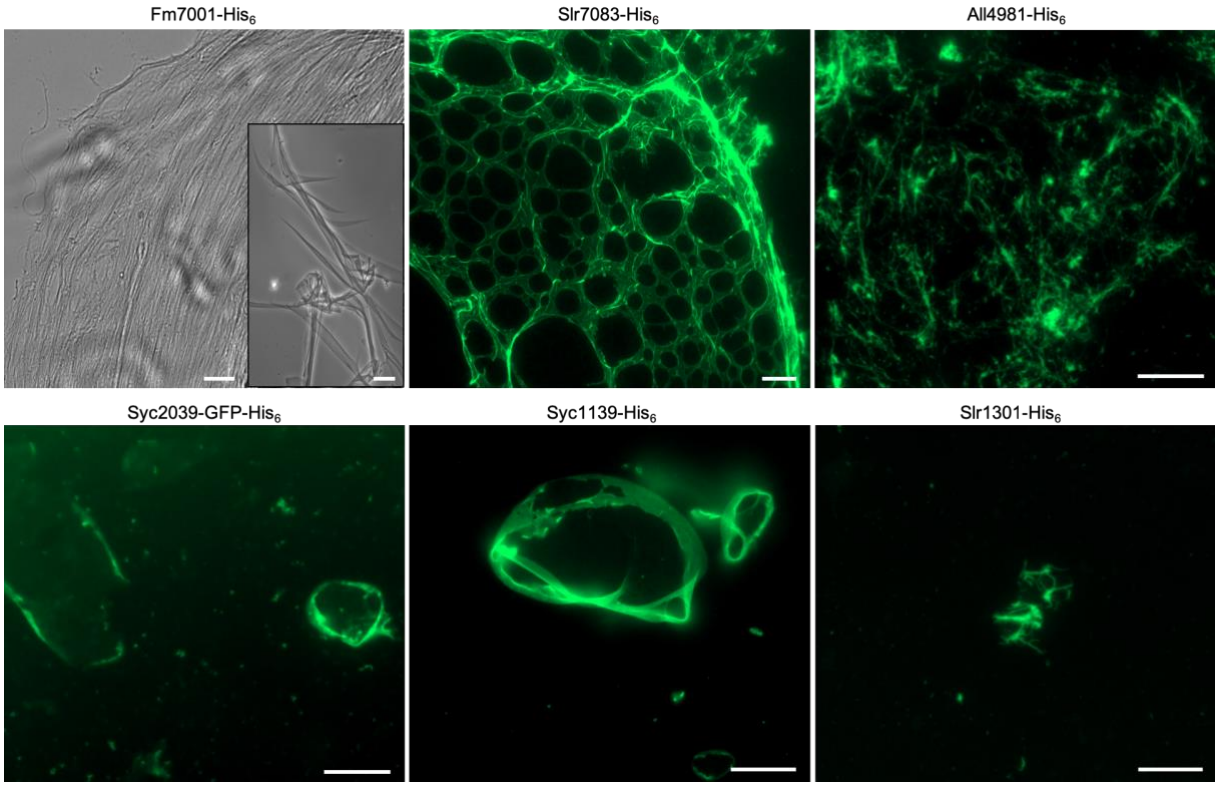

Fig. 2: Cyanobacterial CCRPs assemble into diverse filamentous structures *in vitro*

Bright field and epifluorescence micrographs of filamentous structures formed by purified and renatured Fm7001-His_6 (0.7 mg ml^{-1}), Slr7083-His_6 (1 mg ml^{-1}), All4981-His_6 (0.5 mg ml^{-1}), Syc2039-GFP-His_6 (0.3 mg ml^{-1}), Syc1139-His_6 (0.5 mg ml^{-1}) and Slr1301-His_6 (0.5 mg ml^{-1}). Proteins were dialyzed into 2 mM Tris-HCl, 4.5 M urea pH 7.5 (Fm7001), HLB (Slr7083), PLB (All4981, Syc1139, Slr1301) or BG11 (Syc2039). Renatured proteins were either directly analyzed by bright field microscopy (Fm7001) or stained with an excess of NHS-Fluorescein and analyzed by epifluorescence microscopy. The NHS-Fluorescein dye binds primary amines and is thus incompatible with urea, which is why Fm7001 filaments were visualized by bright field microscopy. Scale bars: 10 µm or (Fm7001 inlay and Slr7083) 20 µm.

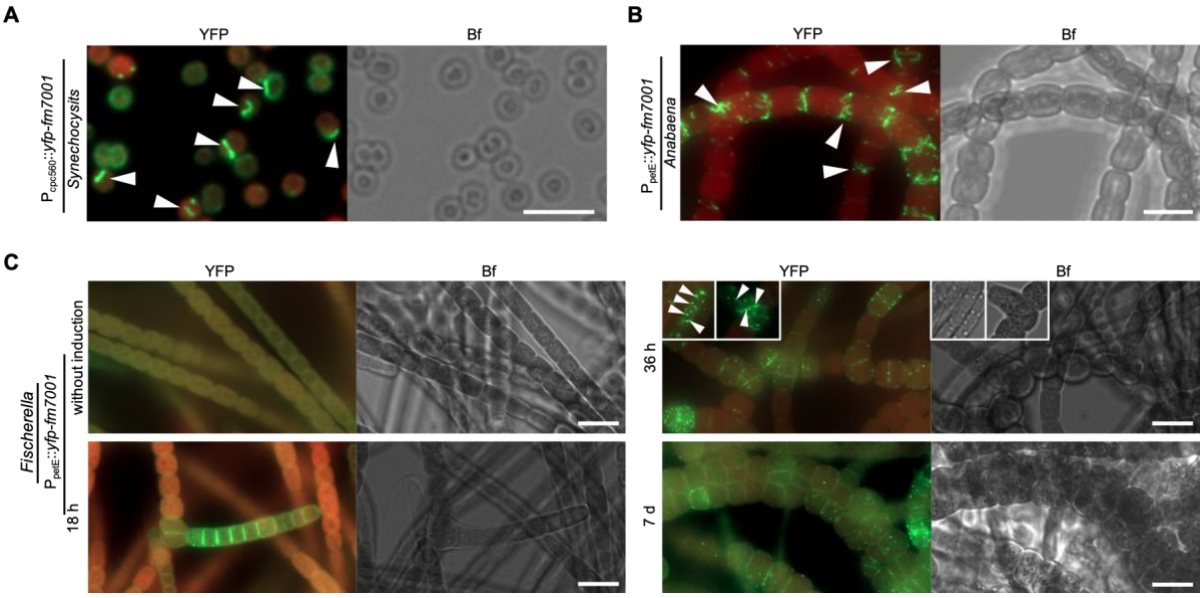

Fig. 3: Host-independency for Fm7001 *in vivo* filamentation

Merged GFP fluorescence and chlorophyll autofluorescence (red) and bright field micrographs of (A) *Synechocystis*, (B) *Anabaena* or (C) *Fischerella* cells expressing YFP-Fm7001. Cells were either grown in (**A**,**B**) BG11 or (C)BG11 without copper and then induced with 0.5 µM $CuSO_4$. (**C**) Micrographs were taken before induction of *yfp-fm7001* expression (without induction) and 18 h, 36 h or 7 d post induction. White triangles point to selected YFP-Fm7001 filamentous strings within the cells. Notably, unlike in *Anabaena* and *Fischerella*, Fm7001-GFP induced a swollen morphotype in *E. coli* and a subpopulation of *Synechocystis* cells (Supplementary Fig. 1E). (**B**): maximum intensity projection of a Z-stack. Scale bars: (**A**,**B**) 5 µm, (**C**) 10 µm.

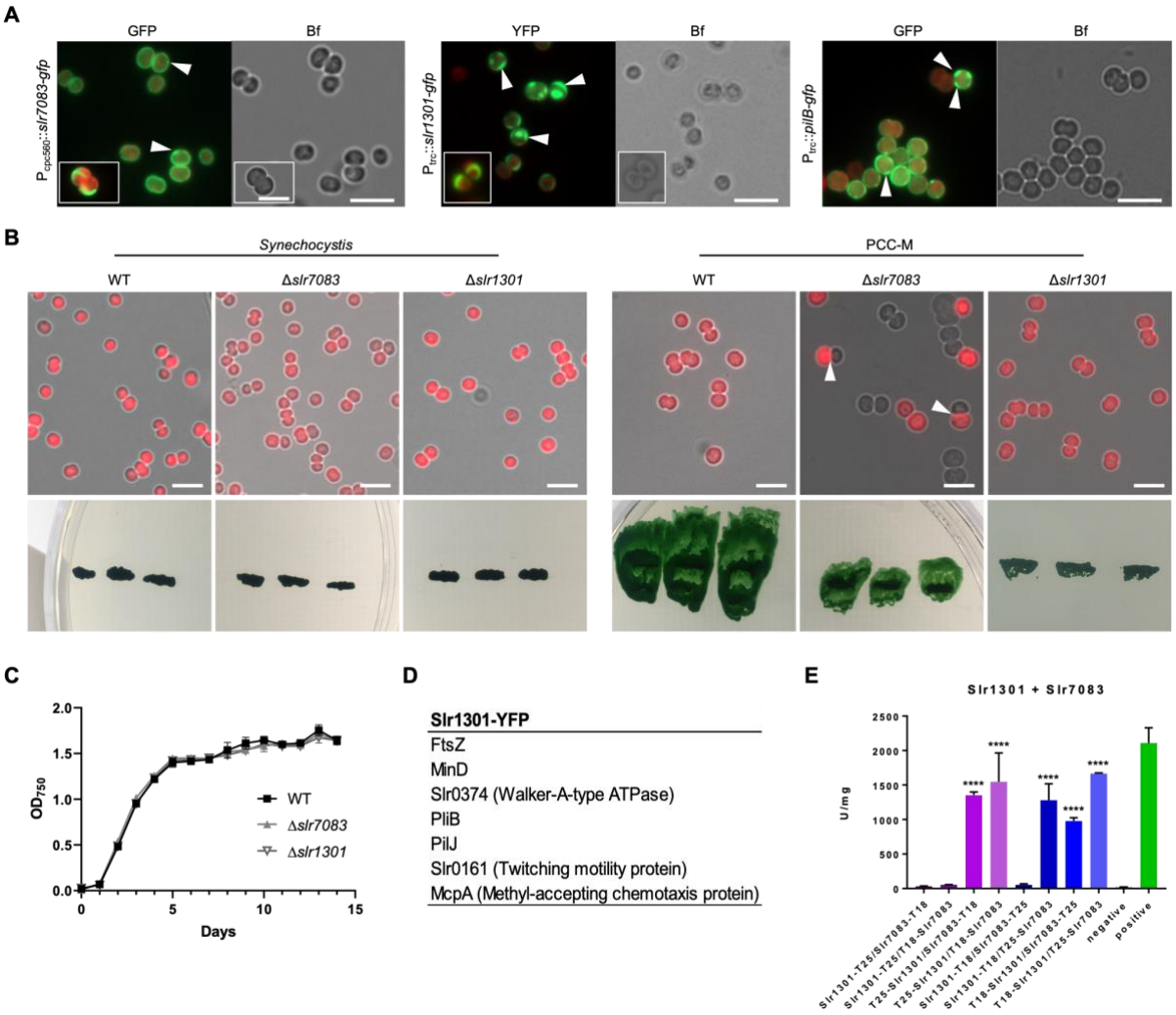

Fig. 4: Slr7083 and Slr1301 are involved in twitching motility in *Synechocystis*

(**A**) Merged GFP fluorescence and chlorophyll autofluorescence (red) and bright field micrographs of *Synechocystis* cells expressing, Slr7083-GFP, Slr1301-YFP or PilB-GFP from P_{cpc560} (Slr7083) or P_{trc} (Slr1301, PilB). Expression of PilB-GFP in PCC-M resulted in the same localization pattern (data not shown). White triangles indicate focal spots and crescent-like formations. Scale bars: 5 µm. (**B**) Merged bright field and chlorophyll autofluorescence micrographs of motile and non-motile *Synechocystis* WT, Δ*slr7083* and Δ*slr1301* mutant cells. Below, motility tests of three single colonies from indicated cells streaked on BG11 plates and illuminated from only one direction are shown. (**C**) Growth curve of *Synechocystis* WT, Δ*slr7083* and Δ*slr1301* mutant strains grown in quadruples at standard growth conditions. OD_{750} values were recorded once a day for 15 d. Error bars show the standard deviation (n=4). (**D**) Excerpt of interacting proteins of interest from mass spectrometry analysis of anti-GFP co-immunoprecipitations of *Synechocystis* cells expressing Slr1301-YFP from P_{trc}. (**E**) Beta-galactosidase assays of *E. coli* cells co-expressing indicated translational fusion constructs of all possible pair-wise combinations of Slr7083 with Slr1301 grown for 1 d at 30 °C. Quantity values are given in Miller Units per milligram LacZ of the mean results from three independent colonies. Error bars indicate standard deviations (n=3). Neg: pKNT25 plasmid carrying *slr1301* co-transformed with empty pUT18C. Pos: Zip/Zip control. Values indicated with * are significantly different from the negative control. *: P<0.05, **: P<0.01, ***: P<0.001, ****: P<0.0001 (Dunnett's multiple comparison test and one-way ANOVA).

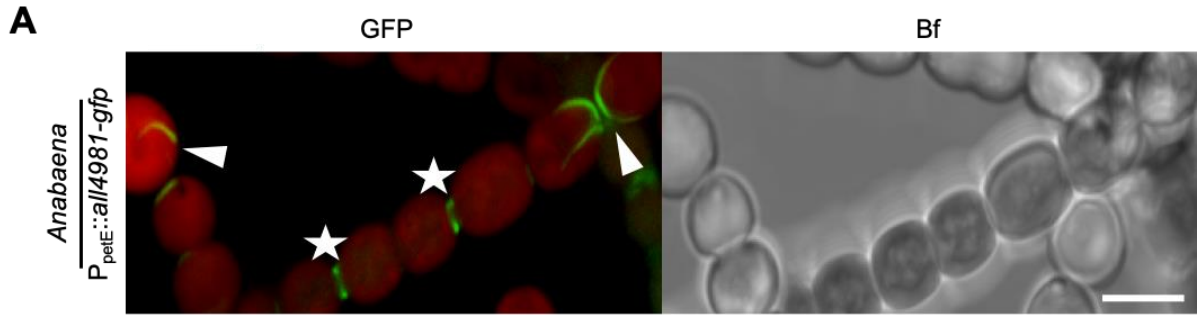

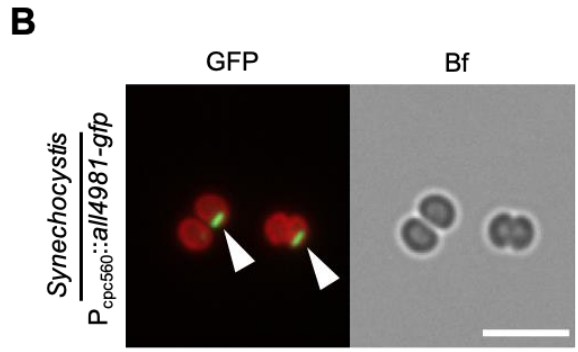

C

YFP-All4981$^{\Delta TPR3-4}$
All4982
All4499 (S-layer)
Alr0834 (S-layer or Porin)
Alr4550 (S-layer)
Alr1819 (S-layer or fascilin)
Alr1295 (Prohibitin)
DevH
FtsH
ParB
MreB
MinD

Fig. 5: All4981 forms cell-traversing filaments in cyanobacteria

(**A**,**B**) GFP fluorescence and merged GFP fluorescence and chlorophyll autofluorescence (red) and bright field micrographs of (**A**) *Anabaena* and (**B**) *Synechocystis* cells expressing All4981-GFP. *Anabaena* cells were grown in $BG11_0$ and *Synechocystis* cells were grown in BG11. (**A**): Maximum intensity projections of a Z-stack. White triangles indicate selected filaments traversing through the cells. White arrows point to spindle-like YFP-All4981 filaments. White stars mark septal formations between two neighboring cells. Scale bars: 5 µm. (**C**) Excerpt of interacting proteins of interest from mass spectrometry analysis of anti-GFP co-immunoprecipitations of *Anabaena* cells expressing YFP-All4981$^{\Delta TPR3-4}$ from P_{petE}.

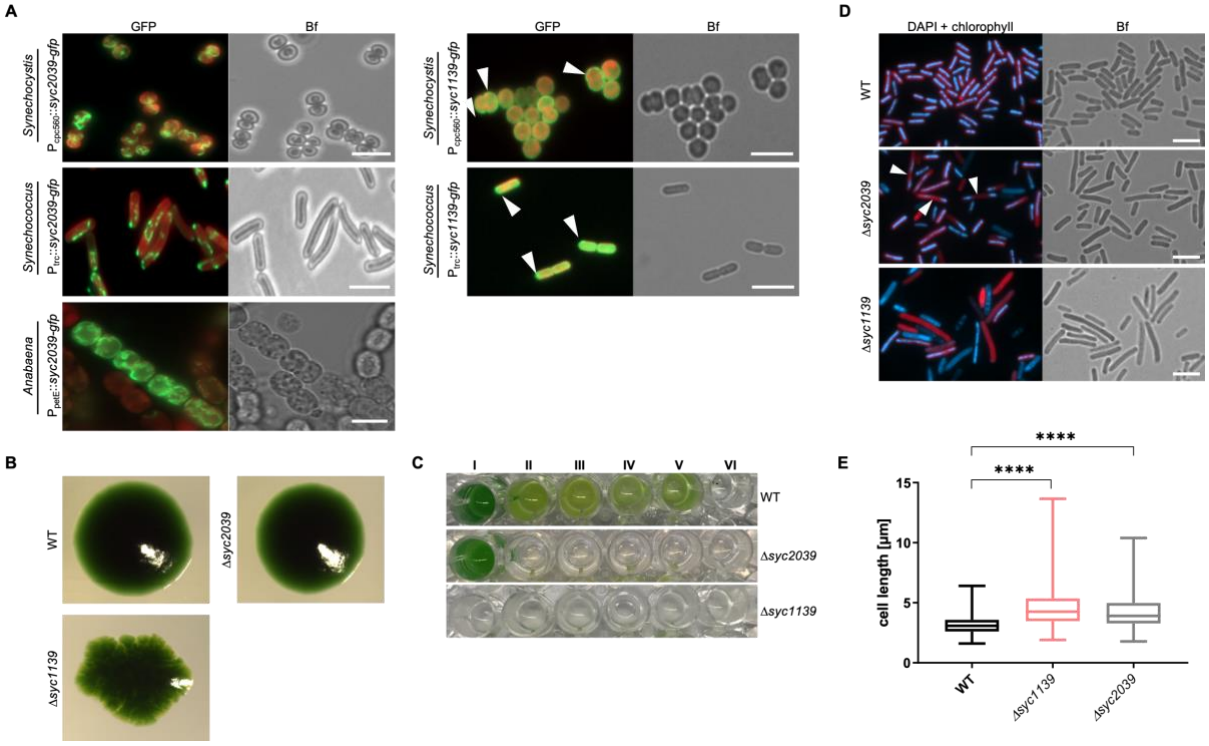

Fig. 6: *Synechococcus* CCRPs affect cytokinesis and cellular integrity

(**A**) Merged GFP fluorescence and chlorophyll autofluorescence (red) and bright field micrographs of *Synechocystis*, *Synechococcus* and *Anabaena* cells expressing Syc2039-GFP or Syc1139-GFP from P_{trc}. *Synechocystis* cells were grown in BG11, *Anabaena* cells were grown in $BG11_0$ supplemented with 0.25 µM $CuSO_4$ for 1 day, and *Synechococcus* cells were grown on BG11 plates supplemented with 0.01 mM (Syc2039) or 1 mM (Syc1139) IPTG. Micrographs of *Synechococcus* and *Anabaena* cells expressing Syc2039-GFP are maximum intensity projections of a Z-stack. White triangles indicate Syc1139-GFP spots. Attempts to translationally fuse a YFP-tag to the N-terminus of Syc2039 were unsuccessful, possibly due to the transmembrane domain predicted to the Syc2039 N-terminus (Supplementary Table 1). (**B**) Colony formation of *Synechococcus* WT and mutant strains on BG11 plates. (**C**) Cell viability of *Synechococcus* WT and mutant strains grown in (I) BG11 or BG11 supplemented with (II) 5 mM glucose, (III) 200 mM glucose, (IV) 2 mM NH_4Cl, (V) 200 mM maltose or (VI) 500 mM NaCl. (**D**) Merged DAPI fluorescence and chlorophyll autofluorescence (red) and bright field micrographs of *Synechococcus* WT and mutant strains grown on BG11 plates and stained with 10 µg ml^{-1} DAPI. White triangles indicate non-dividing cells revealing inhomogeneous DNA placement. (**E**) Cell length of *Synechococcus* WT (n=648), non-segregated Δ*syc1139* (n=417) and Δ*syc2039* (n=711) mutant cells. Values indicated with * are significantly different from the WT. ****: P<0.0001 (one-way ANOVA, using Turkey's multiple comparison test). Scale bars: 5 µm.

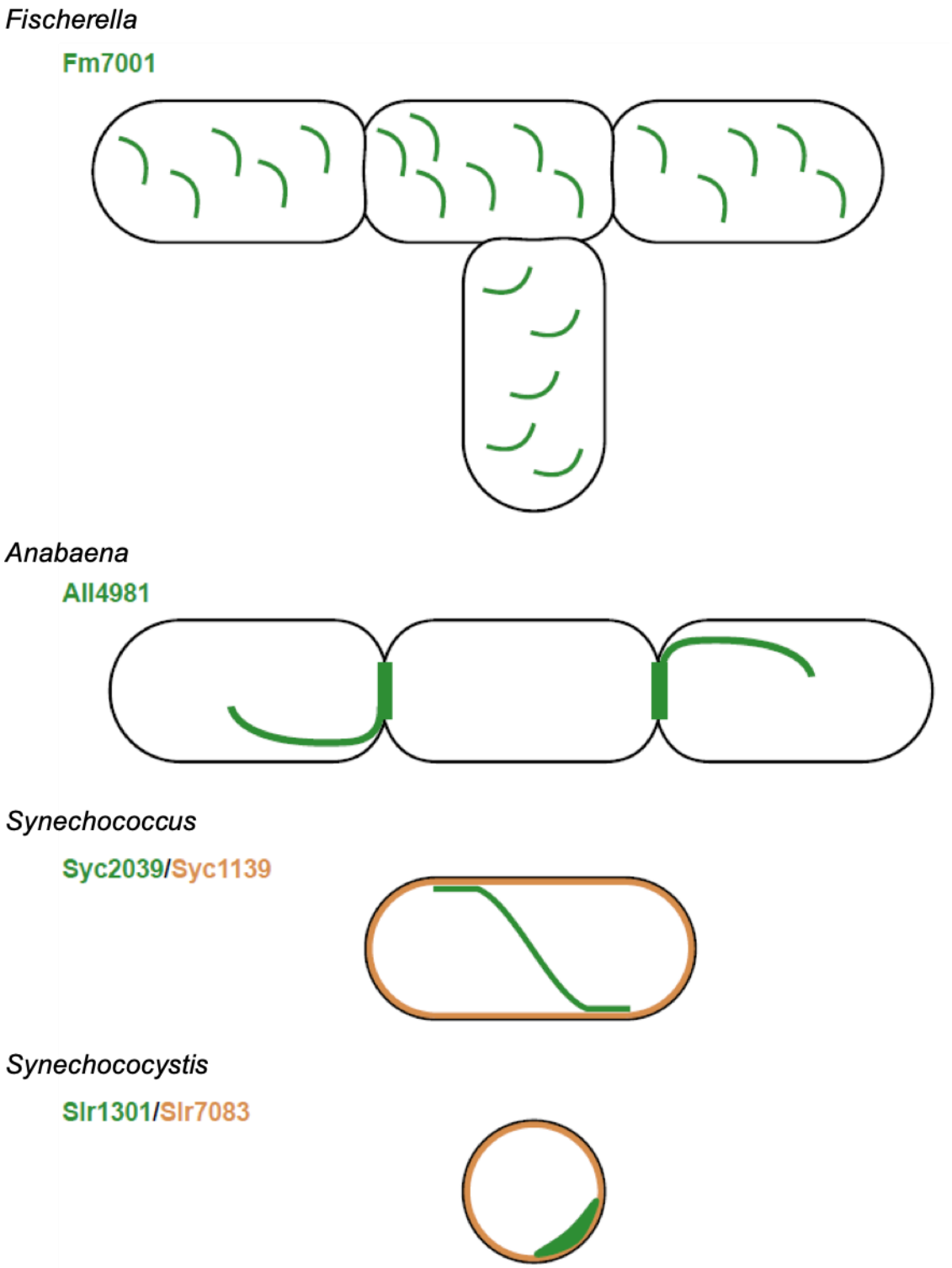

Fig. 7: Cyanobacterial CCRP systems

Schematic models for the *in vivo* localization of cyanobacterial CCRPs in their respective hosts. Fm7001 forms filamentous strings in *Fischerella*. In *Anabaena*, All4981 assembles into pole-arising filaments that traverse through the cell or forms septal-localized bridge-like formations. Syc2039, either independently of other *Synechococcus* proteins, or in direct cooperation with other filamentous proteins, forms long and sometimes helical strings that are often aligned with or in close proximity to the cell periphery. In *Synechococcus*, Syc1139 likely forms a protective proteinaceous layer below the cytoplasmic membrane. In *Synechocystis*, Slr1301 forms crescent-like structures while Slr7083 seemingly underlies the cytoplasmic membrane. Both localization types were also observed for PilB, suggesting a cooperative function.

Supplementary Information

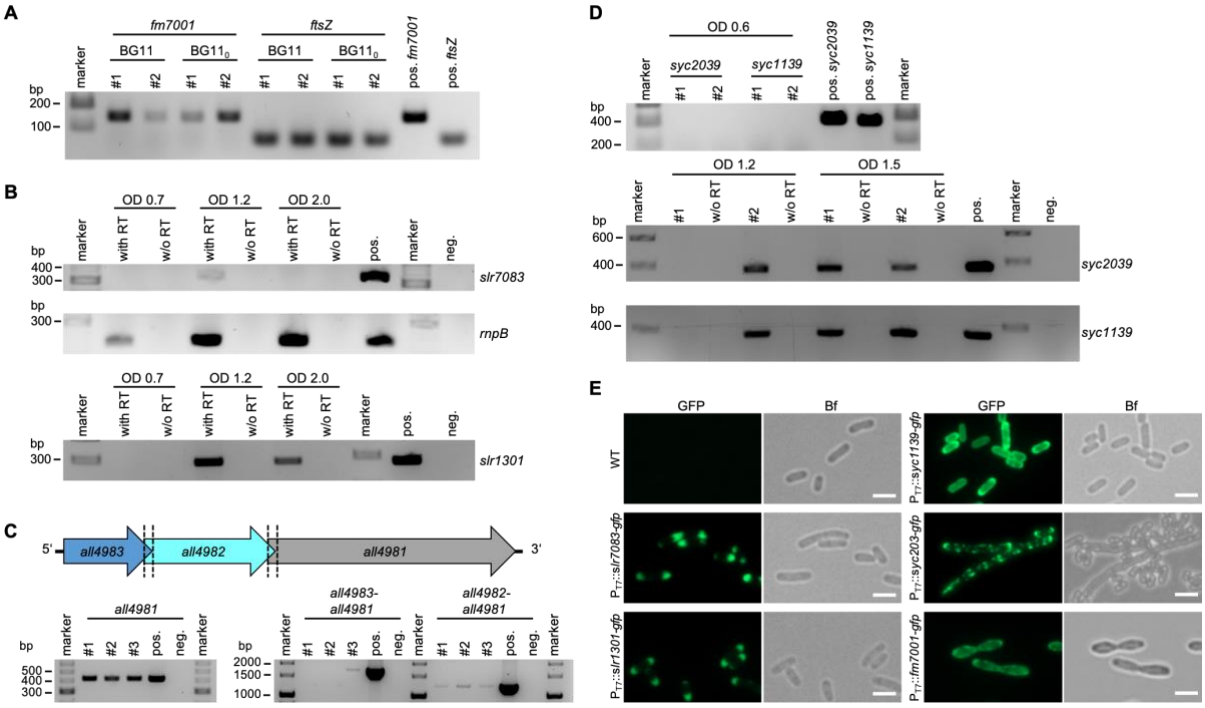

Supplementary Fig. 1: Expression of candidate CCRPs and heterologous expression in *E. coli*

(**A**) RT-PCR of reverse transcribed whole RNA from young *Fischerella* WT cultures grown in BG11 or $BG11_0$ from two independent biological replicates. Gene transcripts were verified using internal *fm7001* gene primers (#1/#2) or internal *ftsZ* gene primers (#3/#4) as a control. (**B**) RT-PCR of reverse transcribed whole RNA from *Synechocystis* WT (OD_{750} 0.7, 1.2 or 2.0) grown in BG11 using internal *slr7083* gene primers (#5/#6) or internal *slr1301* gene primers (#9/#10). Internal *rnpB* gene primers (#7/#8) were included as a control. (**C,** top) Schematic representation of the genomic context of *all4981*. The 3' end of *all4983* overlaps with 4 bp with the 5' region of *all4982*, which has the same overlap with the 5' end of *all4981*. Both overlaps are comprised of the same four nucleotides (ATGA). (**C**, bottom) RT-PCR of reverse transcribed whole RNA from *Anabaena* WT cultures grown in BG11 (OD_{750} 1.8) from three independent biological replicates. *all4981* gene transcript was internal gene primers (#15/#16). For operon structure of *all4983-all4981* or *all4982-all4981*, primer pairs #17/#16 or #18/#16 were used, respectively. Only one replicate showed a common transcript for an *all4983-all4981* operon, which is likely is the result of the long fragment (about 1800 bp). The employed cDNA synthesis kit is optimized for fragments up to 1000 bp, thus making longer reverse transcriptions unlikely. (**D**) RT-PCR of reverse transcribed whole RNA from *Synechococcus* WT (OD_{750} 0.6, 1.2 or 1.5) grown in BG11 from two independent biological replicates. Gene transcripts were verified using internal *syc2039* gene primers (#11/#12) and internal *syc1139* gene primers (#13/#14). (**B**,**D**) RNA was either reverse transcribed in the reaction buffer containing reverse transcriptase (with RT) or without reverse transcriptase (w/o RT) as a control for residual genomic DNA contamination. (**A**-**D**) Genomic DNA of the respective species was included as positive control for the different reactions. (**E**) GFP fluorescence and bright field micrographs of *E. coli* BL21 (DE3) cells expressing Slr7083-GFP, Slr1301-GFP, Syc1139-GFP, Syc2039-GFP or Fm7001-GFP. Cells were grown at 20 °C or (Fm7001-GFP) 16 °C and protein expression was induced with 0.05 mM IPTG for 24 h. Scale bars: 2.5 µm.

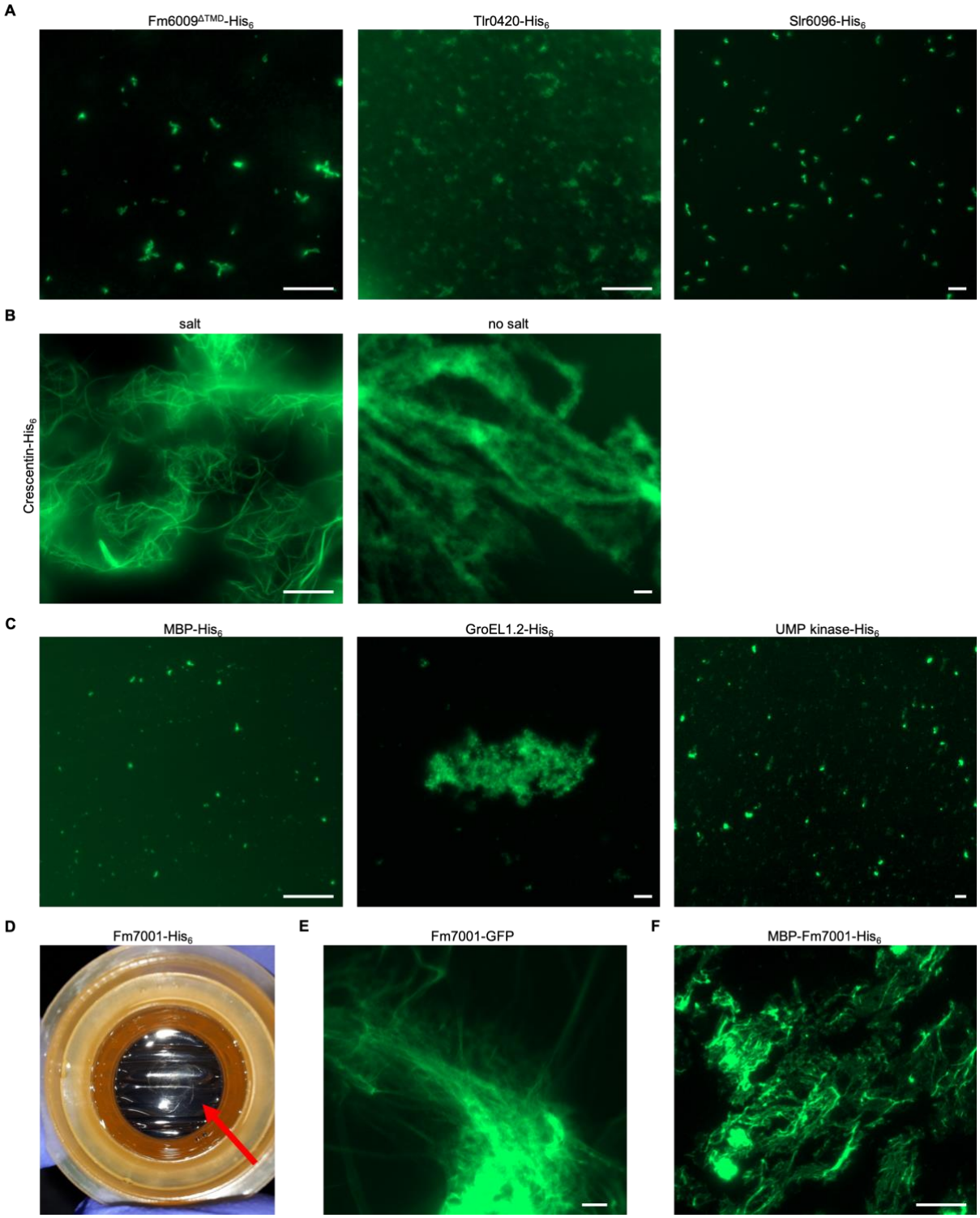

Supplementary Fig. 2: *In vitro* polymerization is dependent on monovalent ions

(A-C) NHS-fluorescein fluorescence micrographs of *in vitro* structures formed by purified and renatured Fm6009$^{\Delta TMD}$-His$_6$ (lacking the transmembrane domain, i.e. the first 91 aa), Tlr0420-His$_6$ or Slr6096-His$_6$ (1 mg ml^{-1} each), Crescentin-His$_6$ (0.7 mg ml^{-1}), MBP-His$_6$ (1 mg ml^{-1}), GroEL1.2 (0.7 mg ml^{-1}) or UMP kinase (0.5 mg ml^{-1}) , in HLB or Crescentin-His$_6$ (0.7 mg ml^{-1}) renatured in 25 mM Hepes, pH 7.4. Note: Crescentin-His$_6$ *in vitro* polymerization into smooth filaments is strictly dependent of the presence of salt in the renaturation buffer as Crescentin-His$_6$ without salt assembles into filamentous aggregates only. (**A**) Proteins were dialyzed in a stepwise urea-decreasing manner and stained with an excess of NHS-Fluorescein. (**D**) Bright field micrograph of a sheet-like flat object floating on top of the dialysate (red arrow) formed upon dialysis of Fm7001-His$_6$ (0.7 mg ml^{-1}) into 2 mM Tris-HCl, 4.5 M urea, pH 7.5. (**E,F**) Epifluorescence micrographs of filamentous structures formed by (**E**)

denatured cell-free extracts of *E. coli* BL21 (DE3) expressing Fm7001-GFP (0.7 mg ml^{-1} whole protein) dialyzed into 2 mM Tris-HCl, 3 M urea, pH 7.5 or by (**F**) natively purified MBP-Fm7001-His_6 (0.8 mg ml^{-1}) stained with NHS-fluorescein in HLB. Scale bars: 10 µm.

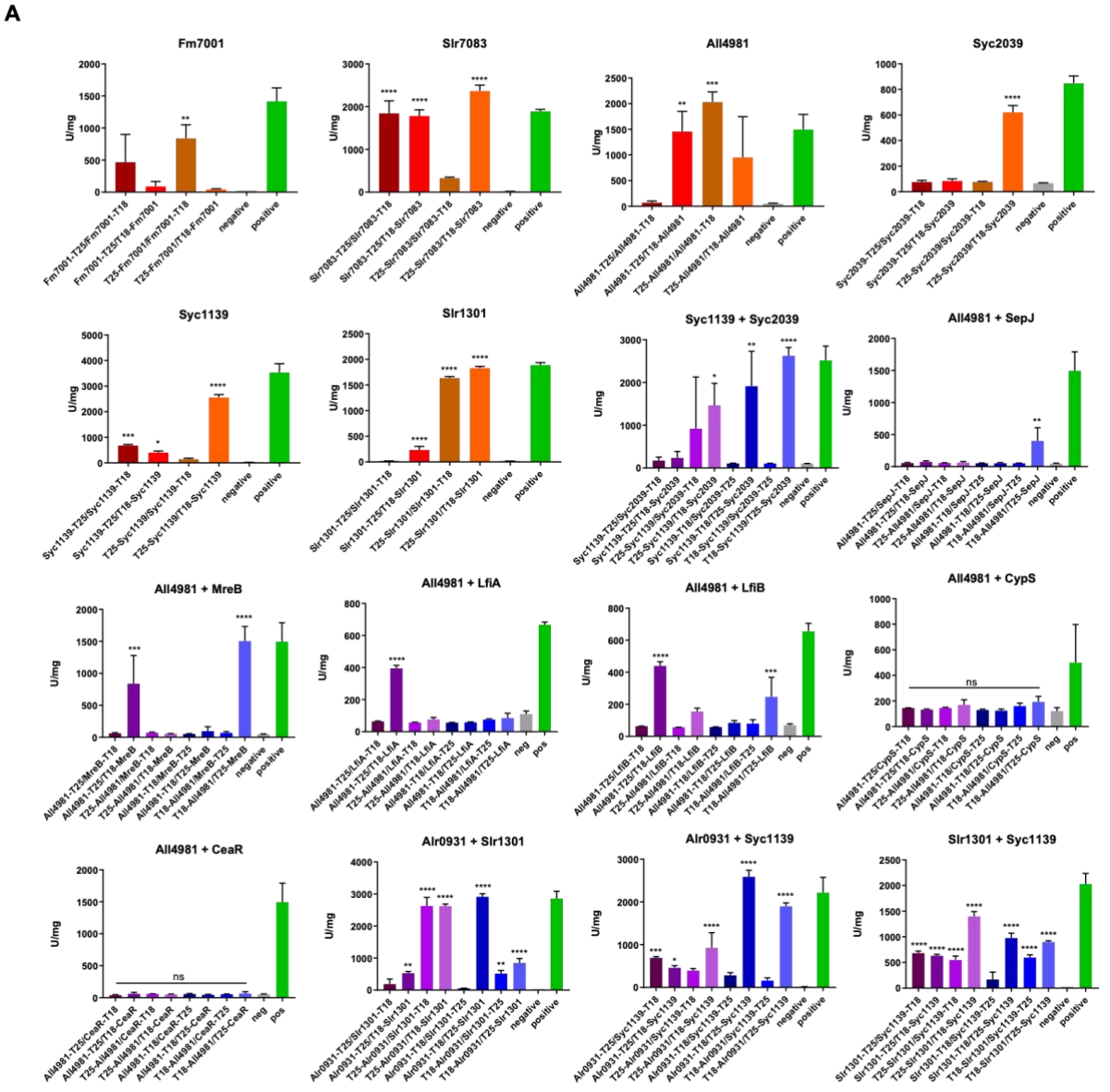

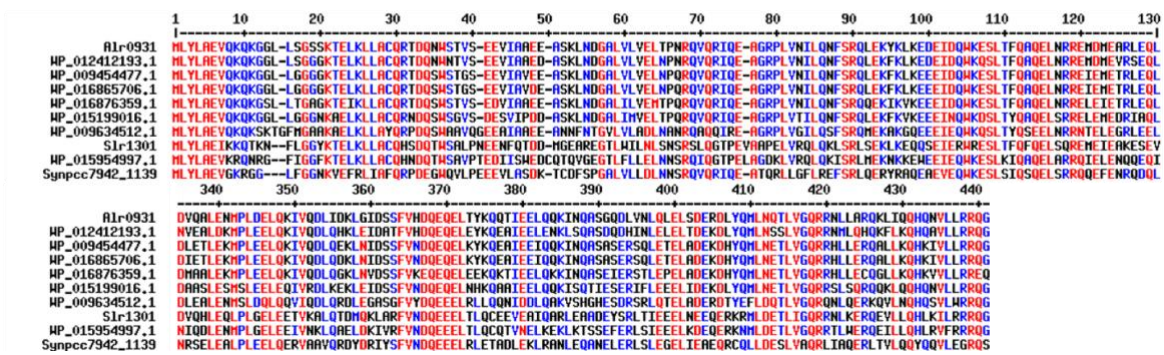

Supplementary Fig. 3: BACTH analysis of cyanobacterial CCRPs

(**A**) Beta-galactosidase assays (BACTH) of *E. coli* BTH101 cells co-expressing indicated T25 and T18 translational fusions of all possible pair-wise combinations from three independent colonies grown for 1 d at 30 °C or 2 d at 20 °C. Quantity values are given in Miller Units per milligram LacZ of the mean results from three independent colonies. Negative: N-terminal T25 fusion construct of the respective protein co-transformed with empty pUT18C. Positive: Zip/Zip control. Error bars indicate standard deviations (n=3). Values indicated with * are significantly different from the negative control. *: P < 0.05, **: P<0.01, ***: P<0.001, ****: P<0.0001 (one-way ANOVA using Dunnett's multiple comparison test). (**B**) Multiple sequence alignment of selected cyanobacterial homologous CCRPs using

MULTALIGN (Corpet, 1988). Alr0931 (termed CypS; *Anabaena*), Slr1301 (*Synechocystis*) and Synpcc7942_1139 (*Synechococcus*) are identified by their designated cyanobase locus tag. Other proteins are given as NCBI accession numbers. WP_012412193.1 (*Nostoc punctiforme* PCC 73102), WP_009454477.1 (*Fischerella thermalis* PCC 7521), WP_016865706.1 (*Fischerella*), WP_016876359.1 (*C. fritschii* PCC 9212), WP_015199016.1 (*Calothrix* sp. PCC 6303), WP_009634512.1 (*Synechocystis* sp. PCC 7509), and WP_015954997.1 (*Cyanothece* sp. PCC 7424). Amino acids from 1-130 and 334-441 are depicted. Red highlighted amino acid residues are conserved among all listed species, blue amino acids are mostly conserved, and black amino acids are not conserved. Characteristic for this group of conserved cyanobacterial CCRPs is a highly conserved N-terminus with a M-L-Y-L-A-E-V sequence motif present in nearly all homologs, followed by a moderately conserved N-terminal region of the first 120 amino acids. Two other highly conserved domains are present in this group, one located around the centre of the proteins (between the 340th and 370th amino acid), and another one shortly thereafter between the 400th and 420th amino acid.

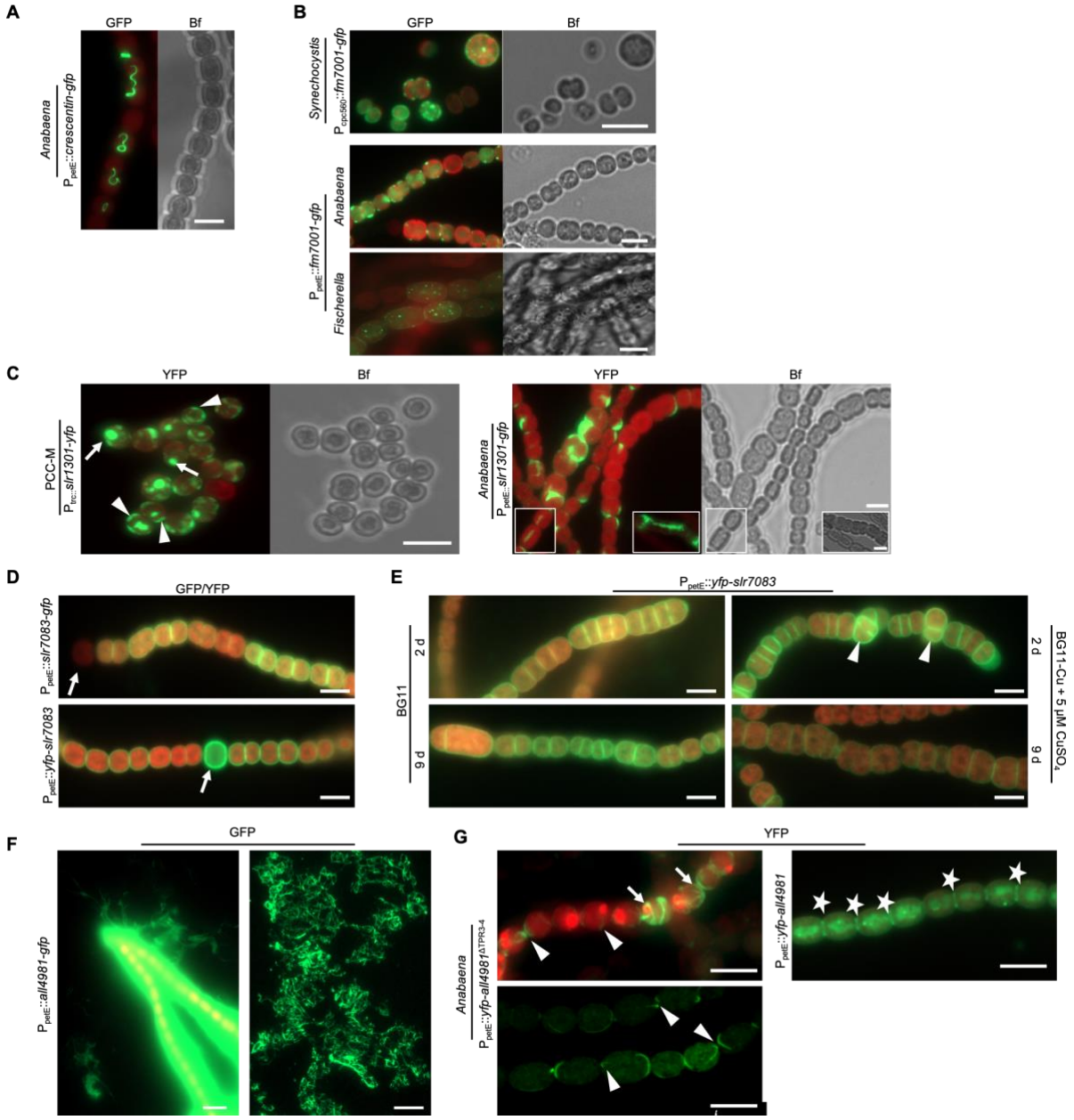

Supplementary Fig. 4: Expression of candidate CCRPs in different cyanobacterial species

GFP fluorescence, chlorophyll autofluorescence (red) and bright field micrographs of *Synechocystis*, *Anabaena* or *Fischerella* cells expressing (**A**) Crescentin-GFP, (**B**) Fm7001-GFP, (**C**) Slr1301-GFP, (**D**) Slr7083-GFP, (**E**) YFP-Slr7083, (**F**) All4981-GFP or (**G**) YFP-All4981$^{\Delta TPR3-4}$ or YFP-All4981 from P_{petE}, P_{trc}, or P_{cpc560}. (**B**) Unlike N-terminal fusion with a YFP tag, no *in vivo* filaments can be observed upon C-terminal fusion of Fm7001 with a GFP-tag in any tested cyanobacterium. (**C**) Besides intracellular filaments (figure inlays), Slr1303 accumulated at the periphery within *Anabaena* cells and induced a partial swollen cell phenotype. White triangles mark crescent-like localizations. White arrows show Slr1301-YFP accumulations. (**D**) *Anabaena* cells were grown on $BG11_0$ plates. White arrows indicate heterocysts. (**E**) *Anabaena* cells expressing YFP-Slr7083 from P_{petE} grown in liquid BG11 or liquid BG11 without copper and induced with 5 µM $CuSO_4$ for 2 and 9 d. White triangles point to multiseriate *Anabaena* trichome growth upon protein overexpression. (**F**) *Anabaena* cells expressing All4981-GFP from P_{petE} grown in BG11 supplemented with 0.5 µM $CuSO_4$ for 2 d. Extended period of overexpression of All4981-GFP led to cell rupture. Protein filaments released from the *Anabaena* trichome are shown in the left image while the right image shows extracellular (*ex vivo*) filaments observed in the growth medium. (**G**) *Anabaena* cells were grown in $BG11_0$ supplemented with 0.5 µM $CuSO_4$. White triangles indicate selected filaments traversing through the cells. White arrows point to spindle-like YFP-All4981$^{\Delta TPR3-4}$ filaments. White stars mark septal localizations. Scale bars: (**A**-**D**,**G**) 5 µm, (**F**, left) 10 µm or (**F**, right) 20 µm.

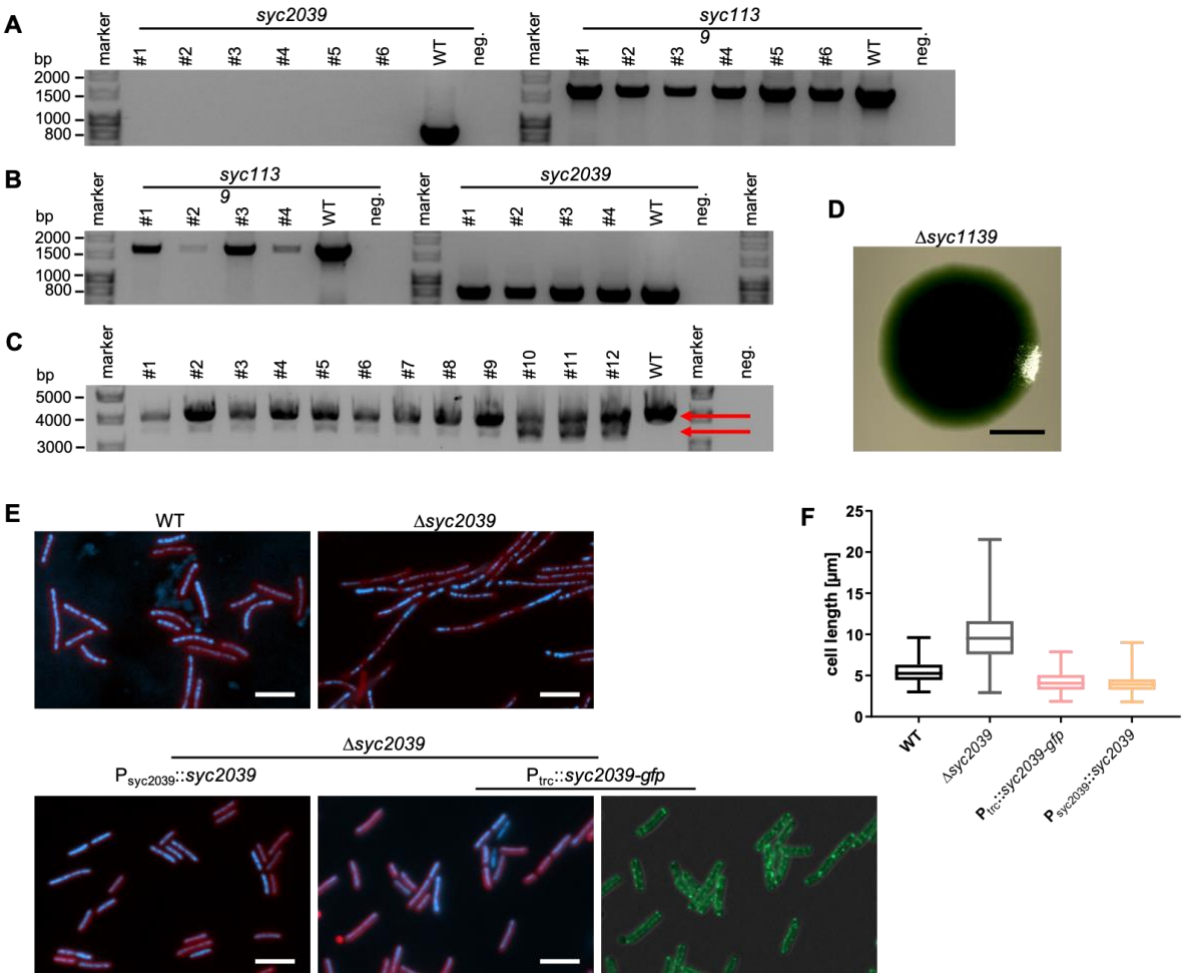

Supplementary Fig. 5: Verification of *Synechococcus* CCRP mutants

(**A**) Colony PCR of six Δ*syc2039* mutant clones using *syc2039* gene primers (#149/#147) and *syc1139* gene primers (#161/#162) as a control. (**B**) Colony PCRs of four non-segregated Δ*syc1139* mutant clones using *syc1139* gene primers (#174/#175) or *syc2039 gene* primers (#159/#160) as a control. (**C**) Colony PCR of twelve non-segregated Δ*syc1139* mutant clones using primers encompassing the homologous flanking regions used for homologous recombination (#238/#239). Upper red arrow indicates WT allele PCR product. Lower red arrow indicates Δ*syc1139* mutant PCR product. As a positive control, *Synechococcus* genomic DNA was included. (**D**) Growth of Δ*syc1139* mutant on non-selective plates leads to a reversal to WT phenotype. (**E**) Merged DAPI fluorescence and chlorophyll autofluorescence (red) and merged GFP fluorescence and bright field micrographs of *Synechococcus* WT, Δ*syc2039* mutant and Δ*syc2039* mutant complemented with $P_{syc2039}$::*syc2039* or P_{trc}::*syc2039-gfp* inserted into the neutral NS1 locus. Cells were grown in BG11 or BG11 supplemented with 0.001 mM IPTG (for strain carrying P_{trc}::*syc2039-gfp*) and stained with 10 µg ml^{-1} DAPI. (**F**) Cell length of *Synechococcus* WT (n=505), Δ*syc2039* mutant (n=517), Δ*syc2039* mutant carrying P_{trc}::*syc2039-gfp* (n=547) and Δ*syc2039* mutant carrying $P_{syc2039}$::*syc2039* (n=529) cells.

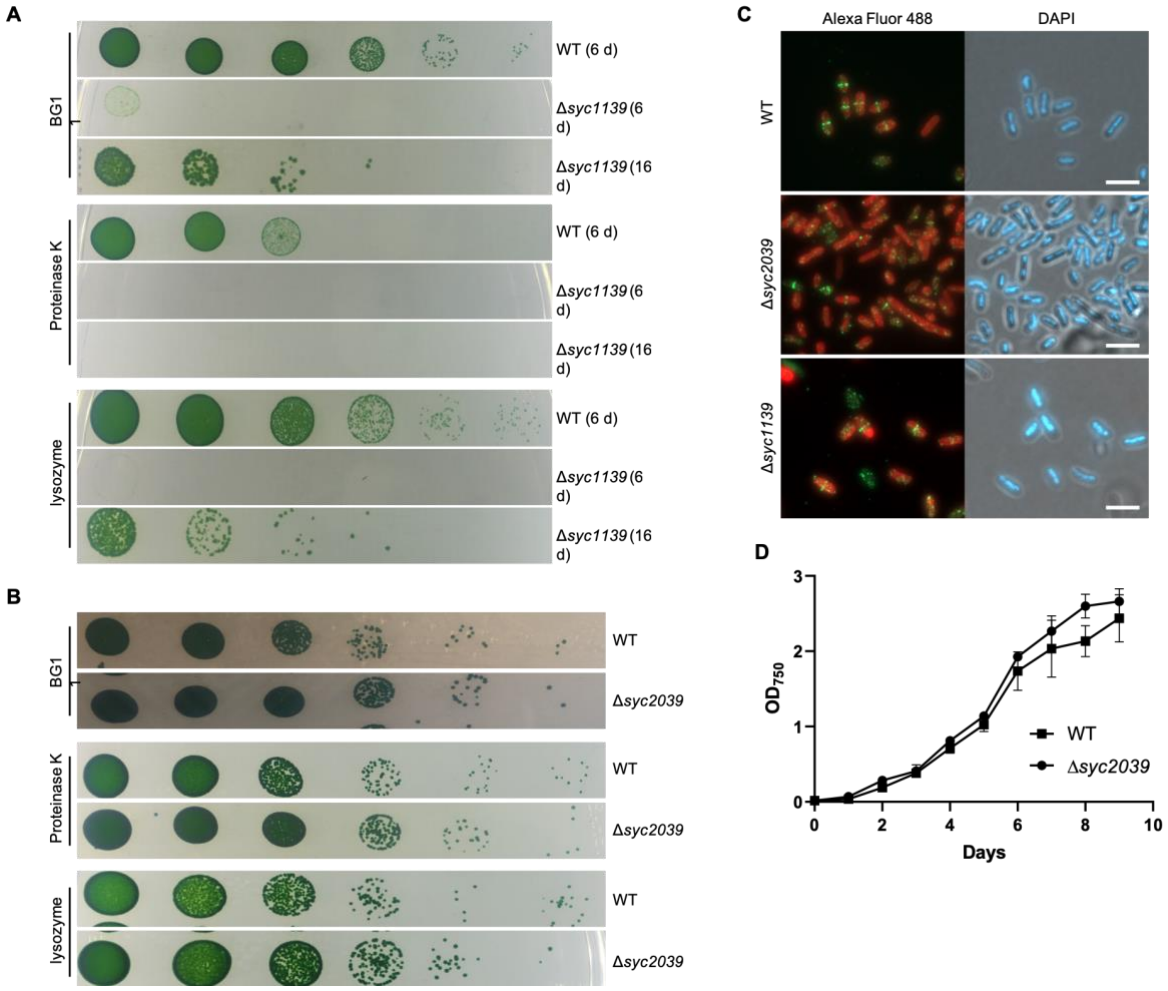

Supplementary Fig. 6: Phenotypic characterization of *Synechococcus* mutant strains

(**A**) *Synechococcus* WT (upper lane, after 6 days) and non-segregated Δ*syc1139* mutant (middle lane: after 6 days and lower lane after 16 days) strains were grown on BG11 plates or BG11 plates supplemented with 50 µg ml^{-1} Km. Cells were resuspended in BG11, adjusted to an OD_{750} of 0.4 and spotted in triplicates of serial 10-fold dilutions on BG11 plates or BG11 plates supplemented with 100 µg ml^{-1} Lysozyme or 50 µg ml^{-1} Proteinase K. Cells were grown until no further colonies arose in the highest dilution. (**B**) *Synechococcus* WT and Δ*syc2039* mutant strains were grown in liquid culture at standard growth conditions until an OD_{750} of about 2.0, diluted in BG11 to an OD_{750} of 0.4 and spotted in triplicates of serial 10-fold dilutions on BG11 plates or BG11 plates supplemented with 100 µg ml^{-1} Lysozyme or 50 µg ml^{-1} Proteinase K. Cells were grown until no further colonies arose in the highest dilution. (**C**) Merged Alexa Flour-488 fluorescence and chlorophyll autofluorescence (red) and merged bright field and DAPI fluorescence micrographs of *Synechococcus* WT, Δ*syc2039* or non-segregated Δ*syc1139* mutant strains grown on BG11 plates and subjected to immunofluorescence staining using an anti-FtsZ primary antibody (Agrisera, raised against *Anabaena* FtsZ) and an Alexa Fluor-488 coated secondary antibody. Cells were mounted in Prolong Diamond antifade mountant with DAPI (Thermo Fischer Scientific). Scale bars: 5 µm. (**D**) Growth curve of *Synechocystis* WT and Δ*syc2039* mutant strain. Cells were grown in BG11, adjusted to an OD_{750} of 0.1 and then grown in triplicates at standard growth conditions. OD_{750} values were recorded once a day for 9 d. Error bars show the standard deviation (n=3).

1234 **Supplementary Table 1: Properties of cyanobacterial CCRPs**

Gene /Locus tag	Genus	Subsection	Homologs distribution	Predicted proteins of similar structure (I-TASSER)	Homolog similarities	Conserved domains	Others
crescentin	*C. crescentus*	n/a	n/a	Cytoplasmic domain of bacterial cell division protein EzrA		SMC, CCDC158	IF-like CCRP
filP	*S. coelicolor*	n/a	n/a	Dynein tail; α-Actinin; Tropomyosin		DUF3552, SMC, RNase_Y	IF-like CCRP
desmin	*Homo sapiens*	n/a	n/a	PI4KIIIa lipid kinase		Filament (pfam00038), SMC, Spc7, MscS_TM	IF protein
vimentin	*Homo sapiens*	n/a	n/a	PI4KIIIa lipid kinase		Filament (pfam00038), SMC, Spc7	IF protein
syc2039	*Synechococcus*	I	I	Tropomyosin		SMC, MukB, CALCOCO1	N-terminal TMD; only in *Synechococcus* sp.
syc1139	*Synechococcus*	I	I, II, III, IV, V	Cytoplasmic domain of bacterial cell division protein EzrA	39%	SMC, MukB, Spc7	Homolog to *slr1301*
slr6096	*Synechocystis*	I	I, III, IV	Cytoplasmic domain of bacterial cell division protein EzrA		SMC	
slr7083	*Synechocystis*	I	I	Plectin		SMC, MscS_TM	Encoded on pSYSA plasmid, only in *Synechocystis* sp.
slr1301	*Synechocystis*	I	I, II, III, IV, V	Cytoplasmic domain of bacterial cell division protein EzrA	39%	SMC, SbcC, APG6, DUF3552	Homolog to *syc1139*
tlr0420	*BP-1*	I	I, III	Plectin		SMC, MscS_TM	
fm7001	*Fischerella*	V	IV, V	α-catenin or vinculin; similarity to acyl-CoA dehydrogenase	63%	Acetyl-CoA carboxylase carboxyl transferase (PLN0322)	Highly expressed; 3' end 9 bp overlap to *fm7000*
fm6009	*Fischerella*	V	V	Structure of β-catenin and HTCF-4		COG0610	
all4981	*Anabaena*	IV	III, IV, V	TTC7B/Hyccin Complex, Clathrin	47%	TPR	5' with a 4 bp overlap to *all4982*

The first column indicates the respective gene name or locus tags of each protein candidate. The second and third column indicate the respective subsection of the corresponding cyanobacterial genus. Column four lists the subsections that contain homologous proteins to the respective CCRP. Column five indicates structural similarities of the candidate to proteins in the Protein Data Bank (PDB) based on I-TASSER (Zhang, 2009; Yang and Zhang, 2015). The sixth column lists predicted sub-domains of protein candidates identified by BLAST Conserved Domain Search. Column seven names other features of interest. Abbreviations: (TMH) Transmembrane helix; (DUF) Domain of unknown function; (CCDC158) Coiled-coil domain-containing protein 158; (SMC) Structural maintenance of chromosomes; (MukB) The hinge domain of chromosome partition protein MukB; (APG6) Autophagy protein Apg6, (SbcC) DNA repair exonuclease SbcCD ATPase; (CALCOCO1) Calcium binding and coiled-coil domain; (Spc7) Spc7 kinetochore protein; (Filament) Intermediate filament protein; (TPR): Tetratricopeptide repeat; (PLN0322) Acetyl-CoA carboxylase carboxyl transferase; (COG0610) Type I site-specific restriction-modification system. *Anabaena* CCRPs CypS, LfiB, CeaR, Alr4393 and All4935 (Springstein *et al.*, 2019) also revealed structural similarities to EzrA. n/a: not applicable.

1243 **Supplementary Table 2: Bacterial strains**

Strain	Genotype	Resistance	Reference
E. coli XL1 blue	*endA*1 *gyrA*96(nal^R) thi-1 *recA*1 *relA*1 *lac gln*V44 F'[::Tn10 *proAB*$^+$ *lacI*^{q} Δ(*lacZ*)M15] *hsd*R17(r$_K^-$ m$_K^+$)	Tet	Stratagene
E. coli HB101	F$^-$ *mcrB mrr hsd*S20(r$_B^-$ m$_B^-$) *recA*13 *leuB*6 *ara*-14 *proA*2 *lacY*1 *galK*2 *xyl-5 mtl*-1 *rpsL*20(Sm^R) *gln*V44 λ$^-$	Sm	(Boyer and Roulland-Dessoix, 1969)
E. coli DH5α	F– Φ80*lacZ*ΔM15 Δ(*lacZ*YA-*arg*F) U169 *recA*1 *endA*1 *hsdR17* (rK–, mK+) *phoA supE*44 λ– *thi*-1 *gyrA*96 *relA*1		(Meselson and Yuan, 1968)
E. coli DH5αMCR	F- *endA*1 *supE*44 *thi-1* λ$^-$ *recA1 gyrA*96 *relA*1 *deoR* Δ(*lacZYA-argF*)U169 Φ80d*lacZ*ΔM15 *mcrA* Δ(*mrr hsdRMS mcrBC*)		(Grant *et al.*, 1990)
E. coli BL21 (DE3)	F$^-$ *ompT gal dcm lon hsdS$_B$*(*r$_B^-$m$_B^-$*) λ(DE3 [*lacI lacUV5-T7p07 ind1 sam7 nin5*]) [*malB*$^+$]$_{K-12}$(λ^S)		(Studier and Moffatt, 1986)s
E. coli BTH101	F$^-$, *cya-99*, *araD139*, *galE15*, *galK16*, *rpsL1* (*Str$_r$*), *hsdR2, mcrA*, *mcrB1*	Sm	Euromedex
Fischerella muscicola PCC 7414	WT		PCC, France
Synechocystis sp. PCC 6803	Glucose tolerant Kazusa substrain WT		PCC, France
BLS4	Δ*slr1301*::CS.3	Sm,Sp	This study
BLS5	Δ*slr7083*::CS.3	Sm,Sp	This study
Synechocystis sp. PCC-M 6803	Glucose tolerant and motile Moscow PCC-M substrain WT		A gift from Annegret Wilde (University Freiburg)
BLS6	Δ*slr1301*::CS.3	Sm,Sp	This study
BLS7	Δ*slr7083*::CS.3	Sm,Sp	This study
Synechococcus elongatus PCC 7942	WT		A gift from Martin Hagemann (University Rostock)
BLS8	Non-segregated Δ*syc2039*::*nptII*	Km	This study
BLS9	Δ*syc2039*::*nptII*	Km	This study
Anabaena sp. PCC 7120	WT		PCC, France

1244

1245 **Supplementary Table 3: Oligonucleotides and Plasmids**

#	Given name	Sequence 5' -> 3'	Purpose
1	Fm7001_intern_A	AGCGGGAAGATGGCTACTATC	RT-PCR
2	7001_northern	TCTGCGGCTTGACTTGATAC	RT-PCR
3	qftsZ7414_fwd	TGGAACTAAAGCTGCCGAGG	RT-PCR
4	qftsZ7414_rev	CTGTACCAGTTCCACCACCC	RT-PCR
5	Syn017_intern_A	TGCAACAGCAAACGGAACAG	RT-PCR
6	Syn017_intern_B	TTGGGAGCTAACTTGCCCAC	RT-PCR
7	rnpb 6803 primer fwd	GGAGTTGCGGATTCCTGTCA	RT-PCR
8	rnpb 6803 primer rev	AAGACCAACCTTTGCCCCTC	RT-PCR
9	Syn708_intern_A	TGGAGTGCCCTGCCTAACG	RT-PCR
10	Syn708_intern_B	CCCTTCTAACCTTTGTCGGGC	RT-PCR
11	Syc484_intern_A	CTACCATTCTTGGTGTGGCGG	RT-PCR
12	Syc484_intern_B	GAAATCCTGCGATCGCTGTTG	RT-PCR
13	Syc879_intern_A	CCTGTGACTTCTCTCCAGGG	RT-PCR
14	Syc879_intern_B	CTTTTAACTCGCGATCGCGGC	RT-PCR
15	Nos389_intern_A	ATCACCTGAATTAGCTGCGG	RT-PCR
16	Nos389_intern_B	CTAATAATGCCGCAATCAGCG	RT-PCR
17	All4982_intern_A	ATCAGATGGTGGAGGGAAGC	RT-PCR
18	All4983_intern_A	AGTAGCTGCATTTATCGGTGC	RT-PCR
19	pET19bmod-Fwd	GGAATTGTGAGCGGATAACAATT	Sequencing of pET21a(+) inserts
20	T7R	CTAATACGACTCACTATAGGGA	Sequencing of pET21a(+) inserts
21	pAM2991_Seq_A	GCGCCGACATCATAACGGTTC	Sequencing of pAM2991 inserts
22	pAM2991_Seq_B	GCTGAAAATCTTCTCTCATCCGCC	Sequencing of pAM2991 inserts
23	pRL153_Seq_Rev	AGGAGATTAACCCGCCCAAG	Sequencing of pRL153 inserts
24	CS3_Seq_Fwd	CGCGCAGATCAGTTGGAAG	Sequencing of gene replacement plasmids
25	CS3_Seq_Rev	AACGTCGGTTCGAGATGGC	Sequencing of gene replacement plasmids
26	GFP_Seq_Rev	TTGTGCCCATTAACATCACCATC	Sequencing of GFP containing plasmids
27	pJET1.2 forward sequencing primer	CGACTCACTATAGGGAGAGCGGC	Sequencing of pJET1.2 inserts
28	pJET1.2 reverse sequencing primer	AAGAACATCGATTTTCCATGGCAG	Sequencing of pJET1.2 inserts
29	pKO_Seq_Fwd	GCCTTTTTACGGTTCCTGGC	Sequencing pTHS121

30	pKO_Seq_Rev	TCTTTTCTACGGGGTCTGACG	Sequencing pTHS121
31	pIGA_Seq_Fwd	TGCGCATAGAAATTGCATCA	Sequencing of pIGA inserts
32	pIGA_Seq_Rev	GTCAGCAACACCTTCTTCA	Sequencing of pIGA inserts
33	pRL271_Seq_Fwd	GCCTGGTGCTACGCCTGAATA	Sequencing of pRL271 inserts
34	pRL271_Seq_Rev	CCAGTTAATAGTTTGCGCAACGTTG	Sequencing of pRL271 inserts
35	pRL278_Seq_Fwd	GGGGCGTAATTTTTTTAAGGCAGTTATTG	Sequencing of pRL278 inserts
36	pSL2680_Seq_A	CAAGAGGGCAAAAAACTCAATTTG	Sequencing of pSL2680 inserts
37	cpf1_1A	TTGGTCATGAGATTATCAAAAAGGATCCT GGAAAACGTTCTTCGGGGC	Amplification of *cpf1* for pTHS123
38	pRL25c_CRISPR_2 B	AGGCCCTTTCGTCTTCAAGAATTCTTTAC ACTGATGAATGTTCCGTTGCG	Amplification of *cpf1* for pTHS123
39	cpf1-1	CTCCAGAAGCTATAAACTATGAAC	Sequencing of *cpf1*
40	cpf1-2	CTACTTCAAGCTAGTGCGGAA	Sequencing of *cpf1*
41	cpf1-3	GTTGAAAATCAAGGCTACAAACTAAC	Sequencing of *cpf1*
42	cpf1-4	CGTTTCAAGGTAGAGAAGCAGG	Sequencing of *cpf1*
43	pRL25c_Seq_Fwd	CTTTGATCTTTTCTACGGGGTCT	Sequencing of pRL25C inserts
44	pRL25c_Seq_Rev	TTGAGGTGAGGGATGAGCG	Sequencing of pRL25C inserts
45	pMAL_Seq_Fwd	AGAAAGGTGAAATCATGCCG	Sequencing of pMAL-c2x inserts
46	pMAL_Seq_Rev	CTGCAAGGCGATTAAGTTGG	Sequencing of pMAL-c2x inserts
47	MB_Seq_A	GGCTCGTATGTTGTGTGG	Sequencing of pKNT25, pKT25 and pUT18 inserts
48	MB_Seq_B	GGCTTAACTATGCGGCATC	Sequencing of pKNT25, pUT18 and pUT18C inserts
49	MB_Seq_C	TAACGCCAGGGTTTTCCCA	Sequencing of pKT25 inserts
50	pKNT25_Seq_Rev	CGTTTGCGTAACCAGCC	Sequencing of pKNT25 inserts
51	pKT25_Seq_Fwd	GATTCGGTGACCGATTACCTG	Sequencing of pKT25 inserts
52	pUT18_Seq_Rev	GATGCGTTCGCGATCCAG	Sequencing of pUT18 inserts

53	pUT18C_Seq_Fwd	TCGCCGGATGTACTGGAAAC	Sequencing of pUT18C inserts
54	N-term_1A	GAGGATCCCCGGGTACC	Amplification of pKNT25 and pUT18
55	N-term_1B	TAGAGTCGACCTGCAGGCA	Amplification of pKNT25 and pUT18
56	pKT25_1A	CCCCGGGTACCTAAGTAAGTAAG	Amplification of pKT25
57	pKT25_1B	ATCCTCTAGAGTCGACCCTGC	Amplification of pKT25
58	pUT18C_1A	CCGAGCTCGAATTCATCGAT	Amplification of pUT18C
59	pUT18C_1B	TACCCGGGGATCCTCTAGAGT	Amplification of pUT18C
60	pET21a_1A	CACCACCACCACCACCAC	Amplification of pET21a(+) for gfp fusions
61	pET21a_1B	ATGTATATCTCCTTCTTAAAGTTAAACAAA ATTATTTCTAGAGG	Amplification of pET21a(+) for gfp fusions
62	pRL271_Fwd	GAGCTCGCGAAAGCTTGCATG	Amplification of pRL271 and pRL278
63	pRL271_Rev	CTCGAGATCTAGATATCGAATTTCTGCCA T	Amplification of pRL271
64	pRL278_Rev	CCGCTTATTATCACTTATTCAGGCG	Amplification of pRL278
65	pETM22_Vec_R	ATGTTTTTCGTATTTTCCCTACCAGAAGAA TGATGATGATGATGG	Amplificaiton of pETM22
66	pETM22_Vec_F	TGGATGAACTATACAAATAAATCCGGCTG CTAACAAAGC	Amplificaiton of pETM22
67	Vector.FOR	TGATGTTCAACTTCGACAGCGAATTCCTC GACCTGCAGGG	Amplification of pIGA
68	Vector.REV	AGGGACTCTTCTCTACAGGTGGTACCCC GGGTTCGAAATCG	Amplification of pIGA
69	YFP_pcpc560_2A	CATAAAGTCAAGTAGGAGATTAATTCAAT GCTGAGCAAGGGCGA	Amplification of YFP with overhang to P_{cpc560}
70	YFP_2A	TACAGGTTAGGAGAACGCCATGCTGAGC AAGGGCG	Amplification of YFP
71	YFP-Myc_2B	CAGATCCTCTTCAGAGATGAGTTTCTGCT CCTTGTACAGCTCGTCCATGC	Amplification of YFP with C-terminal *myc*
72	Myc+Linker_2B	TCCTGAACCCGATCCAGAGCCCAGATCC TCTTCAGAGATGAGTTTC	Amplification of YFP with C-terminal *myc* and a GSGSGSG linker

73	XIII-GFP_1A	GCTAGCGACTCGACCGGTTC	Amplification of pRL153
74	XIII-GFP_1B	GCTTAATTTCTCCTCTTTAATTCTAGGTAC CCG	Amplification of pRL153
75	eYFP_MYC_3A	GAGCAGAAACTCATCTCTGAAGAGGATCT GATGCTGAGCAAGGGCGAG	*yfp* for pTHS82
76	eYFP_3B	AACCGGTCGAGTCGCTAGCTTACTTGTAC AGCTCGTCCATGC	*yfp* for pTHS82
77	GFP_pAM2991_2B	GCCTGCAGGTCGACTCTAGATTATTTGTA TAGTTCATCCATGCCATGTG	*syc1139-gfp* for pTHS74
78	His_pAM2991_2B	GCCTGCAGGTCGACTCTAGATCAGTGGT GGTGGTGGTG	*syc2039-gfp-his* for pTHS75
79	CS.3_Fwd	GATCCGTGCACAGCACCTTG	Amplification of CS.3 cassette
80	CS.3_Rev	TTATTTGCCGACTACCTTGGTGATCT	Amplification of CS.3 cassette
81	nptII_Fwd	ATGATTGAACAAGATGGATTGCACG	Amplification of nptII
82	nptII_Rev	TCAGAAGAACTCGTCAAGAAGGCG	Amplification of nptII
83	pUC_ori_Fwd	TTGAGATCCTTTTTTTCTGCGCGTAATC	Amplification of pUC origin
84	pUC_ori_Rev	TTTCCATAGGCTCCGCCCC	Amplification of pUC origin
85	nptII_A	AAGCTTCACGCTGCCGCAA	Amplification of P_{nptII}::*nptII*
86	nptII_B	TCAGAAGAACTCGTCAAGAAGGCG	Amplification of P_{nptII}::*nptII*
87	GFP_pET21a_2B	AGTGGTGGTGGTGGTGGTGTTTGTATAG TTCATCCATGCCATGTGTAATC	Amplification of *gfp*-fusions for insertion into pET21a(+)
88	7001_EcoRI_Fwd	GCATGAATTCAGGGAAAATACGAAAAACA TTG	*fm7001* for pTHS73
89	7001_His_PstI_R	GCTACTGCAGTCAGTGGTGATGGTGATG ATGGACTAAGGCAGTCATTAAATAGT	*fm7001* for pTHS73
90	Fragment 1.FOR	GATTTCGAACCCGGGGTACCACCTGTAG AGAAGAGTCCCTGAATATCAA	P_{cpc560} for pTHS60
91	Fragment 1.REV	TTTTTCGTATTTTCCCTCATTGAATTAATC TCCTACTTGACTTTATGAGTTGGGA	P_{cpc560} for pTHS60
92	Fragment 2.FOR	TCAAGTAGGAGATTAATTCAATGAGGGAA AATACGAAAAACATTGGAGT	*fm7001* for pTHS60
93	Fragment 2.REV	GCACTAGCAGATGCACTAGCGACTAAGG CAGTCATTAAATAGTGAAGTAAGTAATTAA AGTAAC	*fm7001* for pTHS60
94	Fragment 3.FOR	ATTTAATGACTGCCTTAGTCGCTAGTGCA TCTGCTAGTGCTAGT	*gfp*-tagged genes for pTHS60
95	Fragment 3.REV	CCGACAATCCAAACACCGGTTTATTTGTA TAGTTCATCCATGCCATGTGTAATCC	*gfp*-tagged genes for pTHS60

96	Fragment 4.FOR	TGGATGAACTATACAAATAAACCGGTGTT TGGATTGTCGG	T_{rbcL} for pTHS60
97	Fragment 4.REV	CCCTGCAGGTCGAGGAATTCGCTGTCGA AGTTGAACATCAGTAAGC	T_{rbcL} for pTHS60
98	TrbcL_A	ACCGGTGTTTGGATTGTCGG	Amplification of pIGA containing P_{cpc560} and T_{rbcL} for pTH76
99	pIGA_Pcpc560_1B	TGAATTAATCTCCTACTTGACTTTATGAGT TGGG	Amplification of pIGA containing P_{cpc560} and T_{rbcL} for pTH76
100	YFP_pcpc560_2A	CATAAAGTCAAGTAGGAGATTAATTCAAT GCTGAGCAAGGGCGA	*yfp-fm7001* for pTHS76
101	7001_TrbcL_2B	CCGACAATCCAAACACCGGTTCAGACTAA GGCAGTCATTAAATAGTGAAG	*yfp-fm7001* for pTHS76
102	7001F_BamHI	ACTGGATCCAGGGAAAATACGAAAAACAT TGGA	*fm7001* for pTHS63
103	7001R_NotI	AGCGGCCGCTCAGACTAAGGCAGTCATT AAATAGTG	*fm7001* for pTHS63
104	7001F_BamHI	GGATCCTATGAGGGAAAATACGAAAAAC	*fm7001* for pTHS95, pTHS96, pTHS97 and pTHS98
105	7001R_EcoRI	AGCGAATTCTCAGACTAAGGCAGTCAT	*fm7001* for pTHS96 and pTHS98
106	7001R_SacI	GAGCTCCTGACTAAGGCAGTCATTA	*fm7001* for pTHS95 and pTHS97
107	7120petER_7001ol	GTATTTTCCCTCATACCTGTAGTTTTATTT TTCTTATTTC	*petE* for pTHS83 (overlap PCR)
108	7001F_petEol	AAAACTACAGGTATGAGGGAAAATACGAA AAAC	*fm7001* for pTHS83 (overlap PCR)
109	7001R_SacI_C	AGCGAGCTCTAAGGCAGTCATTAAATAGT G	*fm7001* for pTHS83
110	7001F_NheI	AACTGCTAGCAGGGAAAATACGAAAAAC	*fm7001* for pTHS83
111	7001_3A	CTCTGGATCGGGTTCAGGAATGAGGGAA AATACGAAAAACATTGG	*fm7001* for pTHS84
112	7001_3B	CCTTTCGTCTTCAAGAATTCTTCAGACTAA GGCAGTCATTAAATAGTG	*fm7001* for pTHS84
113	pRL271_7up_F	AGAAATTCGATATCTAGATCTCGAGAGCA ATGTGAGTGAGTTCGTGAGC	Upstream homology for pTHS126
114	7001KO_1B	GTGCTTGCGGCAGCGTGAAGCTTGGGGT TATCCTTAATAGAAGAAGAGTGC	Upstream homology for pTHS126
115	7001KO_2A	CGCCTTCTTGACGAGTTCTTCTGAATCAA GAGCATTCTTGATTTCTGTCTCA	Downstream homology for pTHS126

116	pRL271_7down_R	CAGGCATGCAAGCTTTCGCGAGCTCTGC TACCAAGACGATGCGTTTCATGTC	Downstream homology for pTHS126
117	7001KO_2A2	AATTCGATATCTAGATCTCGAGTTGCGTT TCAAAACACTACAAATTAGTACAAAC	Upstream homology for pTHS127
118	7001KO_2B2	AAGGTGCTGTGCACGGATCGGGGTTATC CTTAATAGAAGAAGAGTGC	Upstream homology for pTHS127
119	7001KO_4A2	CAAGGTAGTCGGCAAATAAATCAAGAGCA TTCTTGATTTCTGTCTC	Downstream homology for pTHS127
120	7001KO_4B2	TGCAAGCTTTCGCGAGCTCCTGAAGACA AAGATGAAGTTTCGATATTACC	Downstream homology for pTHS127
121	trunc7001_2A	CTGAATAAGTGATAATAAGCGGTTGCGTT TCAAAACACTACAAATTAGTACAAA	Truncated *fm7001* for pTHS128
122	trunc7001_2B	TGCAAGCTTTCGCGAGCTCGTATTGATAC TGGGTTGAGAATACTGC	Truncated *fm7001* for pTHS128
123	7001_gRNA_A	AGATGAGTTTTGCACAAAGTTGGA	*fm7001* gRNA for pTHS121 and pTHS123
124	7001_gRNA_B	AGACTCCAACTTTGTGCAAAACTC	*fm7001* gRNA for pTHS121 and pTHS123
125	Fm7001_HL1A	TTGTCTAGCTTTAATGCGGTAGTTGGTAC CAGGAACATCGCGTCTCTACC	Downstream homology repair template for pTHS121 and pTHS123
126	Fm7001_HL1B	AAGAATGCTCTTGATGGGGTTATCCTTAA TAGAAGAAGAGTGC	Upstream homology repair template for pTHS121 and pTHS123
127	Fm7001_HL2A	TATTAAGGATAACCCCATCAAGAGCATTC TTGATTTCTGTCTC	Upstream homology repair template for pTHS121 and pTHS123
128	Fm7001_HL2B	GATTACAGATCCTCTAGAGTCGACGGTAC CTAAGGCAGCAACGTTTTCCG	Downstream homology repair template for pTHS121 and pTHS123
129	Syn017_NdeI_fwd	GCTACATATGACAAGTCAAAATTTTGTTTC TGAT	*slr7083* for pTHS61
130	Syn017_XhoI_wo_rev	GCTACTCGAGTGGTAAATAAGGGGGAGT GG	*slr7083* for pTHS61
131	pIGA_V_017_R	ACAAAATTTTGACTTGTCATTGAATTAATC TCCTACTTGACTTTATGAGTTGG	Amplification of pIGA with P_{cpc560} and T_{rbcL} for pTHS77

132	pIGA_V_017_F	CCACTCCCCCTTATTTACCAGCTAGTGCATCTGCTAGTGCT	Amplification of pIGA with P_{cpc560} and T_{rbcL} for pTHS77
133	pIGA_Syn017_F	TCAAGTAGGAGATTAATTCAATGACAAGTCAAAATTTTGTTTCTGATCAAG	*slr7083* for pTHS77
134	pIGA_Syn017_R	GCACTAGCAGATGCACTAGCTGGTAAATAAGGGGGAGTGGGAC	*slr7083* for pTHS77
135	Syn017_pRL25c_F	TAAAACTACAGGTTAGGAGAACGCCATGACAAGTCAAAATTTTGTTTCTGATCAAGATACC	*slr7083* for pTHS86
136	Syn017_pRL25c_R	CACTAGCACTAGCAGATGCACTAGCTGGTAAATAAGGGGGAGTGGGACG	*slr7083* for pTHS86
137	017_up_Fwd	GTCAGGGGGGCGGAGCCTATGGAAATTTCCCAACAAATTAGTGAATGGCAGG	Upstream homology for pTHS120
138	017_up_Rev	CGTGCAATCCATCTTGTTCAATCATTGTTTTACCAGATTAAAATTAATGATTGAGACAGAATTGAAAAG	Upstream homology for pTHS120
139	017_down_Fwd	TCGCCTTCTTGACGAGTTCTTCTGAGATTTCCAGTCACTTCCGTTTTTTTACTATTAGG	Downstream homology for pTHS120
140	017_down_Rev	TACGCGCAGAAAAAAAGGATCTCAAAATCCTAAAATTCGTGGTTCATCTTTCTTTGT	Downstream homology for pTHS120
141	Syn017_3A	CTCTGGATCGGGTTCAGGAATGACAAGTCAAAATTTTGTTTCTGATC	*slr7083* for pTHS85
142	Syn017_3B	CCTTTCGTCTTCAAGAATTCTCTATGGTAAATAAGGGGGAGTGGG	*slr7083* for pTHS85
143	Syn017_pET_2A	GTTTAACTTTAAGAAGGAGATATACATATGACAAGTCAAAATTTTGTTTCTGATCAAG	*slr7083* for pTHS69
144	017_Seq_A	CCACAGCGGAAACCTTTTTAGATC	Sequencing of Δ*slr7083* plasmids
145	017_Seq_B	AAACGAACAGAGTGGAACTTTGC	Sequencing of Δ*slr7083* plasmids
146	Syc484_2A	GTTTAACTTTAAGAAGGAGATATACATATGAACTACGCTCTTACCCAAG	*syc2039* for pTHS87
147	Syc484_2B	AGTGGTGGTGGTGGTGGTGAGACCCTAACCAGCGGC	*syc2039* for pTHS87
148	Syc484_pIGA_2A	TAAAGTCAAGTAGGAGATTAATTCAATGAACTACGCTCTTACCCAAGC	*syc2039* for pTHS80
149	Syc484_2A2	TACAGGTTAGGAGAACGCCATGAACTACGCTCTTACCCAAG	*syc2039* for pTHS62
150	Syc484_2B2	CACTAGCAGATGCACTAGCAGACCCTAACCAGCGGC	*syc2039* for pTHS62
151	Syc484_pAM2991_2A	CACACAGGAAACAGACCATGAACTACGCTCTTACCCAAGC	*syc2039* for pTHS75
152	Syc484_KO_2A	TGTAGGAGATCTTCTAGAAAGATGTAGGCATCAAAGGCAGGC	Upstream homology for pTHS119

153	Syc484_KO_2B	CTTGCGGCAGCGTGAAGCTTAGCAAAGCAAAAGAAGCGATCG	Upstream homology for pTHS119
154	Syc484_KO_4A	TTCTTGACGAGTTCTTCTGATTCTGCTGCGATGCGTTAGG	Downstream homology for pTHS119
155	Syc484_KO_4B	CTCGAGTTTTTCAGCAAGATCAAGTAAGACTGGCTGCCATG	Downstream homology for pTHS119
156	Syc484_Seq_A	GATGCCACCGAGCAGAATTAG	Verification of Δ*syc2039*
157	Syc484_Seq_B	GGCAGATCAATCAGCAGCTC	Verification of Δ*syc2039*
158	Syc879_pET_2A	GTTTAACTTTAAGAAGGAGATATACATATGCTCTATCTGGCTGAAGTCG	*syc1139* for pTHS66
159	Syc879_pET_2B	CAGTGGTGGTGGTGGTGGTGGGCTGCAATCAGTTGATGACT	*syc1139* for pTHS66
160	Syc879_pIGA_2A	TAAAGTCAAGTAGGAGATTAATTCAGTGCTCTATCTGGCTGAAGTCGG	*syc1139* for pTHS81
161	Syc879_2A	TACAGGTTAGGAGAACGCCATGCTCTATCTGGCTGAAGTCG	*syc1139* for pTHS93
162	Syc879_2B	CACTAGCAGATGCACTAGCGGCTGCAATCAGTTGATGACTG	*syc1139* for pTHS93
163	Syc879_pAM2991_2A	CACACAGGAAACAGACCATGCTCTATCTGGCTGAAGTCGG	*syc1139* for pTHS74
164	Syc879_KO_2A	TGTAGGAGATCTTCTAGAAAGATCTGGAGCGATCGCTATGG	Upstream homology for pTHS133
165	Syc879_KO_2B	CTTGCGGCAGCGTGAAGCTTTATCGATGCCTCGCCTTAATCAATC	Upstream homology for pTHS133
166	Syc879_KO_4A	CCTTCTTGACGAGTTCTTCTGAGCCAGTCCCCCGCGACTA	Downstream homology for pTHS133
167	Syc879_KO_4B	CTCGAGTTTTTCAGCAAGATGGCAAGCGCAACTGAATTCTTAC	Downstream homology for pTHS133
168	Syn708_NdeI_F	GCTACATATGCTCTATCTGGCTGAAATTAAGAAA	*slr1301* for pTHS65
169	Syn708_XhoI_R_w/o	GCTACTCGAGACCGCCAAACAATAGGGTC	*slr1301* for pTHS65
170	Syn708_pET_2A	GTTTAACTTTAAGAAGGAGATATACATATGCTCTATCTGGCTGAAATTAAGAAAC	*slr1301* for pTHS67
171	Syn708_pRL25c_Fwd	TAAAACTACAGGTTAGGAGAACGCCATGCTCTATCTGGCTGAAATTAAGAAACAAAC	*slr1301* for pTHS91
172	Syn708_pRL25c_Rev	CACTAGCACTAGCAGATGCACTAGCACCGCCAAACAATAGGGTCT	*slr1301* for pTHS91
173	Syn708_3A	CTCTGGATCGGGTTCAGGAGTGCTCTATCTGGCTGAAATTAAG	*slr1301* for pTHS92
174	Syn708_3B	CCTTTCGTCTTCAAGAATTCTCTAACCGCCAAACAATAGGGTC	*slr1301* for pTHS92

175	153Syn708_2A	AGAATTAAAGAGGAGAAATTAAGCATGCT CTATCTGGCTGAAATTAAGAAAC	*slr1301* for pTHS82
176	153Syn708_2B	TCAGAGATGAGTTTCTGCTCACCGCCAAA CAATAGGGTC	*slr1301* for pTHS82
177	pJET708_2A	TGTAGGAGATCTTCTAGAAAGATAATAGA CTGCAATGTCAAAAAACTCAG	Upstream homology for pTHS131
178	708KO_CS3_2B	CAAGGTGCTGTGCACGGATCAAGTCGTT GTCCTGAGCAG	Upstream homology for pTHS131
179	708KO_CS3_4A	CCAAGGTAGTCGGCAAATAATTGGGTTG GTTGCCGAC	Downstream homology for pTHS131
180	pJET708_4B	CTCGAGTTTTTCAGCAAGATTTAGCAAGG TGGGGGGAATG	Downstream homology for pTHS131
181	708KO_1Aa	CCTGATTCTGTGGATAACCGTACGTCAAA ATCGAATTCCCGGTC	Upstream homology for pTHS132
182	708KO_1B	TGCTTGCGGCAGCGTGAAGCTTAAGTCG TTGTCCTGAGCAGTG	Upstream homology for pTHS132
183	708KO_2A	CGCCTTCTTGACGAGTTCTTCTGATTGGG TTGGTTGCCGACTTC	Downstream homology for pTHS132
184	708KO_2B	GATTATCAAAAAGGATCTTCACCTTTAGC AAGGTGGGGGGAATGC	Downstream homology for pTHS132
185	Nos389_pET_2A	GTTTAACTTTAAGAAGGAGATATACATAT GAATAGTGAGTTGTTCCAGAAGC	*all4981* for pTHS72
186	Nos389_NdeI_F	GCTACATATGAATAGTGAGTTGTTCCAGA AG	*all4981* for pTHS64
187	Nos389_XhoI_wo_R	GCTACTCGAGGATGTTACTATCACTACTT TGAATTTTT	*all4981* for pTHS64
188	Nos389_2A	CTACAGGTTAGGAGAACGCCATGAATAGT GAGTTGTTCCAGAAGCTAGC	*all4981* for pTHS89
189	Nos389_2B	GCACTAGCAGATGCACTAGCGATGTTACT ATCACTACTTTGAATTTTTTTGAGTTTGGC	*all4981* for pTHS89
190	Nos389_3A	CTCTGGATCGGGTTCAGGAATGAATAGT GAGTTGTTCCAGAAGC	*all4981* for pTHS88
191	Nos389_3B	CCTTTCGTCTTCAAGAATTCTTTAGATGTT ACTATCACTACTTTGAATTTTTTTGAG	*all4981* for pTHS88
192	Nos389_pIGA_2A	TAAAGTCAAGTAGGAGATTAATTCAATGA ATAGTGAGTTGTTCCAGAAGC	*all4981* for pTHS79
193	Nos389_TrbcL_2B	CCGACAATCCAAACACCGGTTTAGATGTT ACTATCACTACTTTGAATTTTTTTGAGTTT G	*all4981* for pTHS78
194	389KO_2A	ATTCGATATCTAGATCTCGAGTGTCAGAT TTAGTACTTTAAATACAAGACTTACACAC	Upstream homology for pTHS129

195	389KO_2B	CAAGGTGCTGTGCACGGATCAGCTGTTC GCTCTTGAGGG	Upstream homology for pTHS129
196	389KO_4A	CCAAGGTAGTCGGCAAATAAAGTAACGC GATGTGCGACT	Downstream homology for pTHS129
197	389KO_4B	ATGCAAGCTTTCGCGAGCTCGATTAATAC CTTTGGTGTTCATGACACTGG	Downstream homology for pTHS129
198	trunc389_2A	CTGAATAAGTGATAATAAGCGGAAGCCAT TTTAGATCGAGAGGCG	Truncated *all4981* for pTHS130
199	trunc389_2B	TGCAAGCTTTCGCGAGCTCGCTAAATTCC AAAACTCACTGCCTT	Truncated *all4981* for pTHS130
200	Nos389_gRNA-A	AGATCAGAAGCTAGCAAAAGCACA	*all4981* gRNA for pTHS124 and pTHS125
201	Nos389_gRNA-B	AGACTGTGCTTTTGCTAGCTTCTG	*all4981* gRNA for pTHS124 and pTHS125
202	Nos389_HL1A	TTTGTCTAGCTTTAATGCGGTAGTTGGTA CCGTGTGGGGTAATTTGCGGG	Upstream homology for pTHS124 and pTHS125
203	Nos389_HL1B	ATAAGTCGCACATCGCGTTACTTCATAGC TGTTCGCTCTTGAGG	Upstream homology for pTHS124 and pTHS125
204	Nos389_HR2A	CCTCAAGAGCGAACAGCTATGAAGTAAC GCGATGTGCGACTTATTC	Downstream homology for pTHS124 and pTHS125
205	Nos389_HR2B	GGATTACAGATCCTCTAGAGTCGACGGTA CCGGACACCACCAGCCATTTC	Downstream homology for pTHS124 and pTHS125
206	MB_1A	TGCCTGCAGGTCGACTCTAATGAATAGTG AGTTGTTCCAGAAGC	*all4981* for pTHS107 and pTHS109
207	MB_1B	TCGGTACCCGGGGATCCTCGATGTTACT ATCACTACTTTGAATTTTTTTGAGT	*All4981* for pTHS107 and pTHS109
208	MB_2A	AGGGTCGACTCTAGAGGATATGAATAGT GAGTTGTTCCAGAAGC	*all4981* for pTHS108
209	MB_2B	CTTACTTAGGTACCCGGGGGATGTTACTA TCACTACTTTGAATTTTTTTGAGT	*all4981* for pTHS108
210	MB_4A	TCTAGAGGATCCCCGGGTAATGAATAGT GAGTTGTTCCAGAAGC	*all4981* for pTHS110
211	MB_4B	TCGATGAATTCGAGCTCGGGATGTTACTA TCACTACTTTGAATTTTTTTGAGT	*all4981* for pTHS110
212	MB_9A	TGCCTGCAGGTCGACTCTAATGCTCTATC TGGCTGAAATTAAGAAAC	*slr1301* for pTHS111 and pTHS113

213	MB_9B	TCGGTACCCGGGGATCCTCACCGCCAAA CAATAGGGT	*slr1301* for pTHS111 and pTHS113
214	MB_10A	AGGGTCGACTCTAGAGGATATGCTCTATC TGGCTGAAATTAAGAAAC	*slr1301* for pTHS112
215	MB_10B	CTTACTTAGGTACCCGGGGACCGCCAAA CAATAGGGTC	*slr1301* for pTHS112
216	MB_12A	TCTAGAGGATCCCCGGGTAATGCTCTATC TGGCTGAAATTAAGAAAC	*slr1301* for pTHS114
217	MB_12B	TCGATGAATTCGAGCTCGGACCGCCAAA CAATAGGGTC	*slr1301* for pTHS114
218	MB_13A	TGCCTGCAGGTCGACTCTAATGACAAGTC AAAATTTTGTTTCTGATCAAG	*slr7083* for pTHS99 and pTHS101
219	MB_13B	TCGGTACCCGGGGATCCTCTGGTAAATA AGGGGGAGTGGGAC	*slr7083* for pTHS99 and pTHS101
220	MB_14A	AGGGTCGACTCTAGAGGATATGACAAGT CAAAATTTTGTTTCTGATCAAG	*slr7083* for pTHS100
221	MB_14B	CTTACTTAGGTACCCGGGGTGGTAAATAA GGGGGAGTGGGAC	*slr7083* for pTHS100
222	MB_16A	TCTAGAGGATCCCCGGGTAATGACAAGT CAAAATTTTGTTTCTGATCAAG	*slr7083* for pTHS102
223	MB_16B	TCGATGAATTCGAGCTCGGTGGTAAATAA GGGGGAGTGGGAC	*slr7083* for pTHS102
224	MB_33A	TGCCTGCAGGTCGACTCTAATGCTCTATC TGGCTGAAGTCG	*syc1139* for pTHS115 and pTHS117
225	MB_33B	TCGGTACCCGGGGATCCTCGGCTGCAAT CAGTTGATGACT	*syc1139* for pTHS115 and pTHS117
226	MB_34A	AGGGTCGACTCTAGAGGATATGCTCTATC TGGCTGAAGTCG	*syc1139* for pTHS116
227	MB_34B	CTTACTTAGGTACCCGGGGGGCTGCAAT CAGTTGATGACT	*syc1139* for pTHS116
228	MB_36A	TCTAGAGGATCCCCGGGTAATGCTCTATC TGGCTGAAGTCG	*syc1139* for pTHS118
229	MB_36B	TCGATGAATTCGAGCTCGGGGCTGCAAT CAGTTGATGACT	*syc1139* for pTHS118
230	MB_45A	TGCCTGCAGGTCGACTCTAATGAACTACG CTCTTACCCAAG	*syc2039* for pTHS103 and pTHS105
231	MB_45B	TCGGTACCCGGGGATCCTCAGACCCTAA CCAGCGGC	*syc2039* for pTHS103 and pTHS105
232	MB_46A	AGGGTCGACTCTAGAGGATATGAACTAC GCTCTTACCCAAG	*syc2039* for pTHS104
233	MB_46B	CTTACTTAGGTACCCGGGGAGACCCTAA CCAGCGGC	*syc2039* for pTHS104
234	MB_48A	TCTAGAGGATCCCCGGGTAATGAACTAC GCTCTTACCCAAG	*syc2039* for pTHS106

235	MB_48B	TCGATGAATTCGAGCTCGGAGACCCTAACCAGCGGC	*syc2039* for pTHS106
236	708_Seq_A	CCAACAAACTACCTACCACCAGTC	Verification of *Δslr1301*
237	708_Seq_B	CCGTAGGGATGCCTGATAAACC	Verification of *Δslr1301*
238	Syc879_Seq_A	CATCAGGAATGGATGCAGGAGG	Verification of *Δsyc1139*
239	Syc879_Seq_B	GGCCGCTAATCACTTTCAGTG	Verification of *Δsyc1139*

Plasmids	**Description**	**Resistance**	**Reference**
pJET1.2/ blunt	*E. coli* subcloning vector	Amp	Thermo Fischer Scientific
pMAL-c2x	Bacterial vector for expressing N-terminal MBP-tagged proteins in *E. coli* with a Factor Xa cleavage site	Amp	A gift from Axel Scheidig (University of Kiel)
pet21a(+)	Bacterial vector for expressing C-terminal 6His-tagged proteins in *E. coli*	Amp	Novagen
pRL25C	Shuttle cosmid vector for cyanobacteria and *E. coli*	Km, Nm	(Wolk *et al.*, 1988)
pRL623	Methylation plasmid	Cm	(Wolk *et al.*, 1988)
pRL443	Conjugation plasmid	Amp	(Wolk *et al.*, 1988)
pRL271	*sacB* containing plasmid to select for double homologous recombination in *Anabaena*	Cm	(Cai and Wolk, 1990)
pRL278	*sacB* containing plasmid to select for double homologous recombination in *Anabaena*	Km, Nm	(Cai and Wolk, 1990)
pSL2680	Cpf1-mediated CRISPR editing plasmid	Km, Nm	(Ungerer and Pakrasi, 2016)
pRL25c-CRISPR	Functional CRISPR cassette from pSL2680 transferred into EcoRI and BamHI digested pRL25c by GIBSON assembly	Km, Nm	This work
pSM2-Pcpc560ter	pMD18-T derivate for insertion into *pta*, containing P_{cpc560}::*ter*::T_{rbcL} expression cassette	Km, Amp	A gift from Yin Li (Chinese Academy of Science). (Zhou *et al.*, 2014)
pIGA	Cyanobacterial vector for insertion into neutral locus (RS1 and RS2) of *slr0168* in *Synechocystis*	Amp, Km	A gift from Martin Hagemann (University Rostock), (Kunert, Hagemann and Erdmann, 2000)
pRL153-GFP	Mobilizable broad host range vector, P_{trc}-*gfp*	Km, Nm	(Tolonen, Liszt and Hess, 2006)

pKNT25	P_{lac}::-*T25*	Km	Euromedex
pKT25	P_{lac}::*T25*-	Km	Euromedex
pUT18	P_{lac}::-*T18*	Amp	Euromedex
pUT18C	P_{lac}::*T18*-	Amp	Euromedex
pKT25-zip	pKT25; P_{lac}::*T25-zip*	Km	Euromedex
pUT18C-zip	pUT18C, P_{lac}::*T18-zip*	Amp	Euromedex
pAM2991	Cyanobacterial vector for expression of proteins under the control of P_{trc} that inserts into the NS1 site of *Synechococcus*	Sm, Sp	A gift from Susan Golden (Addgene plasmid # 40248)
pTHS1	pRL25C, P_{petE}::*alr4504-gfp*	Km, Nm	(Springstein *et al.*, 2019)
pTHS33	pKNT25, P_{lac}::*sepJ-T25*	Km, Nm	(Springstein *et al.*, 2019)
pTHS34	pKT25, P_{lac}::*T25-sepJ*	Km, Nm	(Springstein *et al.*, 2019)
pTHS35	pUT18, P_{lac}::*sepJ-T18*	Amp	(Springstein *et al.*, 2019)
pTHS36	pUT18C, P_{lac}::*T18-sepJ*	Amp	(Springstein *et al.*, 2019)
pTHS37	pKNT25, P_{lac}::*ftsZ-T25*	Km, Nm	(Springstein *et al.*, 2019)
pTHS38	pKT25, P_{lac}::*T25-ftsZ*	Km, Nm	(Springstein *et al.*, 2019)
pTHS39	pUT18, P_{lac}::*ftsZ-T18*	Amp	(Springstein *et al.*, 2019)
pTHS40	pUT18C, P_{lac}::*T18-ftsZ*	Amp	(Springstein *et al.*, 2019)
pTHS41	pKNT25, P_{lac}::*mreB-T25*	Km, Nm	(Springstein *et al.*, 2019)
pTHS42	pKT25, P_{lac}::*T25-mreB*	Km, Nm	(Springstein *et al.*, 2019)
pTHS43	pUT18, P_{lac}::*mreB-T18*	Amp	(Springstein *et al.*, 2019)
pTHS44	pUT18C, P_{lac}::*T18-mreB*	Amp	(Springstein *et al.*, 2019)
pTHS60	pIGA, P_{cpc560}::*fm7001-gfp*::T_{rbcL}	Amp, Km	This study
pTHS61	pET21a(+), P_{T7}::*slr7083-his*	Amp	This study
pTHS62	pET21a(+), P_{T7}::*syc2039-his*	Amp	This study
pTHS63	pET21a(+), P_{T7}::*fm7001-his*	Amp	This study

pTHS64	pET21a(+), P_{T7}::*all4981-his*	Amp	This study
pTHS65	pET21a(+), P_{T7}::*slr1301-his*	Amp	This study
pTHS66	pET21a(+), P_{T7}::*syc1139-his*	Amp	This study
pTHS67	pET21a(+); P_{T7}::*slr1301-gfp*	Amp	This study
pTHS68	pET21a(+), P_{T7}::*syc1139-gfp*	Amp	This study
pTHS69	pET21a(+), P_{T7}::*slr7083-gfp*	Amp	This study
pTHS70	pET21a(+), P_{T7}::*fm7001-gfp*	Amp	This study
pTHS71	pET21a(+), P_{T7}::*syc2039-gfp*	Amp	This study
pTHS72	pET21a(+), P_{T7}::*all4981-gfp*	Amp	This study
pTHS73	pMAL-c2x; P_{tac}::*mbp-fm7001-his*	Amp	This study
pTHS74	pAM2991, P_{trc}::*syc1139-gfp*	Sm, Sp	This study
pTHS75	pAM2991, P_{trc}::*syc2039-gfp-his*	Sm, Sp	This study
pTHS76	pIGA, P_{cpc560}::*yfp-fm7001*::T_{rbcL}	Amp, Km	This study
pTHS77	pIGA, P_{cpc560}::*slr7083-gfp*::T_{rbcL}	Amp, Km	This study
pTHS78	pIGA, P_{cpc560}::*yfp-all4981*::T_{rbcL}	Amp, Km	This study
pTHS79	pIGA, P_{cpc560}::*all4981-gfp*::T_{rbcL}	Amp, Km	This study
pTHS80	pIGA, P_{cpc560}::*syc2039-gfp*::T_{rbcL}	Amp, Km	This study
pTHS81	pIGA, P_{cpc560}::*syc1139-gfp*::T_{rbcL}	Amp, Km	This study
pTHS82	pRL153, P_{trc}::*slr1301-yfp*	Km, Nm	This study
pTHS83	pRL25C, P_{petE}::*fm7001-gfp*	Km, Nm	This study
pTHS84	pRL25C, P_{petE}::*yfp-fm7001*	Km, Nm	This study
pTHS85	pRL25C, P_{petE}::*yfp-slr7083*	Km, Nm	This study
pTHS86	pRL25C, P_{petE}::*slr7083-gfp*	Km, Nm	This study
pTHS87	pRL25C, P_{petE}::*syc2039-gfp*	Km, Nm	This study
pTHS88	pRL25C, P_{petE}::*yfp-all4981*	Km, Nm	This study
pTHS89	pRL25C, P_{petE}::*all4981-gfp*	Km, Nm	This study
pTHS90	pRL25C, P_{petE}-*creS-gfp*	Km, Nm	This study
pTHS91	pRL25C, P_{petE}::*slr1303-gfp*	Km, Nm	This study
pTHS92	pRL25C, P_{petE}::*yfp-slr1303*	Km, Nm	This study
pTHS93	pRL25C, P_{petE}::*syc1139-gf*	Km, Nm	This study
pTHS94	pRL25C, $P_{all4982}$::*all4982-ecfp*	Km, Nm	This study
pTHS95	pKNT25, P_{lac}::*fm7001-T25*	Km, Nm	This study

pTHS96	pKT25, P_{lac}::*T25-fm7001*	Km, Nm	This study
pTHS97	pUT18, P_{lac}::*fm7001-T18*	Amp	This study
pTHS98	pUT18C, P_{lac}::*T18-fm7001*	Amp	This study
pTHS99	pKNT25, P_{lac}::*slr7083-T25*	Km, Nm	This study
pTHS100	pKT25, P_{lac}::*T25-slr7083*	Km, Nm	This study
pTHS101	pUT18, P_{lac}::*slr7083-T18*	Amp	This study
pTHS102	pUT18C, P_{lac}::*T18-slr7083*	Amp	This study
pTHS103	pKNT25, P_{lac}::*syc2039-T25*	Km, Nm	This study
pTHS104	pKT25, P_{lac}::*T25-syc2039*	Km, Nm	This study
pTHS105	pUT18, P_{lac}::*syc2039-T18*	Amp	This study
pTHS106	pUT18C, P_{lac}::*T18-syc2039*	Amp	This study
pTHS107	pKNT25, P_{lac}::*all4981-T25*	Km, Nm	This study
pTHS108	pKT25, P_{lac}::*T25-all4981*	Km, Nm	This study
pTHS109	pUT18, P_{lac}::*all4981-T18*	Amp	This study
pTHS110	pUT18C, P_{lac}::*T18-all4981*	Amp	This study
pTHS111	pKNT25, P_{lac}::*slr1301-T25*	Km, Nm	This study
pTHS112	pKT25, P_{lac}:: *T25-slr1301*	Km, Nm	This study
pTHS113	pUT18, P_{lac}::*slr1301-T18*	Amp	This study
pTHS114	pUT18C, P_{lac}::*T18-slr1301*	Amp	This study
pTHS115	pKNT25, P_{lac}::*syc1139-T25*	Km, Nm	This study
pTHS116	pKT25, P_{lac}::*T25-syc1139*	Km, Nm	This study
pTHS117	pUT18, P_{lac}::*syc1139-T18*	Amp	This study
pTHS118	pUT18C, P_{lac}::*T18-syc1139*	Amp	This study
pTHS119	pJET1.2/blunt with ~1000 bp upstream and downstream of *syc2039* flanking *nptII*	Amp	This study
pTHS120	Circularized pUC ori with 1000 bp upstream and downstream of *slr7083* flanking *nptII* assembled by GIBSON assembly	Km, Nm	This study
pTHS121	pSL2680 with *fm7001* gRNA and homologous repair templates 1000 bp upstream and downstream of *fm7001*	Km, Nm	This study
pTHS122	pRL25C containing *cpf1*, *lacZα* and pre-crRNA array with tandem spacer-repeat sequences from *Francisella novicida*	Km, Nm	This study
pTHS123	pTHS122 with *fm7001* gRNA and homologous repair templates 1000 bp upstream and downstream of *fm7001*	Km, Nm	This study

pTHS124	pSL2680 with *all4981* gRNA and homologous repair templates 1000 bp upstream and downstream of *all4981*	Km, Nm	This study
pTHS125	pTHS122 with *all4981* gRNA and homologous repair templates 1000 bp upstream and downstream of *all4981*	Km, Nm	This study
pTHS126	pRL271 containing 1000 bp upstream and downstream of *fm7001* flanking *nptII*	Km, Nm, Cm	This study
pTHS127	pRL278 containing 2000 bp upstream and downstream of *fm7001* flanking CS.3	Km, Nm, Sm, Sp	This study
pTHS128	pRL278 containing 2000 bp upstream of *fm7001* and the first 398 bp of *fm7001*	Km, Nm	This study
pTHS129	pRL278 containing 1000 bp upstream and downstream of *all4981* flanking CS.3	Km, Nm, Sm, Sp	This study
pTHS130	pRL278 containing 151 bp upstream of *all4981* and the first 449 bp of *all4981*	Km, Nm	This study
pTHS131	pJET1.2/blunt with ~1000 bp upstream and downstream of *slr1303* flanking CS.3 inserted by GIBSON assembly	Amp	This study
pTHS132	Circularized pUC ori with 1000 bp upstream and downstream of *slr1301* flanking *nptII* assembled by GIBSON assembly	Km, Nm	This study
pTHS133	pJET1.2/blunt with ~1000 bp upstream and downstream of *syc1139* flanking *nptII* inserted by GIBSON assembly	Amp	This study

Restriction sites or overlapping sites are underlined.

Sm: streptomycin resistance; Sp: spectinomycin resistance; Amp: ampicillin resistance, Km: kanamycin resistance, Nm: neomycin resistance; Cm: chloramphenicol resistance.

- 1) The eYFP is C-terminally followed by a myc-tag, which is then followed by a heptapeptide of glycine and serine. Abbreviated: *yfp*.
- 2) Modified *gfpmut3.1* in which the internal NdeI site was removed by replacing CAT by the synonymous CAC codon. The GFP is N-terminally preceded by 12 alanine and serine residues. Abbreviated: *gfp*. (Stucken *et al.*, 2012).